

An Experimental Investigation on the Flow Properties of Bulk Solids

A Dissertation Submitted
in partial fulfillment of the requirements
for the degree of

Master of Engineering
in
Thermal Engineering

by

Lokesh Rohilla

Registration No.: 801483013

Under Supervision of

Dr. S.S. Mallick

(Associate Professor)

and

Mr. Gautam Setia

(Lecturer)



MECHANICAL ENGINEERING DEPARTMENT

THAPAR UNIVERSITY, PATIALA

JULY, 2016

CERTIFICATE

I hereby declare that the thesis entitled “**An Experimental Investigation on the Flow Properties of Bulk Solids**” is an authentic record of my work carried out as requirements for the award of the degree of **Master of Engineering in Thermal Engineering** at **Thapar University, Patiala** under the supervision of **Dr. S.S. Mallick**, Associate Professor and **Mr. Gautam Setia**, Lecturer, Department of Mechanical Engineering, Thapar University, Patiala during July, 2015 to July, 2016. No part of the matter embodied in this report has been submitted to any other university or institute for the award of any degree.

Date: *5-July-2016*


Lokesh Rohilla

It is certified that the above statement made by the student is correct to the best of our knowledge and belief.



Dr. S.S. Mallick
Department
Thapar University, Patiala - 147004



Mr. Gautam Setia
Department
Thapar University, Patiala - 147004

Countersigned by



Head, Mechanical Engineering Department
Thapar University, Patiala - 147004



Dean of Academic Affairs
Thapar University, Patiala - 147004

*Dedicated to
My Parents*

Acknowledgements

I would like to acknowledge my supervisors Dr. S.S. Mallick and Mr. Gautam Setia for introducing me to the fundamentals of research. They provided an excellent atmosphere necessary for a research scholar to carry out his research work. Their advice and pointers were priceless and had a deep impact on my analytical thinking and research work as well.

The research grant provided by Thapar University, Patiala for Powder Flow Tester is highly appreciated. GATE scholarship provided by Ministry of Human Resource and Development (MHRD) allowed me to carry out my research work.

I owe a special debt to all the authors and researchers whose work I have used and duly cited to carry out my research. Last but not least, I would like to thank my parents, brother and friends from the bottom of my heart for their constant encouragement and support.

Lokesh Rohilla

Abstract

This thesis results from an ongoing investigation on the effects of powder physical properties on flow properties of fine powders. Seven fly ash samples (F type, median particle size $139\mu\text{m}$ - $21\mu\text{m}$; particle density 2013 - 2015 Kg/m^3 ; bulk density 670.2 Kg/m^3 - 794.9 Kg/m^3) were collected directly from electrostatic precipitator hoppers (ESP hopper) corresponding to seven ESP fields. Their powder flow properties were measured by using Brookfield Powder Flow tester. It was found that fly ash samples collected from first four stages were easy flowing and fly ash samples collected from later stages were of cohesive nature according to Jenike (1964) classification. Transition particle size which caused change in flow properties of fly ash was found experimentally. Transition particle size was identified by using flowability classification and compaction dynamics. Transition in flow behaviour was probably due to large magnitude of inter-particle forces among powder particles as compared to weight of the particle. All powder flow properties like cohesion, unconfined yield strength etc showed asymptotic behaviour after transition particle size. Additionally, twenty two fly ash samples (median particle size $139\mu\text{m}$ - $4\mu\text{m}$; particle density 2960 - 2013 Kg/m^3 ; bulk density 794.9 Kg/m^3 - 494.3Kg/m^3) of different flowability were evaluated for their feasibility to flow from an ESP hopper of specified dimensions. It was found that only easy flowing fly ash samples can flow reliably from ESP hopper under gravity while cohesive and very cohesive fly ash samples will require discharge aids. A qualitative idea about magnitude of aeration rate necessary has been given on the basis of minimum fluidisation velocity and permeability factor. It was observed that all fly ash samples do not require same aeration rate which is generally the practice in industries. A new cohesion model has been developed by using only powder physical properties. The new model eliminates the need of conducting shear testing of fine powders to find cohesion and gives 20% more accuracy as compared to existing cohesion models. Finally, a new model for unconfined yield strength has been proposed which can be used to rank powders according to their flowability without conducting their shear testing.

Keywords: Powder Characterization; Powder flow properties; Fly ash; Hopper/silo design; Powder Flow Tester; Cohesion model.

Contents

List of Figures.....	viii
List of Table.....	xii
Nomenclature	xiv
1 Introduction and Objectives	1
1.1 Introduction	1
1.2 Objectives.....	3
2 Literature Review.....	4
2.1 Introduction	4
2.2 Common problems with bulk solids.....	4
2.3 Mohr circle analysis of bulk solids.....	7
2.4 Principle of shear testing.....	10
2.5 Flowability tests.....	13
2.6 Flow function tests.....	13
2.7 Time consolidated flow function.....	15
2.8 Wall friction test.....	15
2.9 Bulk density test	16
2.10 Flowability variation with depth of hopper.....	16
2.11 Previous research work on flow properties of powders.....	17
2.12 Previous research work related to powder rheology and shear testing.....	24
2.13 Previous research work related to particle properties, shear testing and AFM.....	27
3 Material and methods	30
3.1 Introduction	30
3.2 Samples	30
3.3 Physical properties measurement	31

3.3.1 SEM images and particle size measurement	31
3.3.2 Particle density measurement	32
3.3.3 Hausner ratio (HR) measurement.....	32
3.4 Chemical composition of fly ash.....	32
3.5 Annular shear tester	33
3.5.1 Powder Flow Tester	33
3.5.2 Calibration of Powder Flow Tester	34
3.5.3 Operating procedure for powder flow tester.....	35
3.6 Flow properties measurement.....	36
3.6.1 Yield locus and flow function curves.....	36
3.6.2 Wall friction and bulk density tests.....	39
3.7 Hopper design procedure	41
3.7.1 Critical dimensions of mass flow hopper	41
3.7.2 Hopper design for funnel flow	41
3.7.3 Hopper design by using Jenike charts	42
3.8 Exploring link between flowability and fluidizability	43
4 Effect of Physical Properties of Fly Ash on its Flow Properties	45
4.1 Introduction	45
4.2 Analysis of physical properties of fly ash.....	45
4.3 Flowability classification of fly ash.....	47
4.4 Effect of particle size on cohesion.....	48
4.5 Effect of particle size on angle of internal friction.....	50
4.6 Effect of particle size on unconfined yield strength	52
4.7 Effect of particle size on wall friction angle	53
4.8 Effect of aerated bulk density on Flow Index (FI)	54
4.9 Effect of aerated bulk density on cohesion	55
5 Effect of Flow Properties of Fine Powers on Hopper Geometry	57

5.1 Introduction	57
5.2 Effect of flow properties of fly ash on mass flow hopper geometry	57
5.3 Effect of flow properties of fly ash on funnel flow hopper geometry	63
6 Modeling cohesion and unconfined yield strength for fine powders	67
6.1 Introduction	67
6.2 Existing correlations between particle physical properties and cohesion.....	67
6.2.1 Unconfined yield strength ratio model.....	67
6.2.2 Trend line modeling based cohesion model	72
6.3 Modeling cohesion on the basis of particle size distribution	73
6.3.1 Particle size distribution model (PSD model).....	73
6.3.2 Physical significance of model parameters.....	75
6.3.3 Relative importance of model parameters	75
6.3.4 Evaluation of applicability and error in the model.....	76
6.4 Modeling unconfined yield strength on the basis of particle size distribution.....	80
6.5 Comparison of maximum and minimum error in the models	84
7 Conclusion and future scope.....	85
7.1 Conclusion.....	85
7.2 Future scope	86
References.....	87
Web references	92
Appendix A.....	93
Appendix B.....	98
Appendix C.....	100
Communications.....	101

List of Figures

Figure 2.1	Arching (Schulze, 2008)	4
Figure 2.2	Funnel flow (Schulze, 2008)	5
Figure 2.3	Flooding (Schulze, 2008)	5
Figure 2.4	Non uniform discharge (Schulze, 2008)	6
Figure 2.5	Segregation (Schulze, 2008)	6
Figure 2.6	Buckling (Schulze, 2008)	7
Figure 2.7	Powder element with vertical stress and complimentary Horizontal stress (Schulze, 2008)	8
Figure 2.8	Stress on any plane of powder element (Schulze, 2008)	8
Figure 2.9	Yield limit and failure strength of the powder element (Schulze, 2008)	10
Figure 2.10	Powder Flow Tester	11
Figure 2.11	Plotting of yield locus curve by shear ring tester (Schulze, 2008)	12
Figure 2.12	Axial and torsional load variation with time for a powder	12
Figure 2.13	Flowability test (Schulze, 2008)	14
Figure 2.14	Flow function curve (ff) (Schulze, 2008)	15
Figure 2.15	Formation of cohesive arch (Schulze, 2008)	17
Figure 3.1	Brookfield Powder Flow Tester (PFT)	34
Figure 3.2	(a) Standard flow function vane lid (b) Standard 304 s/s wall friction lid	34
Figure 3.3	Yield locus for F1 fly ash at 0.317, 0.610, 1.207, 2.44 and 4.819 kPa	37
Figure 3.4	Flow function curves for seven fly ash samples	38
Figure 3.5	Variation of effective angle of internal friction with major consolidation stress	38
Figure 3.6	Wall yield locus for F7 fly ash sample	39
Figure 3.7	Trends of effective angle of wall friction with major consolidation stress	40
Figure 3.8	Bulk density curves for seven fly ash samples	40

Figure 4.1	SEM images of seven fly ash samples F1 to F7 at 500 times magnification	46
Figure 4.2	Effect of median particle size on cohesion in seven fly ash samples at different Pre shear stresses	50
Figure 4.3	Effect of particle size on angle of internal friction	51
Figure 4.4	Effect of particle size on unconfined yield strength	52
Figure 4.5	Effect of particle size on wall friction angle at different normal stresses	53
Figure 4.6	Effect of aerated bulk density on FI	55
Figure 4.7	Effect of aerated bulk density on cohesion in sample	56
Figure 5.1	Mass flow hopper geometry for easy flowing fly ash	59
Figure 5.2	Mass flow hopper geometry for cohesive fly ash	60
Figure 5.3	Mass flow hopper geometry for very cohesive fly ash	61
Figure 5.4	Mass flow hopper geometry for samples (F1 to F7) collected From consecutive ESP hoppers	62
Figure 5.5	Critical rathole diameter profile for easy flowing fly ash	64
Figure 5.6	Critical rathole diameter for cohesive fly ash samples	65
Figure 5.7	Critical rathole diameter for cohesive fly ash samples	66
Figure 6.1	Comparison of experimental cohesion and modelled cohesion by using Saw et al. (2013) model at stress 1	68
Figure 6.2	Comparison of experimental cohesion and modelled cohesion by using Saw et al. (2013) model at stress 2	69
Figure 6.3	Comparison of experimental cohesion and modelled cohesion by using Saw et al. (2013) model at stress 3	69
Figure 6.4	Comparison of experimental cohesion and modelled cohesion by using Saw et al. (2013) model at stress 4	70
Figure 6.5	Comparison of experimental cohesion and modelled cohesion by using Saw et al. (2013) model at stress 5	70
Figure 6.6	Comparison of experimental cohesion and modelled cohesion by using	71

	Saw et al. (2013) model at all pre shear stresses	
Figure 6.7	Comparison between experimental and modelled cohesion by using Saw et al. (2015) model at all pre shear stresses	73
Figure 6.8	Comparison of experimental cohesion and modelled cohesion by using newly developed particle size distribution model at stress 1	77
Figure 6.9	Comparison of experimental cohesion and modelled cohesion by using newly developed particle size distribution model at stress 2	77
Figure 6.10	Comparison of experimental cohesion and modelled cohesion by using newly developed particle size distribution model at stress 3	78
Figure 6.11	Comparison of experimental cohesion and modelled cohesion by using newly developed particle size distribution model at stress 4	78
Figure 6.12	Comparison of experimental cohesion and modelled cohesion by using newly developed particle size distribution model at stress 5	79
Figure 6.13	Comparison of experimental cohesion and modelled cohesion by using Particle size distribution model at stress 1 to stress 5	79
Figure 6.14	Comparison of experimental cohesion and modelled unconfined yield strength (UYS) at all pre shear stresses	80
Figure 6.15	Comparison of experimental and modelled unconfined yield strength (UYS) at stress 1	81
Figure 6.16	Comparison of experimental and modelled unconfined yield strength (UYS) at stress 2	81
Figure 6.17	Comparison of experimental and modelled unconfined yield strength (UYS) at stress 3	82
Figure 6.18	Comparison of experimental and modelled unconfined yield strength (UYS) at stress 4	82
Figure 6.19	Comparison of experimental and modelled unconfined yield strength (UYS) at stress 5	83
Figure 6.20	Comparison of experimental and modelled unconfined yield strength (UYS) at all pre shear stresses	83

Figure A.1	Dependence of major consolidation stress on wall friction angle (W.2)	94
Figure A.2	Stress distribution in a silo (Schulze, 2008)	96

List of Tables

Table 3.1	Physical properties of fly ash samples	31
Table 3.2	Silicon oxide and Aluminium oxide content in fly ash samples	33
Table 3.3	Calibration table for PFT	35
Table 3.4	Flow mode classification of fly ash sample	44
Table 4.1	Comparison of range of angle of internal friction with fly as flowability	52
Table 4.2	Aerated bulk density of 7 fly ash samples	54
Table 5.1	Minimum fluidisation velocity ash permeability factor for sample F1 to F7 (Chawla, 2015)	63
Table 6.1	Particle size distribution model parameters for 25 tested powders	74
Table 6.2	Pre shear stress level and magnitude	75
Table 6.3	Evaluation of error in different models	84
Table B.1	Comparison of maximum and minimum error in cohesion models at stress 1	98
Table B.2	Comparison of maximum and minimum error in cohesion models at stress 2	98
Table B.3	Comparison of maximum and minimum error in cohesion models at stress 3	98
Table B.4	Comparison of maximum and minimum error in cohesion models at stress 4	99
Table B.5	Comparison of maximum and minimum error in cohesion models at stress 5	99
Table C.1	Comparison of maximum and minimum error in cohesion models at stress 5	100
Table C.2	Comparison of maximum and minimum error in cohesion models at stress 5	100
Table C.3	Comparison of maximum and minimum error in cohesion models at stress 5	100

Table C.4	Comparison of maximum and minimum error in cohesion models at stress 5	100
Table C.5	Comparison of maximum and minimum error in cohesion models at stress 5	100

Nomenclature

B_o	= Bond number
C	= Cohesion, kPa
d	= Particle diameter, μm
D_c	= Minimum opening size for hopper, mm
D_f	= Rathole diameter for funnel flow hopper, m
F_a	= Force of attraction between particles, N
ff	= Flow factor
ff_c	= Flowability factor
g	= Acceleration due to gravity, m/s^2
K	= Stress ratio
mg	= Particle weight, N
Q	= Discharge rate, m^3/s
R_a	= Average roughness, μm
Z	= Depth of powder, m

Greek symbols

δ	= Effective angle of internal friction, $^\circ$
δ^*	= Effective angle of internal friction, $^\circ$
θ	= Hopper half angle, $^\circ$
κ	= Elastic plastic contact consolidation coefficient
κ_a	= Elastic plastic contact area coefficient
κ_p	= Plastic contact repulsion coefficient

ρ_a	= Aerated bulk density, kg/m ³
ρ_b	= Bulk density, kg/m ³
ρ_o	= Loose pour bulk density, kg/m ³
ρ_p	= Particle density, kg/m ³
σ'	= Abutment stress, kPa
σ	= Consolidation stress or normal stress, kPa
σ_1	= Major principle stress, kPa
σ_1'	= Stress in an arch or abutment stress, kPa
σ_c	= Unconfined yield strength, kPa
σ_h	= Horizontal stress, kPa
σ_{pre}	= Pre shear stress, kPa
σ_v	= Vertical stress, kPa
σ_α	= Normal stress at angle α , kPa
τ, τ_{xy}	= Shear stress, kPa
τ_α	= Shear stress on plane at α angle, kPa
φ	= Angle of internal friction, °
φ_f	= Hopper half angle for funnel flow hopper, °
φ_w	= Wall friction angle, °

Acronyms

AFM	≡	Atomic Force Microscope
C.I	≡	Compressibility Index
EDS	≡	Energy Dispersive Spectroscopy
ESP	≡	Electrostatic Precipitator
FI	≡	Flow Index
HR	≡	Hausner Ratio

HSC ≡ High Sensitivity Circularity
PFT ≡ Powder Flow Tester
RH ≡ Relative Humidity
SEM ≡ Scanning Electron Microscope

Chapter 1

Introduction and Objectives

1.1 Introduction

Determination of flow properties of bulk solids and powders (such as cement, fly ash, pulverised coal, food products etc) are of paramount importance. Flow properties of bulk solids affect the geometry of storage and handling equipment. Fine powders are encountered in various stages of manufacturing in different industries related to pharmaceuticals, food products, powder metallurgy etc. Fine powders have to be stored, handled and transported from one point to another. Fine powder is a complex assembly of solid particles which shows the behaviour of both solids and liquids (Schulze, 2008). On the one hand they flow out of the hopper like any liquid while on the other hand they support shear stress in static state like solids resulting in formation of the powder heap. This dual nature of powder under different conditions causes difficulty in providing any general analytical theory applicable to them under all conditions. Their flow properties are affected by many factors like particle physical properties, moisture content, temperature, net intermolecular forces etc. Researchers rely on the experiments and experimental data to propose tailor made solution for every powder and its application. One of the foremost applications of powder flow properties is the designing of mass flow and funnel flow storage vessels. Problems related to storage vessels are like arching, ratholing, flooding, unreliable discharge etc. Such problems are encountered when the storage vessels or hoppers/ silo are not designed by considering flow properties of powders. Jenike (1964) did pioneering work by deducing the relation between hopper critical dimensions and flow properties of powders. Recently many researchers have used Jenike design technique to propose tailor made solution to the flow problems of different powders. Ripp et al. (2015) recently conducted a study on flow properties of tef flour and seeds and designated the optimum mass flow storage vessel for them by using Jenike methodology. They also showed the effect of wall material on the flow properties of bulk solids. Liu et al. (2015) studied the effect of particle size of pulverised coal on the discharge behaviour from a mass flow hopper. Lu et al. (2015) investigated the flow properties of pulverised coal and found the dominant forces causing gravity discharge at different particle sizes. Lee et al.

(2015) investigated the flow properties of soybean powder and applied the image analysis to explain the cause of particular flow behaviour of irregularly shaped soybean powders. Teunou et al. (1993) and Iqbal et al. (2006) studied the effect of moisture content, particle size, time consolidation and chemical composition of food powders on their flow properties. Some researchers like Chirone et al., (2015); Colbert et al., (2015) and Capece et al., (2015) have taken a step further in powder characterization by correlating magnitude of microscopic force of attraction between particles with its bulk flow behaviour. Different researchers like Leturia et al., (2014); Krantz et al., (2009) and Freeman (2007) have performed an experimental investigation on flow properties of air and fine powder mixture to comment on their flowability and fluidizability. Another indirect application of powder flow properties is in pneumatic conveying systems. There is interaction between fine powder and pipe wall during various modes of conveying. Solid friction factor is affected by powder flow properties. Pan and Wypych (2000) derived an analytical model for predicting pressure drop in slug conveying mode by using powder flow properties like angle of internal friction and wall friction angle. Pressure drop prediction is very important for reliable and low operating cost of pneumatic conveying system (Mallick and Wypych, 2009). Difference in powder flow properties affects the performance of pneumatic conveying system.

Fly ash is a fine powder which has been classified as cohesive powder according to various researchers (Pan, 1999; Wypych, 1999). Indian coal used in thermal power stations has nearly 40% ash content (Sarkar, 1974). The quantity of fly ash is approximately 80% out of the total fly ash (rest 20% is bottom ash). Fly ash is suspended in flue gases and is generally separated by using an electrostatic precipitator (ESP). There are several number of ESP units in the thermal power station according to the number of boilers. An ESP consists of charged plates on which fine fly ash particles stick while passing through them. Rapping action is used to dislodge fly ash particles from ESP plates. Dislodged fly ash particles are collected in the ESP hoppers present under the ESP plates. Typically, there are seven fields in an ESP unit to collect fine fly ash particles. Coarse fly ash is collected in first few stages of ESP hopper and finer fly ash is collected in the later stages. Fly ash collected in ESP hoppers has to be evacuated continuously to ensure proper working of power plant. Fly is transported to buffer hoppers by pneumatic conveying system and further to the remote silo.

Fly ash handling and transportation also require the consideration of powder flow properties like other powders. ESP hoppers and remote silos have to be designed by considering the flow properties of different fly ash so that problems like arching and unreliable discharge can

be avoided. A storage vessel designed according to powder flow properties will be able to evacuate fly ash reliably under gravity or with the help of little aeration provided by the aeration pads.

1.2 Objectives

On the basis of above discussion, it can be concluded that flow properties of fly ash have to be investigated for reliable design of storage and handling equipment like ESP hoppers, remote silo, pressure drop prediction in pneumatic conveying system etc. The objectives of thesis in view of the above discussion are,

- 1) To measure instantaneous flow properties of fly ash and classify them according to their flowability.
- 2) To evaluate the effect of physical properties of fly ash on their flow properties.
- 3) To investigate mass flow and funnel flow storage vessels critical dimensions by using powder flow properties.
- 4) To model cohesion and unconfined yield strength for fine powders of different flowability by using powder physical properties.

Chapter 2

Literature Review

2.1 Introduction

In this chapter, the basics of flow properties of bulk solids have been discussed. Various practical problems faced by the industries will be comprehensively discussed. Basic physics behind the shear testing of powders has also been included in this chapter. Powder flow Tester and its measuring principles have also been discussed. A comprehensive review has been performed on stresses produced in storage vessels containing bulk solids. Finally, the work of different researchers on powder characterization and powder flow properties has been reviewed.

2.2 Common problems with bulk solids

When a power plant is designed, very less attention is paid to the design of silos, hoppers and bins. But in the long run, power plant owners face problems with this bulk solid storage and handling equipment. The most common problem faced is arching as shown in Fig. 2.1. Arching is formation of stable arch just above the outlet of hopper. (Schulze, 2008)

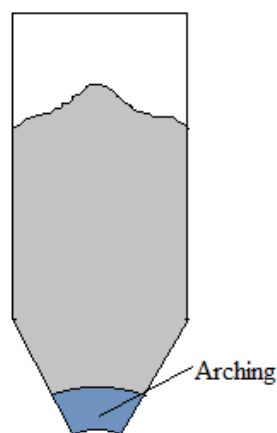


Figure 2.1: Arching (Schulze, 2008)

Arching is due to cohesive strength in fine powders and due to interlocking in coarse particles. Funnel flow and rat holing are also the major problems faced during the discharge. The funnel flow is shown in Fig. 2.2.

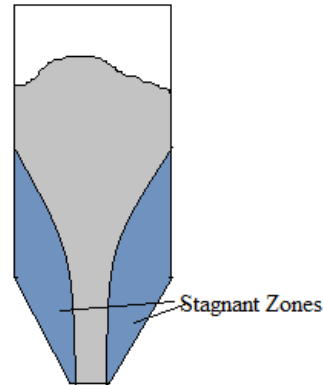


Figure 2.2: Funnel flow (Schulze, 2008)

The funnel flow mainly occurs due to large hopper half angle and high wall friction. Due to large hopper angles, the material remains stagnant with the walls and over the time gain the strength. Further the residence time is the major problem in the funnel flow silo. The material which is filled recently comes out of the silo without complete de-aeration and the fine powder flow like the fluid flooding the outlet of the silo. Flooding is shown in Fig. 2.3. Flooding causes dust generation near the silo region (Schulze, 2008).

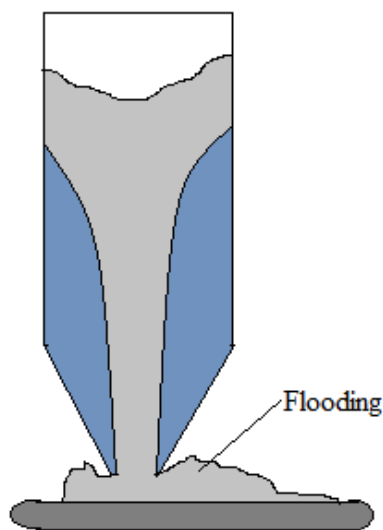


Figure 2.3: Flooding (Schulze, 2008)

The hoppers with screw feeders face the problem of non uniform discharge as shown in Fig. 2.4. Material at the extreme left of the hopper is actively discharged while rest of the feeder does not give any discharge.

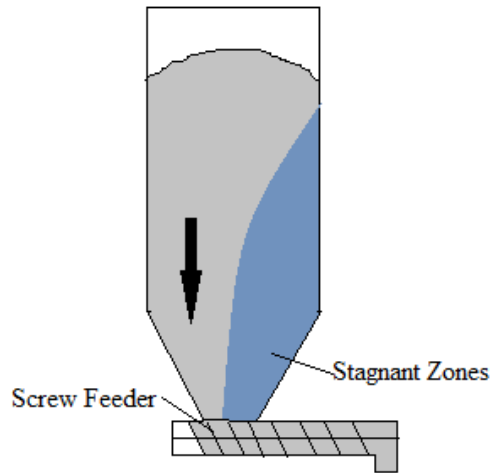


Figure 2.4: Non uniform discharge (Schulze, 2008)

Funnel flow discharge in hoppers reduce the quality of material at the outlet of silo as shown in Fig. 2.5. Segregation occurs in the silo when it is centrally charged. The fines accumulate at the centre of the silo while the coarse particle roll down the walls of the silo and further during discharge the fine particles come out of the hopper first and then followed by coarse particles. Segregation is the major problem in chemical and pharmaceutical industries as different types of medicine powder have different size and they segregate during handling operation. (Schulze, 2008)

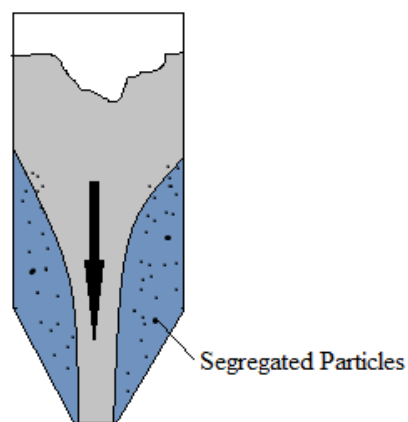


Figure 2.5: Segregation (Schulze, 2008)

An eccentric discharge in the silo is shown in Fig. 2.6; this is caused due to unsymmetrical loading over the silo during discharge of the silo. This causes buckling in the silo and further changes the flow pattern in the silo (Schulze, 2008).

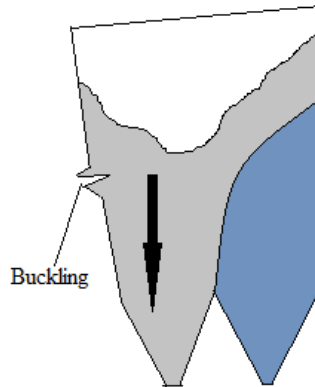


Figure 2.6: Buckling (Schulze, 2008)

2.3 Mohr circle analysis for bulk solids

The bulk solids are those materials which are having properties in between that of the solids and the liquids. The bulk solids or powders support shear stress in steady state like solids and flow out of the hopper like liquids. The pseudo solid nature of the powders can be observed in the heap of sands supporting shear stress at steady states while the liquids which do not support shear at steady state have flat surfaces and do not form heap. Powder is the complex assembly of fine solid particle, gases (in form of interstitial gases in voids) and liquid (in form of moisture content) which makes their analysis very difficult (Lumay et al., 2012). Studying each particle interaction under different conditions is a cumbersome task and the results predicted have very less practical applicability. Therefore the approach adopted by many researchers has been experimental and empirical to explain the powder behaviour. It is easy to perform analysis on the powder by assuming a continuum approach rather than considering individual particle interaction. This assumption greatly simplifies the analysis of powders. They are studied like solids subjected to different condition of stresses. Jenike (1964) performed initial investigation on powder flowability by assuming it as a pseudo solid.

Two dimensional Mohr circle analysis can be applied to the powders after assuming them as pseudo solids.

Application of some vertical stress σ_v over the powder in the confined container will produce some horizontal stress σ_h as shown in Fig. 2.7.

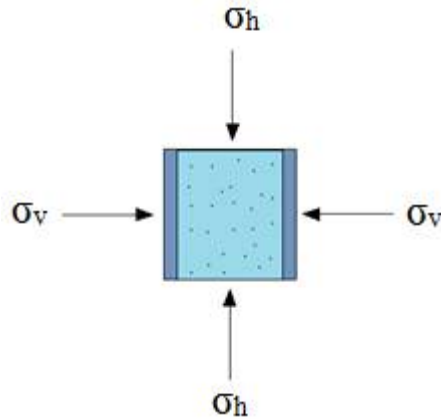


Figure 2.7: Powder element with vertical stress and complimentary horizontal stress (Schulze, 2008)

The ratio of horizontal stress to the vertical stress is lesser than 1 and typically its value lies between 0.4 - 0.6. These stresses are equal in case of the liquids and that is why they do not support any shear stress in the steady state. Both σ_v and σ_h can be assumed as principle stresses by assuming friction less walls of the confining container. This is not the case with real life problems because the walls are always rough and provide some shear stress τ_{xy} to the powders. The condition of the powder element in actual case is shown in Fig. 2.8.

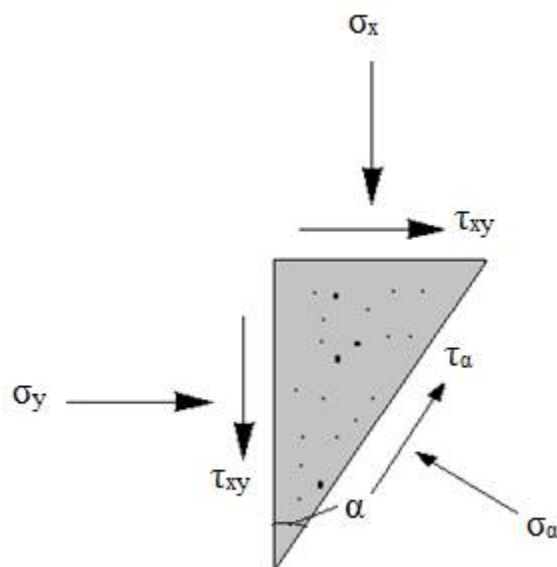


Figure 2.8: Stresses on any plane of powder element (Schulze, 2008)

Normal stress (σ_α) and shear stress (τ_α) at any defined angle α within the powder element can be found by Eq. (2.1) and (2.2).

$$\sigma_\alpha = \frac{\sigma_x + \sigma_y}{2} + \frac{\sigma_y - \sigma_x}{2} \cos 2\alpha + \tau_{xy} \sin 2\alpha \quad (2.1)$$

$$\tau_\alpha = \frac{\sigma_y - \sigma_x}{2} \sin 2\alpha - \tau_{xy} \cos 2\alpha \quad (2.2)$$

In ideal solids, yield locus or yield limit is a straight line passing through the origin and it is tangential to the Mohr circle. The powder do not show this behaviour of ideal solids but rather its yield locus has some intercept on ordinate signifying cohesion at zero normal stress. The yield locus for the powder is not a straight line actually but it deviates from linear nature especially at the low normal stresses. This behaviour of the powder can be captured with very sensitive shear testers (PFT also captures this behaviour). This curved nature of yield locus is neglected for all practical storage vessels designing procedure and the yield locus is assumed as a straight line which follows Mohr-Coulomb failure behaviour which can be represented by Eq. (2.3).

$$\tau = \sigma \tan \phi + C \quad (2.3)$$

where, τ is shear resistance in kPa, σ is normal stress in kPa, ϕ is angle of internal friction and C is the cohesion of the sample in kPa. The significance of yield locus is that this curve shows the shear stress necessary to initiate flow in the powder consolidated at a particular normal. A little consideration will reveal that whatsoever is the stress state of the powder element but its Mohr circle can never overshoot the yield locus. The powder will fracture or there will be incipient flow of powder when the shear stress above the critical limit is applied over the consolidated sample. The relation between failure of powder element under various conditions and yield limit under using Mohr circle analysis is shown in Fig. 2.9.

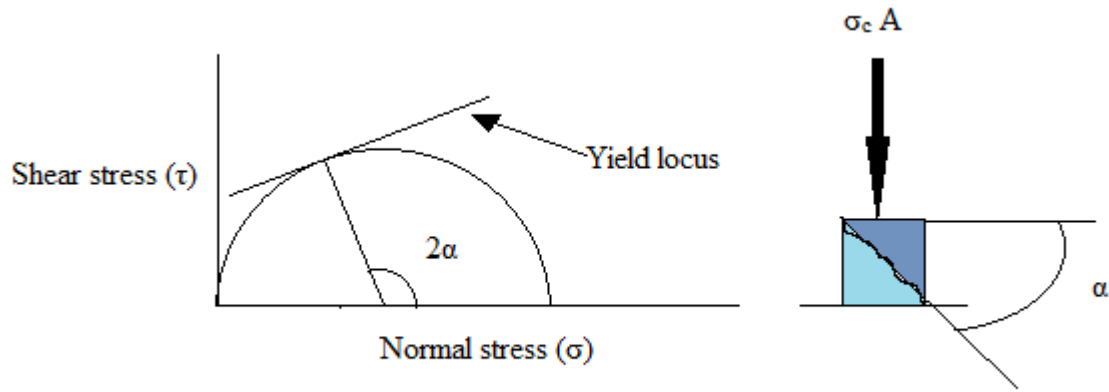


Figure 2.9: Yield limit and failure strength for the powder element (Schulze, 2008)

2.4 Principle of shear testing

The application of Mohr circle analysis to the powder has been discussed in previous section. Shear testers apply the same principle for characterization of the powders. There are many commercially available shear testers like Jenike shear testers, RST- XS Schulze ring tester, Brookfield powder flow tester and FT4 powder rheometer. The latter three shear testers are annular shear testers and have the advantage of infinite translational distance as compared to the Jenike translational shear tester which has limited translational movement. It is difficult to achieve homogeneity in the material represented by the constant bulk density with finite shearing of powder as in case of the Jenike translational shear tester. This distinct advantage is the main reason for popularity of annular shear testers. The principle of shear testing can be easily understood by understanding working of the Powder Flow Tester.

The main advantage of the shear ring tester is that it can be used to perform as large as deformation necessary because of its circular ring, but on the other hand in case of translational shear tester deformation only up to some millimetre is possible. An annular shear cell in PFT is shown in Fig. 2.10.

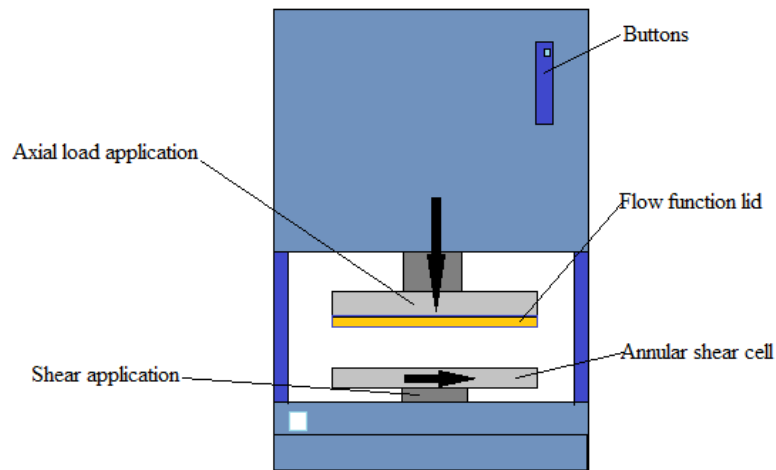


Figure 2.10: Powder Flow Tester Diagram

For performing the flow function test, firstly the powder is compacted under the known consolidation stress σ_{pre} , during this time pre shearing of the powder occurs due to friction between the different layers of the powders and further after some time the value of the shear stress becomes constant as shown in Fig. 2.11. During this time it is assumed that the material is in critical consolidation state, meaning that the shear strength of the powder will not increase further and the density of the powder is also constant. This pre-shearing of the sample is necessary before conducting the shear testing because this process homogenises the material removing excessive voids and human involvement in final observations. The load above the powder is reduced to some value lower than the initial pre-shearing load and the powder is sheared by moving the annular shear cell. The sample is already in consolidated form because of pre-shearing process at higher normal load. In the next step, the sample is sheared under normal stress lower than pre-shear stress and the sample is said to be as over-consolidated sample (as it is already consolidated under higher pre-shear stress). There is a sudden reduction in the value of the shear stress signifying that the powder has failed or the yield shear stress has been achieved in some plane, this is called incipient flow point as shown in Fig. 2.11. Further, these incipient points are projected to plot the yield locus curve as shown in the diagram below. The load over the bulk solid is reduced in each step to measure the yield locus. The Powder Flow Pro software, an interface with powder flow tester also measures this raw data as normal load/ axial load and the shear stress versus time as shown in Fig. 2.12.

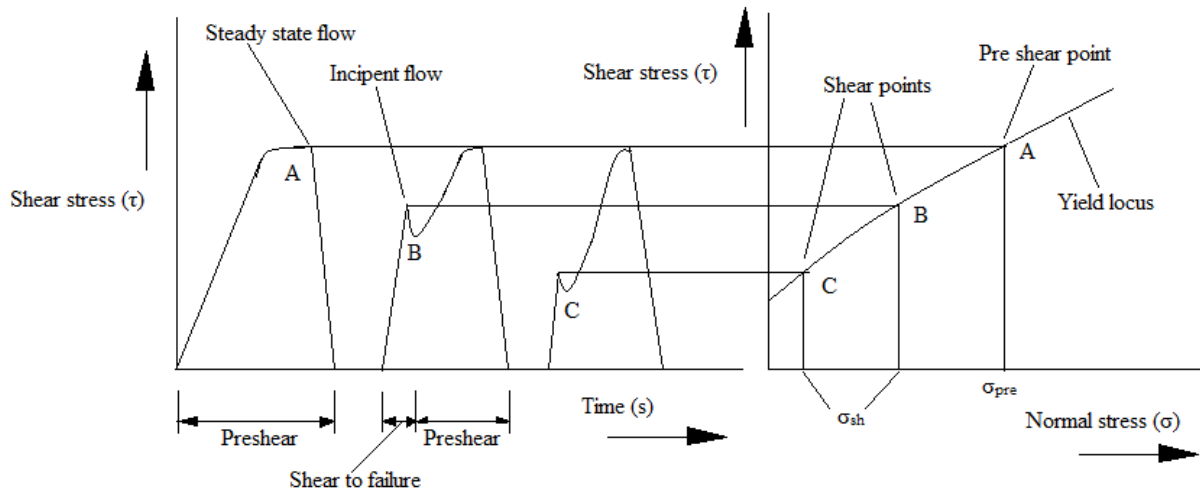


Figure 2.11: Plotting of yield locus curve by the shear ring tester (Schulze, 2008)

Further using the same shear tester with the friction lid made up of the same material as that of the hopper, the wall friction angle can be measured.

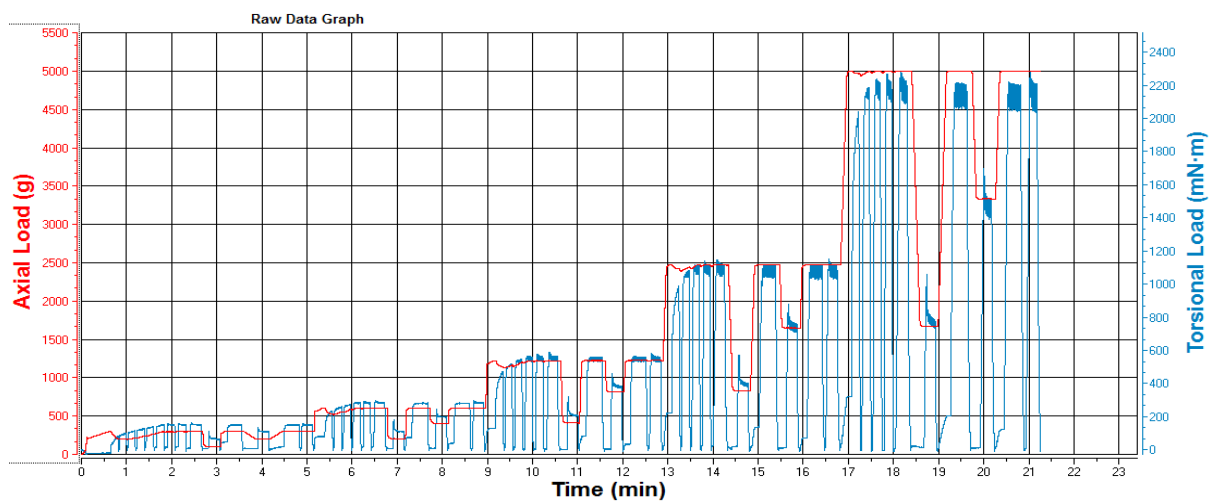


Figure 2.12: Axial load and torsional load variation with time for a powder

2.5 Flowability tests

The following flowability tests are performed to determine the flowability ranking of the powders. These tests are also performed for the designing of storage and handling vessels.

Various flowability tests are as follows,

- 1) Flow function tests: This test is used to measure the internal strength of powder under a state of compaction. This test also measures the angle of friction and the flow index which classifies the powders as cohesive or free flowing. Further the results from the tests can be used to measure arching or ratholing potential of the powders (Ripp et al., 2015).
- 2) Time consolidation test: Sometimes the material in the silo has to be stored for a long time and with the passage of time its flow properties are changed. Generally, the powders do not come out of the opening after such a long time of storage. This test quantifies the opening size and the hopper slope for the material to flow out of the silo (Ripp et al., 2015; Fitzpatrick et al., 2004).
- 3) Wall friction test: The friction between the wall and the powder is one of the important factors which cause the funnel flow or mass flow to occur for the given powder. This test provides the chute angle or wall friction angle necessary for the material to flow (Iqbal et al., 2006).
- 4) Bulk density test: This test is performed to find the density of the material under the state of compaction. This test is useful in obtaining the capacity of silo for designing purpose (Schulze, 2008).

2.6 Flow function test

The significance of the flow function test is to measure the amount of the strength a powder gains under the state of compaction. The simple flow function test is shown in Fig. 2.13. This test is similar to the condition of material at just the outlet of silo.

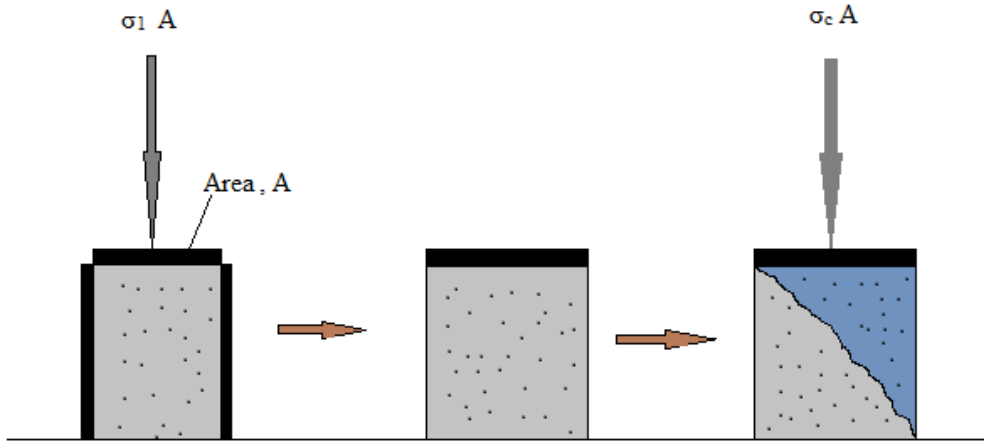


Figure 2.13: Flowability test (Schulze, 2008)

Firstly the material is compacted under the known compaction stress, σ_1 and then the confining cylinder around the bulk solid is removed making the surface free. Then from above σ_c compression stress is increased to measure the peak stress at which the powder fails above, the consolidation stress is increased until the powder element fails or flows. This is known as unconfined yield strength (σ_c). The test is performed at the different initial consolidation stress (σ_1) to generate a flow function curve which signifies flowability (ff_c) as shown in the Fig. 2.14. Different flow zones have been made to classify the powder as cohesive or free flowing under given compaction stress. In the flowability test, several times it becomes difficult to rank the material because the flow function curves of the two powders intersect each other. To eliminate this problem critical arching diameter (D_c) is used which is the diameter required to eliminate the arching in silo. Similarly critical rat-hole diameter is used to rank the powders. The Flow Index which is the inverse of slope of flow function curve at a particular pre shear stress and is used for comparison between two powders when the depth of material is more than 1 m. The flow intercept is the intercept of the best fit line with the unconfined failure strength; this parameter is used to compare powders when the depth of compaction is less than 0.15 m. (Bian et al., 2015)

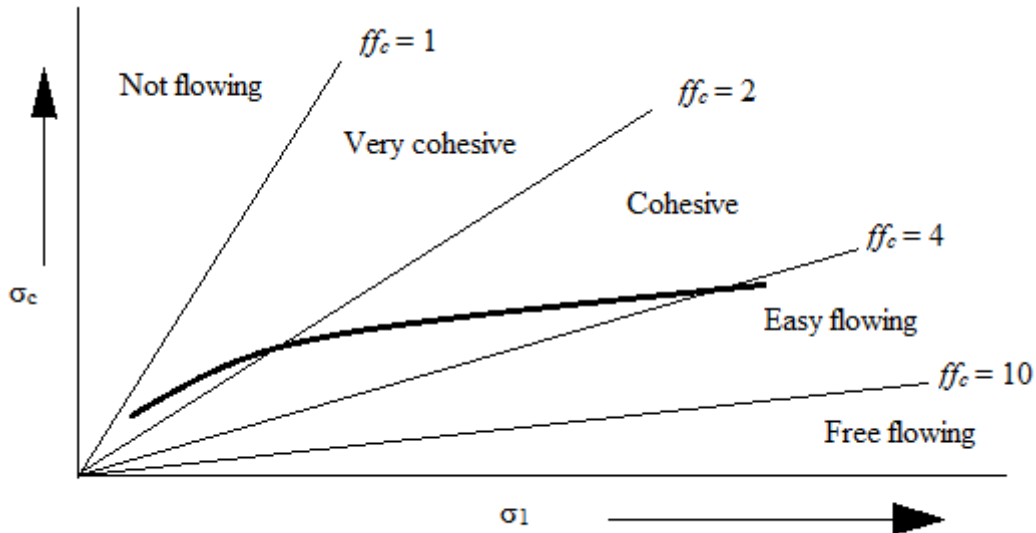


Figure 2.14: Flow function curve showing flowability (ff_c) (Schulze, 2008)

2.7 Time consolidated flow function

This is used to find the strength the powder has gained over the period of time due to flow interruption of a few seconds to days. The measurement process is similar to the flow function test but before shearing the material is left to consolidate for the given period of time. (Ripp et al., 2015)

2.8 Wall friction test

Wall friction has significant effect on the distribution of the stress in silo and the hoppers. As the wall friction increases, the wall friction angle increases (Iqbal et al., 2004). With this increase in the wall friction angle, the powder is supported by the wall and there is less compaction experienced by the powder as shown by Eq. (2.10).

$$\sigma_1 = \frac{\rho g D}{4k \tan \phi} \left(1 - e^{-\frac{4k \tan \phi Z}{D}} \right) \quad (2.10)$$

Where σ_1 is the major consolidation stress, k is the stress ratio ($k = 0.4$ generally) which is the ratio of horizontal to vertical stress acting on the powder element, Z is the depth of powder, D is the diameter of silo, ρ is the bulk density of the solid. The wall friction angle is similar to the chute angle (Schulze, 2008).

The wall friction test gives the graph between σ and τ , and the curve is known as wall friction locus. The wall friction shear test yields the minimum hopper half angle necessary for the mass flow of the powder. The intercept of the wall friction yield locus with the ordinate gives the coefficient representing the stickiness of the powder or the ability of the powder to support itself with the wall.

2.9 Bulk density test

It is the weight of the powder that controls the stress acting on the powder when it is flowing or is in a static storage condition. Generally, the free flowing powders do not have any significant increase in the bulk density under state of compaction. The value of the bulk density is used during the calculation of the minimum opening required for the mass flow to happen.

2.10 Flowability variation with the depth of the hopper

The flowability (ff_c) is the ratio of the major principle consolidation stress σ_1 and unconfined yield strength σ_c . The value of σ_1 is zero at the hopper apex and increases with the height of the hopper as shown in Fig. 2.15. Similarly, σ_c variation is shown with the hopper height. It can be easily observed from the curve that the value of the flowability factor ff_c , approaches to zero at the hopper apex. Due to reduction in flow area in hopper section, the material having cohesive nature can support itself to form a stable arch (Ripp et al., 2015). Appendix A briefly describes the stresses in hoppers.

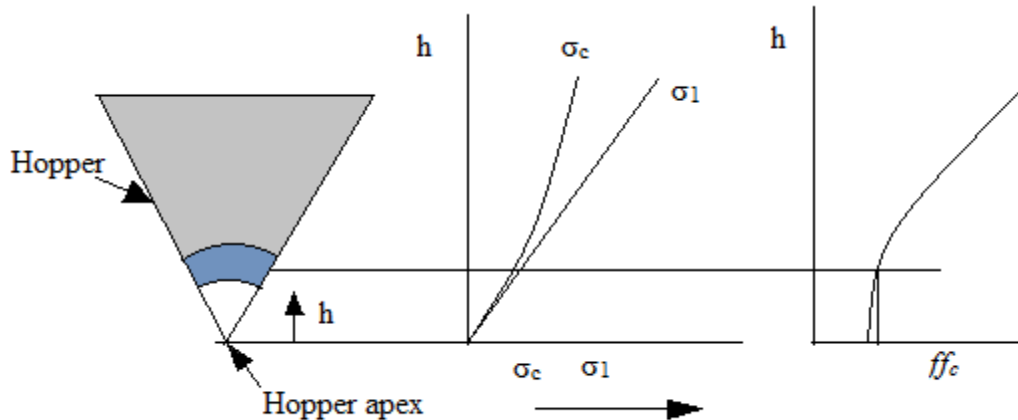


Figure 2.15: Formation of cohesive arch (Schulze, 2008)

Various factors which influence the flow properties of the powders are particle size and particle size distribution, particle shape, particle density, moisture content, stress state and time consolidation. Various researchers have independently conducted powder characterization tests on different powders with different end applications and by using different characterization techniques.

2.11 Previous research work on the flow properties of the powders

Particle size is the most influential parameter which affects the flow behaviour of the powders. This fact has been reported by many researchers during their research.

Ripp et al. (2015) determined the flow properties of tef flour (8.81-517.2 μm) and its seeds (452-1337 μm) by measuring the yield locus, wall yield locus and time consolidated flow properties. Further parameters like unconfined yield strength, angle of internal friction, wall friction angle were used for silo design. They also considered the effect of time consolidated flow properties. The flour having the small particle size was more cohesive as compared to its seeds. Similar results were seen in the flow index of bulk solids. The cohesive flour required the larger opening size and steeper hopper half angle as compared to tef seeds. They measured the wall yield locus for different wall materials like Plexiglas, Aluminium alloy AlMg₃, V4-A stainless steel. The friction angle was the highest for AlMg₃ and wheat flour combination while on the other hand tef seeds and V4-A stainless steel combination showed

the highest value. The flow properties were also measured after 72 hours of storage, tef flour was initially cohesive and after storage further gained strength while tef seeds remained relatively free flowing. There was increase in opening size and decrease in the hopper half angle for both the bulk solids after time storage. The silo design was based upon the design diagrams proposed by Jenike.

Lee et al. (2015) investigated black soybean powder of different particle size at constant moisture content. The flow behaviour was investigated by a Brookfield, Powder Flow Tester. The largest particle size showed less hopper angle and outlet dimension, while the fine soybean powder required large hopper angle and opening. The fine powders were located in the cohesive ranges during powder flowability tests and there was a sharp increase in their bulk density with increase of consolidation stress. The internal friction angle of soya bean powder was influenced by both particle shape and size. The particle shape was determined by High Sensitivity Circularity (HSC). HCS was least for coarse powder sample P1 (1180-1400 μm) and the highest for fine sample powder P4 (425-600 μm). The fine powder due to high HCS (P4) showed less value of internal angle of friction than coarse powder sample (P1). The results of internal friction angle were not in exact agreement with the results of the flow function test. Finest particle were mostly affected by particle size than shape. This indicates that there is a trade-off between particle shape and size. By regression analysis, the relation was found between the flow index (FI) and outlet dimension (OD). Further, by regression analysis the relation was found between FI and hopper half angle (θ). A correlation was given in between the cohesion (C) of powder and consolidation stress (σ).

Liu et al. (2015) investigated the effect of the particle size on the flow behaviour of pulverized coal. The pulverized coal sample was sieved into 7 samples of different particle size ranging from 223.8 μm to 17.7 μm . An annular shear tester was used to measure the flow properties and a transparent Plexiglas hopper was used to determine the discharge behaviour of different particle sizes. The bulk density tests were conducted to classify the sample as coarse or fine. The sample having particle size above 100 μm was classified as the coarse sample while below it the sample was called fine sample. The bulk density value took a constant value after 100 μm and the samples having size smaller than 100 μm were called as fine samples. In coarse region, angle of internal friction and wall friction angle were not sensitive to the particle size but in fine region these angles were significantly affected. The mass flow hopper was designed by Jenike's methodology for each particle size. The results were in agreement with other researchers (Ripp et al. 2015; Lu et al., 2015). The smallest

particle size (17.7 μm) showed the steepest hopper angle (13.41 $^\circ$) and the coarse particle size sample (223.8 μm) showed more value of the hopper half angle (21.68 $^\circ$). They also studied the effect of particle size on the relative flow rate of each sample from the Plexiglas hopper. The discharge behaviour of the sample was classified in 3 categories on the basis of discharge pattern as arching region, unstable region and stable region. Particle size below 40 μm was not flowing out of the model hopper due to arching and hence was classified as arching region powder. The particle size range between 40-100 μm showed higher flow rate and the flow was unstable and hence classified to be in unstable region. Finally the particle size above 100 μm gave the stable discharge behaviour from the hopper. The authors were of the view that the pulverized coal is a complex powder showing a lot of diversity with particle size rheological properties can give a better view about its discharge behaviour and the flow properties.

Saw et al. (2015) gave the correlation between the flow properties measured on the shear tester and Hausner ratio (HR). The tests were performed on 13 milled (size range 28.9 μm -223 μm) and 2 spray dried (size range 35.8 μm , 102.2 μm) lactose powder, 3 sand samples (28.7-76.9 μm) and 3 refractor dust (size range 23.3 μm -66.6 μm) samples. By shear testing the powders were classified as very cohesive, cohesive, easy flowing, free flowing. Milled lactose powders with smaller particle size 28.9 μm and 58 μm were classified as very cohesive and cohesive respectively. Sieved milled lactose powders were free flowing. Sand and refractory dust samples were free flowing despite of their particle size showing that the particle size cannot be regarded as ultimate criteria to classify powder as cohesive or non cohesive. A correlation was given between Hausner ratio (HR) and cohesion (C) value for the pre shear stress value σ_{pre} ranging from 0.31kPa-4.85kPa. Further they gave a correlation to estimate the ratio of major consolidation stress (σ_c) and unconfined yield strength (σ_y) by using Hausner ratio. The correlations predicted well for cohesive and very cohesive powders but gave high correlation error for easy flowing and free flowing powders.

Bian et al. (2015) measured the bulk flow properties of hard red winter (HRW) and soft white winter (SWW) wheat flours. The average particle size of the powders was 48.77 μm and 48.20 μm respectively. Physical properties like compressibility index (CI), Hausner ratio (HR), angle of repose (AOR) of the powders were measured. AOR of the powders were nearly same (40.90 $^\circ$ and 41.57 $^\circ$) but there was a huge difference between the values of CI (8.20 and 41.57). CI was low in case of HRW because its bulk density was lower as compared to SSW. Further, the authors also studied the dynamic flow properties of the powders. The dynamic testing involves the testing of the powders having some kinetic energy. This

involves testing the flow properties of the powder under the aerated and un-aerated condition by using powder rheometers. The Basic flow energy (BFE) gives the measure of powder flowability and it was lower in the case of HRW. Total flow energy is the measure of energy required of breaking the inter-particle cohesion by aerating the powder. The Total flow energy attained a constant value (6mm/s) as the air velocity was increased.

Jager et al. (2015) used Jenike approach to design a large scale (3150L) conical hopper to store pharmaceutical chemicals. Their test products were seven grades of micro crystalline cellulose (MCC). Further the wall materials used for the tests were #2B and #8 surface finish. 2B surface finish is coarser and unfinished while #8 is smoother. They discussed about the effect of overestimating of unconfined yield strength. The flow function curve is generally approximated as linear straight line. The major highlight of their research work was the selection of optimum outlet opening and minimum hopper half angle when the hopper has to be used for different flowability material.

Recently, Xantakis et al. (2015) performed a study on the flow properties of titan, alumina and silica based nanopowders by using the Powder Flow Tester (PFT). The nanopowders taken for the study were of both hydrophobic and hydrophilic nature had the same particle size. The nanopowders were made hydrophobic or hydrophilic by surface modification technique called Hydrophobization. The nanopowder samples were of same material and particle size but still their flowability represented on the flow function curve was quite different. They found that hydrophobic nanopowder samples had less flow function curve slope as compared to hydrophilic ones in every case. An important inference can be drawn from this study that only the particle size cannot be regarded as the only criteria to judge the flowability of the powder.

Zafar et al. (2015) investigated the flowability of cohesive particles at very low consolidation stresses. They performed experiments on spherical glass ballotini and fluid catalytic cracking (FCC) powders. Both the samples were of free flowing nature according to Jenike flow calculations and median particle sizes were ranging from $87\mu\text{m}$ - $44\mu\text{m}$. The author gave a comprehensive review of commercially available techniques to characterise powder at very low consolidation stresses. The experiments were performed on Schulz ring tester, Sevilla powder tester, raining bed method and recently developed ball indentation method. They provided the comprehensive review of measuring principle of all the equipments and compared their tensile strength results at very low stresses ranging from 0-10 kPa.

Indentation hardness was reported in case of ball indentation method which was considered as the measure of yielding behaviour of the sample. The samples were initially consolidated and a known indentation load was applied by spherical ball. There was some elastic deformation in the sample which recovered itself after removal of load leaving behind only plastic deformation part. The hardness of the consolidated powder was having a good correlation between yield locus found from shear testing. It was observed during the experiments that Schulze ring tester overestimates the value of tensile strength as compared to SPT and RBM. This is because of linear extrapolation of yield locus. It was found that SPT gives more reproducible and reliable observations as compared to other methods. They suggested that further work should involve use of DEM to find the accurate reason for difference caused due to measurement equipment.

Marrup et al. (2014) have developed a simple mono-axial shear tester to investigate the flow properties of raw meal cement at 3 consolidation stresses 0.94kPa, 1.87kPa, 2.79kPa and temperature up to 850°C. The flowability of the powder was expressed by the flow factor which was found to be more or less constant up to 550°C, but above it large deviations were found in flowability of the powder. The flowability of the powder was reduced above 550°C due to Calcination and Belite formation. The results from the experiments showed that preheated or Calcinated raw meal flows more poorly than unheated raw meal. The raw meal flowability is greatly affected by the presence of CO₂, alkali sulphates, SO₂, chlorides.

Lumay et al. (2012) measured the flow properties of the powders and the grains. Their study included experiments on silicon carbide, Flour and rice. They advocated that granular material is a complex system in which transitions of the states take place. They defined the three states of a powder. First is the static state followed by a quasi-static state and finally dynamic state. The steady state of the powder can be represented by the heap of the powder having some angle of repose. They gave classification of the powder on the basis of angle of repose. Quasi static state is a transition between steady and dynamic state which can be represented by small movement of particles in the sample. The quantitative measure of the quasi-static state can be made by conducting Hausner ratio tests. HR includes tapping of the sample in which the powder bed is in motion partially. The experiments observed that the two powders may have the same HR in the end but their compaction dynamics could be entirely different. They showed this phenomenon by plotting curves between void fraction and the number of tapings given to the sample. $\eta_{1/2}$ represented number of the tapings at which the void fraction of the sample is reduced to half. The dynamic state of the sample was analysed

by rotating drum showing a dynamic angle of repose for a product. Cohesiveness increases the dynamic angle of repose and further reduces the frequency of avalanche falling for the given material. The main highlight of their research work was the study on the effect of size, size distribution and shape on the flow properties of products. Flow properties of the material were quantified by the properties of the material measured under different state of granular material. They also re-established the fact of occurrence of particular particle size for every material after which their flow properties became poorer. The authors also measured the flow properties of rice and found the effect of increasing their aspect ratio on HR, AOR and dynamic flow angles. They modelled rice grains as ellipse with some major axis and minor axis ratio. The packing fraction of the products increases with the elongation of the rice grain particles.

Geldart et al. (2009) have studied the relation between Angle of repose (AOR) and flowability of the powder. Three standard flowability measuring equipment naming Johnson indicizer cohesion tester, warren Bradford spring cohesion tester, Jenike shear tester results were used to find correlation between flowability of the powder and AOR. The AOR increased with the percentage of fine material in mixture. The mixture of two powder BRACO FRF (flame retardant filters) having chemical formula $Al_2O_3 \cdot 3H_2O$ of different particle size $63\mu m$ and $6\mu m$ were used for making blend. Mark 4 AOR tester was developed by the author to directly find the qualitative measure of the flowability of powder by correlating with angle of repose. The cohesion(C) of powder was the reciprocal of the flowability of powder.

Ganeshan et al. (2008) reviewed various factors influencing the flowability of powders like moisture content, humidity, pressure, temperature and particle size etc. The flow properties of Distilleries Dried grains with soluble (DDGS) were measured. DDGS is the by-product left after the ethanol production from maize and used in food products as the source of protein. The flow properties like angle of repose, the bulk density, and the frictional forces were reviewed and defined. The authors have further reviewed various empirical formulas given by other researchers for the qualitative and quantitative measurement of the flow properties. The different test methods like Jenike shear tester, Carr index, ring shear tester and direct shear tester were discussed with their principle of measurement.

Iqbal et al. (2006) investigated the effect of storage conditions like temperature, storage time, relative humidity on the wall yield locus and further showed its effect on the hopper design. The food powders under investigation were flour ($73\mu m$), tea powder ($25\mu m$), and whey-

permeate (98 μm). The powders were stored for 7 days and there significant change in the flow properties of hygroscopic powders while the wall yield locus of flour remained unchanged. This study indicated the role of measuring the flow properties of powders under different storage conditions before proposing a storage vessel design.

Fitzpatrick et al. (2004) measured the flow properties of 13 food powders ranging from tomato powder, salt, and coco powder to yellow corn flour. The maximum particle size was 320 μm and minimum was 12 μm . The particle density was ranging from 1490-2200 kg/m^3 . The effective angle of internal friction ranged from 40° to 65°. The authors showed that there was no strong relationship between the flow properties and physical properties. Further, the authors applied the Jenike's approach to give the hopper half angle and minimum opening size for the hopper. The authors showed the sensitivity of Jenike's method for hopper design. The method is sensitive if the flow factor line intersects the flow function curve near the origin. This gives the low value of unconfined yield strength and hence the low value of outlet opening. The powders with flat flow function curve when extrapolated backwards to intersect flow function line might result is very large value of outlet opening but actually the flow function will be having curved shape at low consolidation stress.

Johanson and Berletta (2003) reported the flow properties of silica powder and FCC powder. The novelty in their research was that they conducted the flow properties tests under aerated conditions by modifying the Schulze ring tester. The base of the shear cell was having an air chamber and the top lid was permeable to allow the air to come through the sample. It was observed that the unconfined yield strength of the sample reduces as the pressure drop across the powder bed is increased. In both the cases of FCC and silica, the unconfined yield strength decreased with the aeration rate. On the other hand angle of internal friction showed slightly opposite tend. The unconfined yield strength decreased with significant decrease in aeration rate for silica powder but in case of FCC it was not so. The reason cited for this difference was the different flowability of the material. The authors also observed that the decrease in unconfined yield strength occurs at high pressure drop depending upon the nature of material. There was no substantial decrease in the angle of internal friction at lower pressure drop. The authors advocated that aeration of sample causes substantial decrease in cohesion of sample. The angle of internal friction approaches effective angle of internal friction when the cohesion in the sample approaches zero. Their study has applications in flat bottom silos with air slides in which air slides are used to keep the material alive. The air slides must cover approximately 15% of the area of the flat bottom silo.

Abdullah and Geldart (1999) conducted experiments on FRF and FCC and suggested the bulk density as the measure of cohesiveness. Their experiments reconfirmed the fact that cohesion of the sample decreases with increase in particle size. According to the authors, the particles having large inter-molecular attraction have large intermolecular friction as well. They form stable structure which is the main cause of porous structure. On the other hand, the powders with low intermolecular friction do not make a stable structure giving a dense packing. The more important from their research was that the density of sample is maximum at some optimum mixture of fines and coarse particles. They approximated the range as 20-40% fines for FRF and 38% FCC. The authors suggested that the samples having HR less than 1.25 are not affected by the intermolecular forces. For powders having HR between 1.25-1.4 lies in AC boundary and their cohesiveness decrease with particle size. They suggested that Hosokawa powder tester gives better results than Copley volumemeter for aerated and tapped bulk density because of its large tapping height.

Teunou et al. (1993) characterized the flow properties of flour (73 μ m), milk powder (197 μ m), tea (25 μ m) and whey-permeate (98 μ m). They used annular shear tester to measure the flow properties of powders. Physical properties of powders like the bulk density, particle size, particle density, water sorption isotherms and differential scanning calorimetry (DSC) thermographs were measured to define the powder. The instantaneous flow functions were measured for differential humidity and surrounding temperature. The flow parameters were further applied to estimate the critical dimensions of the mass flow hopper. The tea powder was having small particle and was hygroscopic in nature which showed that it can cause serious flow problems at high %RH (relative humidity). The flour was cohesive in nature and its flowability did not change significantly from 25% RH to 65% RH. The skim milk and whey-permeate caked readily at low moisture level due to presence of amorphous lactose, hence there was significant change in the measured values of the flow functions.

2.12 Previous research work related to the powder rheology and shear testing

Some researchers also tried to correlate the results of the powder rheology and the shear testing.

Koynov et al. (2015) performed a comparison between the results of the three rotational shear testers commercially available. The experiments were performed on RST-XS annular shear tester, FT4 rheometer and Brookfield PFT shear cell by using the two grades of γ -aluminium. The test materials were having free flowing and cohesive behaviour with particle size 59 μm and 44 μm . Each sample was examined for eight responses from the equipment. The eight responses studied were: cohesion, bulk density, unconfined yield strength, pre shear stress, and effective angle of internal friction, major principle stresses and flow function coefficient. The results of experiments showed that each equipment is capable of differentiating between cohesive and free flowing sample but the care has to be taken while ranking the material in the free flowing regimes. During the case studies it was found that the test material is always a significant factor on the results of the equipment. Each equipment ranked the sample in the same order of cohesiveness. The authors concluded that the power flowability established under small pre shear stress is independent of type of the shear cell used. The authors were of the view that there is a geometrical difference between each shear cell which is the main cause of different results. Normal consolidation stresses do not vary linearly with the depth of the shear cell. FT4 rheometer has more depth as compared with the other two equipments. This difference in the shear cell causes unequal loading on the powders and has significant effect on the output results. The shear cell used for the characterization of the sample must be mentioned. During the statically analysis, it was found that the shear cell had significant effect on angle of internal friction as compared to the other responses. The flow function is the ratio of the major consolidation stress and unconfined yield strength. The material properties had the highest effect on unconfined yield strength and the initial consolidation state had the highest effect on the major consolidation stress. Therefore the flow function can be interpreted as the ratio of consolidation state of material and material properties.

Leturia et al. (2014) compared the traditional and new testing methods used for characterization of the powders. The investigation was performed on seven powders ranging from nano particles to group B powders. Traditional testing methods were classified in 3

categories as testing under aerated conditions, free surface conditions and packed bed conditions. Classification was based upon the stress level involved in the test. The authors were of the view that flow properties of the powders cannot be indicated by only one index but rather several characterization methods results should be combined to get the complete understanding of behaviour of powder during storage and transportation. The state of compaction and bed voidage were cited as the main factors which influence the flowability of powders. FT4 powder rheometer (developed by Freeman technology) was used for the comparison with the results of traditional testing methods. Flow rate index (FRI) ranked the material in same order as Hausner Ratio (HR) did but the other parameters like basic flow energy were difficult to interpret due to the complex physical phenomenon involved during the tests. The authors concluded that further understanding of blade testing phenomenon is required to get better insight of powder flow phenomenon.

Krantz et al. (2009) investigated the flow properties of the two sample fine powders with median particle size between 21 μ m and 31 μ m under the different stress states. The tests performed ranged from static tests like shear testing to dynamic tests like angle of repose, avalanche angle and bed expansion ratio test (BER). The authors advocated that the selection of characterization technique should be based upon the application. For example the dynamic tests can closely predict the behaviour of the powder during fluidization process while the static testing methods are more suitable for predicting the cohesion and agglomeration phenomenon. The authors concluded that the flow behaviour of the powder depends upon the stress state and no single technique can fully characterize the powder. They also suggested that if the powder is subjected to multiple handling processes like storage, transportation, fluidization than multiple testing techniques should be used to predict the behaviour of the powder. These conclusions are very similar to the results of Leturia et al. (2014)

Freeman (2007) compared the flowability results from the two different methodologies available from the FT4 powder rheometer. The results of the blade testing method were more empirical because of a complex testing phenomenon involved but on the other hand gave a good idea about the energy required to produce three dimensional flow patterns. The results from the dynamic upward and downward testing were compared with the results of the shear testing. The results of the upward testing technique of FT4 rheometer correlated well with the data of the shear cell however surprisingly, the downward testing technique which actually shears and compact the powder showed significantly different results. The author advocated that the aerated powders cannot be evaluated using a shear cell but can be assessed using the

blade testing methods which show very significant difference in the flow energies. The authors concluded that the dynamic testing methods provide better differentiation between the powders with similar rheological properties in the packing states.

2.13 Previous research work related to particle properties, shear testing, and Atomic force microscope (AFM)

Many researchers have tried to correlate the flow properties results from the shear testing and an atomic force microscope. Further, some researchers used the concept of Bond number to explain the flowability of the powders.

Chirone et al. (2016) investigated the effect of temperature on the ceramic powders. They found that the ceramic samples having particle size less than 20 μm were affected by temperature which changed with cohesion. The rest of the samples remained interestingly unaffected by the change in temperature. The main highlight of their paper was the use of inter particle contact mechanics to predict the bulk behaviour. They used models proposed by Rumpf and Molerus to correlate the tensile stress observations found from an annular ring shear tester. Rumpf model gives iso-static tensile stress for a given sample. Iso-static tensile stress is nothing but the tensile stress which can separate two particles attracted by inter-particle forces. In other words, it is the stress equivalent to the force needed to separate two particles under given conditions. This expression proposed by Rumpf needs the value of van der Waals force which was found by the model proposed by Molerus. Both these models and detailed theoretical framework is mentioned in their paper.

Colbert et al. (2015) attempted to correlate the measurements taken from atomic force microscope with the shear testing results taken from FT4 rheometer. They tested the flow properties of crystalline and amorphous (semi crystalline) Lactose powder. The shear testing experiments were performed at 20% to 60% moisture level. The authors also used atomic force microscope for the same sample conditions. A good correlation was found in between the adhesion measurements from the atomic force microscope and cohesion readings from the FT4 rheometer. By analyzing the force distance curves the authors concluded that the nature

of force between the particles was due to capillary action. A small force peak was absent while approach of lactose powder particle which ruled out the possibility of van-der Waals force of attraction between the particles. Although a singularity was found in case of amorphous lactose powder at 50% moisture content which was explained by the fact that the additional moisture content acted as the fuel to cause phase transition of semi crystalline lactose powder to crystalline phase.

Lu et al. (2015) studied the flow properties of pulverized coal ranging from 18 μm -224 μm . They studied the effect of particle size and the flow mode of the pulverized coal during its discharge from the mass flow hopper. The authors concluded that as the particle size increases, the discharge from the mass flow hopper shows transition from arching to discontinuous flow and finally to continuous discharge. The authors used the FT4 rheometer to simulate the mechanically forced flow by using upward testing method and downward testing method. The authors were of the opinion that the Basic flow energy (BFE) found during the mechanically induced flow is correlated to the discharge behaviour of the pulverized coal. A qualitative study was done to find cause of gravity induced flow. The forces considered during the analysis were inter-particle force, drag force and effective weight force. All these forces are the function of particle size and the point of intersection of these forces gives the range of particle in which continuous gravity flow can be achieved.

Capece et al. (2015) recently gave the innovative concept of multi granular Bond number (Bo). Bo is the ratio of inter-particle forces and particle weight. The inter-particle forces include van-der Waals forces, capillary forces, forces due to electrostatic charge etc. The authors firstly correlated the concept of Bo with the flow function and found a very good correlation between them. They further extended the approach by generalising their model for mixture of different components having different particle size. Their novel approach of predicting behaviour of the powder by using fundamental properties can be used for the modelling purposes like predicting solid friction factor in pneumatic conveying systems.

Sindel and Zimmermann (2001) studied the sphere-surface type contact between a lactose particle attached to a probe and lactose tablet used as substrate. They did the comparison of an average adhesion per particle in case of the shear cell, the tensile tester and an atomic force microscope (AFM). The shear cell gave the highest adhesion followed by the tensile tester. There was a huge difference between the observations from AFM and Jenike shear

tester. The authors concluded that it is very difficult to approximate the flow properties of a sample by individual particle contact. These conclusions are contradictory to the conclusions made by Colbert et al. (2015) who found a very good correlation between the adhesion values from AFM and cohesion values found from FT4 rheometer. The FT4 rheometer is a superior equipment as compared to the Jenike shear tester and further it uses the blade rheology which can very well differentiate between the pseudo similar samples.

Lee et al. (1999) characterized the fly ash made from class F type coal collected directly from the ESP hopper. They found that farther the samples were taken from the boiler, finer were the fly ash samples greater was their bulk density and more was their Blain surface area. The fly ash samples collected from the third ESP hopper were having more Al_2O_3 and glass content as compared to the first ESP hopper. Silicon oxide content was also low in the third ESP hopper samples. The colour of the fly ash also varies due to the presence of iron oxide content in it. The authors concluded that due to this difference in iron oxide content of the fly ash the fly ash samples collected farther from the boiler are brighter as compared to those collected from the vicinity of the boiler. The authors advocated that the fly ash produced from the boiler operating at part load produces the ash with more fine content as compared to the full load operating condition. This is mainly due to less probability of collision between the fly ash particles resulting in agglomeration at part loads as compared to the full load condition.

Danjo et al., (1989) studied the effect of particle shape on the flowability of powder. They concluded that there is an increase in the flowability of the bulk solid when there is an increase in the shape factor of the particles contained in the bulk solid. They introduced the new concept of apparent adhesion which they defined as the ratio of the inter-particle forces and the external forces. If the external forces are less as compared to the inter-particle forces holding the particle above the void then the void fraction of the bulk solid will not increase appreciably until the external forces are large enough to force the particle into the void.

Chapter 3

Material and methods

3.1 Introduction

This chapter provides details about the various tested samples, testing equipment, calibration and operating procedure. The flow properties of various fly ash samples collected directly from ESP hopper have been studied. The detailed discussion about the experimental results has been done in subsequent chapters.

3.2 Samples

For this study, seven fly ash samples equivalent to seven ESP fields were collected from seven consecutive ESP hoppers. The fly ash was at 80°C during the sampling process. To ensure that the results of flow properties are correct, each sample was preheated in a baking oven at 103°C for 3 hours to remove any moisture content. During the shear testing process samples were at nearly 80°C temperature, although there was a drop of 3-4°C during the testing process but it can be neglected. For the sake of simplicity each fly ash sample will be named by F1, F2, F3 etc representing the ESP hopper from which the sample has been collected. F1 to F7 samples were considered for the hopper design and the powder flow properties analysis. Apart from these samples, several other samples of the fine powders like fly ash from different power plant and cement were used to model cohesion in fine powders. Sample R1 to R7 are fly ash samples collected from respective ESP hoppers. H1, H2, P1, P2, Rel 1 and Rel 2 are fly ash samples collected from different power stations (numerical value with alphabet represents ESP field from which sample has been collected). Cements are very cohesive as compared to fly ash, therefore cement sample JK, JKW and CC were used for developing cohesion models. TUF and CF are also fly ash samples. Table 3.1 shows the physical properties of the fine samples.

Table 3.1: Physical properties of fly ash samples

Sample Name	Sample Type	d ₁₀ (µm)	d ₅₀ (µm)	d ₉₀ (µm)	ρ _b (kg/m ³)	ρ _p (kg/m ³)	HR	FI	Flowability classification
F1	Fly ash	42	139	316	794.9	2015	1.07	7.46	Easy Flowing
F2	Fly ash	23	102	235	781.6	2014	1.15	5.97	Easy flowing
F3	Fly ash	23	97	213	729.7	2018	1.20	6.37	Easy Flowing
F4	Fly ash	18	69	170	732.7	2025	1.36	5.85	Easy Flowing
F5	Fly ash	14	53	141	798.7	2032	1.42	4.10	Easy Flowing/Cohesive
F6	Fly ash	12	41	108	766.8	2030	1.25	3.63	Cohesive
F7	Fly ash	6	21	63	670.2	2025	1.45	2.41	Cohesive
R1	Fly ash	6	28	120	686.8	2140	1.11	3.16	Cohesive
R2	Fly ash	3	21	112	677.4	2120	1.14	2.24	Cohesive
R3	Fly ash	2	17	111	674.0	2290	1.21	2.30	Cohesive
R4	Fly ash	1	8	69	596.3	2051	1.20	1.52	Very cohesive
R5	Fly ash	1	4	29	590.2	2500	1.33	1.69	Very Cohesive
R6	Fly ash	1	4	25	611.2	2430	1.48	1.84	Very Cohesive
R7	Fly ash	1	4	33	494.3	2560	1.6	1.94	Very Cohesive
JK	Cement	3	17	53	923.4	2930	1.30	2.72	Cohesive
JKW	Cement	3	19	49	952.6	2960	1.2	2.17	Cohesive/Very Cohesive
CC	Cement	3	19	75	808.1	2910	1.5	1.82	Very Cohesive
CF	Fly ash	4	22	83	665.6	2370	1.2	1.85	Very Cohesive
TUF	Fly ash	3	19	140	693.3	1950	1.45	2.29	Cohesive
Rel 1	Fly ash	38	126	202	677	2060	1.10	5.23	Easy Flowing
Rel 2	Fly ash	5	48	170	857.8	2200	1.20	2.60	Cohesive
H1	Fly ash	16	87	238	798.7	2080	1.33	3.76	Cohesive
H2	Fly ash	7	35	105	777.1	2078	1.53	3.05	Cohesive
P1	Fly ash	20	106	235	794.4	2030	1.25	3.35	Cohesive
P2	Fly ash	4	25	103	769.5	2299	1.27	3.65	Cohesive

3.3 Physical properties measurement

The physical properties of fly ash include its shape, particle size distribution, particle density, Hausner Ratio (HR) and the bulk density. A brief description about measuring the physical properties of the samples has been described in subsequent articles.

3.3.1 SEM images and particle size measurement

Particle size and particle size distribution was measured by the Laser diffraction method on Mastersizer 2000 (Malvern Instruments Ltd, Worcestershire, UK) at Arbro Pharmaceuticals

Ltd, Delhi and Malvern Amil Limited, Delhi. The particle size distribution was characterized as d_{10} , d_{50} , d_{90} . It indicates that 10%, 50% and 90% of the particles have diameter lower than this value respectively. Particle size for 7 fly ash samples is shown in Table 3.1. SEM images of F1 to F7 samples are shown in Fig 4.1 with description and analysis. SEM images were taken by JEOL 6510 LV model at SAI labs Thapar University, Patiala.

3.3.2 Particle density measurement

The particle density for each sample was measured by the water displacement method. A known volume of water was poured into the beaker and its weight was measured. The fly ash sample was added into the water which changed the volume in the beaker and further this beaker was weighed again. The particle density is the ratio of sample mass added and the change in the volume of the beaker. Each sample was measured of particle density at least 5 times till the repeatability in the results was achieved. The particle density of the samples is given in Table 3.1.

3.3.3 Hausner ratio (HR) measurement

Hausner ratio is the ratio of tapped density and loose pour density. This parameter is extensively used in the industries for characterization of the powders because these tests can be easily conducted on the spot. The Hausner ratio for each sample was measured manually. A known volume of sample was taken in a beaker and was tapped gently with amplitude of approximately 3mm till the level of sample saturated in the beaker. The measured values of Hausner ratio are shown in Table 3.1. The powders classification according to Hausner ratio was reported by Smoldurs and Baeyens. (2003). They used Geldart diagram to classify the powder. The powders having $HR > 1.25$ belonged to Group A, $1.25 < HR < 1.4$ belonged to Group A or C and $HR > 1.4$ belonged to Group C.

3.4 Chemical composition of the fly ash

The chemical composition of the fly ash of F1 to F7 sample was tested to determine the grade of the fly ash. The Energy Dispersive Spectroscopy (EDS) technique was used to identify the

presence of different elements and their oxides. The fly ash mainly consists of silicon and aluminium oxides. Some un-burnt carbon was also found in the initial samples of the fly ash (observed by spectrograph). Table 3.2 reports the chemical composition of seven samples of the fly ash. Total four spectrums were tested and the average results were used to evaluate grade of the fly ash. It was found that the tested fly ash samples were of F grade fly ash because the total silica and alumina content observed was more than 70% (W.1).

Table 3.2: Silicon and Aluminium oxide content in fly ash samples

Sample	SiO ₂ content (%)	Al ₂ O ₃ content (%)	Fly ash class
F1	65.22	34.92	F
F2	58.85	32.56	F
F3	56.37	35.42	F
F4	54.9	35.43	F
F5	61.8	26.75	F
F6	56.38	36.56	F
F7	52.23	30.47	F

3.5 Annular shear tester

3.5.1 Powder Flow Tester

The Brookfield Powder Flow Tester (PFT) at Laboratory for Particle and Bulk Solid Technologies, Thapar University was used to measure the flow properties of the fly ash samples (shown in Fig. 3.1). It is basically an annular shear tester in which the sample is filled in an annular shear cell and the lid on the top increases the consolidation stress over the powder. The shear cell is rotated at a known angular velocity to produce shear in the sample at a given consolidation stress. There are two lids which are used to conduct the flow function test and the wall friction test on PFT. Flow function lid (shown in Fig. 3.2 (a)) is used to measure yield locus in the powder. The vanes are provided on the flow function lid to completely hold the sample and ensure that the shear takes place between the layers of powder only. The wall friction tests were conducted with standard wall friction lid made up of 304 stainless steel having 2B surface finish (Shown in Fig. 3.2 (b)). The equipment was calibrated with BCR-116 limestone powder before conducting the experiments. All the experiments were conducted at 45% RH and 25°C temperature.



Figure 3.1: Brookfield Powder Flow Tester (PFT)

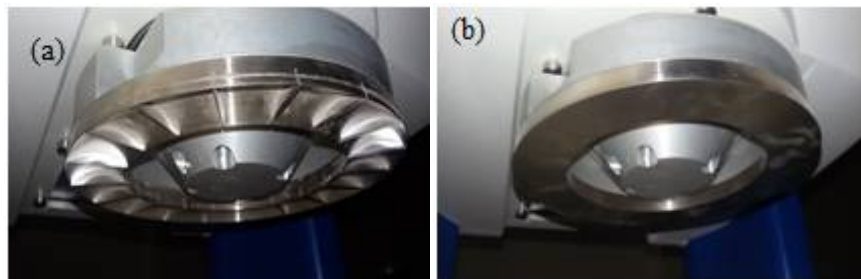


Figure 3.2: (a) Standard flow function vane lid (b) Standard 304 s/s wall friction lid

The equipment operates with accompanying Powder Flow Pro software which analyses the raw data and provides yield locus, flow function curves, trends for wall friction angle and angle of internal friction for powders.

3.5.2 Calibration of Powder Flow Tester

The Brookfield Powder Flow Tester has been calibrated by using BCR116 limestone powder before conducting experiments. The Lime stone powder has been certified by European Research, Joint Research Centre, Belgium. The relative humidity and temperature were ranging between 40 - 50% and 22° - 30°C during calibration. The limestone sample is filled in the trough and 5 flow function tests are conducted on it. The results are the major

consolidation stress and the failure stress (or unconfined yield strength) in kPa. These results are compared with the stress range specified in PFT manual. All the tests were conducted after calibrating the equipment.

Table 3.3: Calibration Table for PFT

S.No	Major consolidation stress (σ_1) in kPa	Permissible σ_1 range in kPa
1	0.552	0.566-0.685
2	1.075	1.110-1.278
3	2.158	2.209-2.487
4	4.324	4.426-4.842
5	8.756	8.959-9.840

3.5.3 Operating procedure for the Powder Flow Tester (PFT)

Flow function test

1. Level the PFT by using base screws and spirit level.
2. Connect the equipment with a PC with Powder Flo Pro software and turn on the power supply.
3. Operate buttons on the PFT panel to ensure proper working of the equipment.
4. Open powder Flo Pro software in PC and connect it with PFT by using setup tab.
5. Weigh annular shear cell on a weighing machine. (Approximately 702.3 gm)
6. Put the powder sample in the annular shear cell and make characteristic shape of the sample by using scrapping tool which is compatible for the flow function test.
7. Weigh the annular shear cell again and deduce the weight of the powder.
8. Set the flow function lid on PFT and adjust shear cell under it.
9. Open test tab in Powder Flo Pro software and enter the powder name, batch name and the powder weight in grams.
10. Select the standard testing method and click on ‘display test stress’ to view estimated time and loads during testing procedures.
11. Click on ‘Run test’.
12. Save the results after the test is complete before conducting any other test.
13. Use buttons on the PFT to remove the sample.

Wall friction and bulk density test

1. The sample preparation process is the same except the shape of the powder in an annular shear cell. It has to be made flat by using the scrapper tool so as to be compatible with the wall friction lid.
2. Set up the wall friction lid on PFT and load the sample.
3. Select the standard wall friction test from the Powder Flo Pro software.
4. Run the test and finally save the results.

3.6 Flow properties measurement

3.6.1 Yield locus and flow function curves

Yield locus of the powder signifies the shear stress (τ) necessary to initiate the flow in it at given consolidation stress (σ) (Schulze, 2008). Yield locus is a curve between normal consolidation load and the shear stress. Yield locus for an ideal solid passes through the origin, but on the other hand it has some intercept on the ordinate for the powders signifying some initial yield stress is necessary to the initiate flow in them at zero normal load. This intercept made by the yield locus at the ordinate is called cohesion (C) (Schulze, 2008). Yield locus at any given pre-shear stress can be represented by Eq. (3.1).

$$\tau = \sigma \tan \varphi + C \quad (3.1)$$

Where, φ is the angle of internal friction representing the magnitude of friction between the layers of powder. Yield locus curve for F1 fly ash sample has been shown in Fig. 3.3. The yield locus curve is drawn at different pre-shear stresses (σ_{pre}). The yield locus was drawn at five pre-shear stresses (0.317 kPa, 0.610 kPa, 1.207 kPa, 2.414 kPa and 4.819kPa represented by Stress 1 to Stress 5) and three over consolidation stress points were measured on each yield locus. Each yield locus provides the major consolidation stress (σ_1) on the powder element and unconfined yield strength (σ_c) of the powder. Unconfined yield strength signifies the strength of an unsupported vertical column of the powder consolidated with the known pre-shear stress which is analogous to the state of the powder element at the outlet of the hopper. More details about the procedure for deducing the major consolidation stresses and

unconfined yield strength from the yield locus can be found elsewhere see (Schulze, 2008). Flow function curve is plotted between σ_1 and σ_c . Figure 3.4 shows the flow function curves for the seven fly ash samples. The flow function curve has been divided in four parts on the basis of Jenike (1964) flowability classification reported by Saw et al. (2015). The classification was based on the range of ratio σ_1/σ_c as follows: $\sigma_1/\sigma_c < 2$ for very cohesive powders, $2 < \sigma_1/\sigma_c < 4$ for cohesive powders, $4 < \sigma_1/\sigma_c < 10$ for the easy flowing powders and $\sigma_1/\sigma_c > 10$ for free flowing powders. Flow index (FI) which is reciprocal of flow function curve slope (σ_1/σ_c) represents the relative flowability of the samples. FI and flowability classification of all fine powders at $\sigma_{pre} = 1.2$ kPa has been reported in Table 3.1. The effective angle of internal friction (δ) is the ratio of the major consolidation stress and minor consolidation stress over the powder element in steady state flow. The variation of effective angle of internal friction with the major consolidation stress is given in Fig. 3.5.

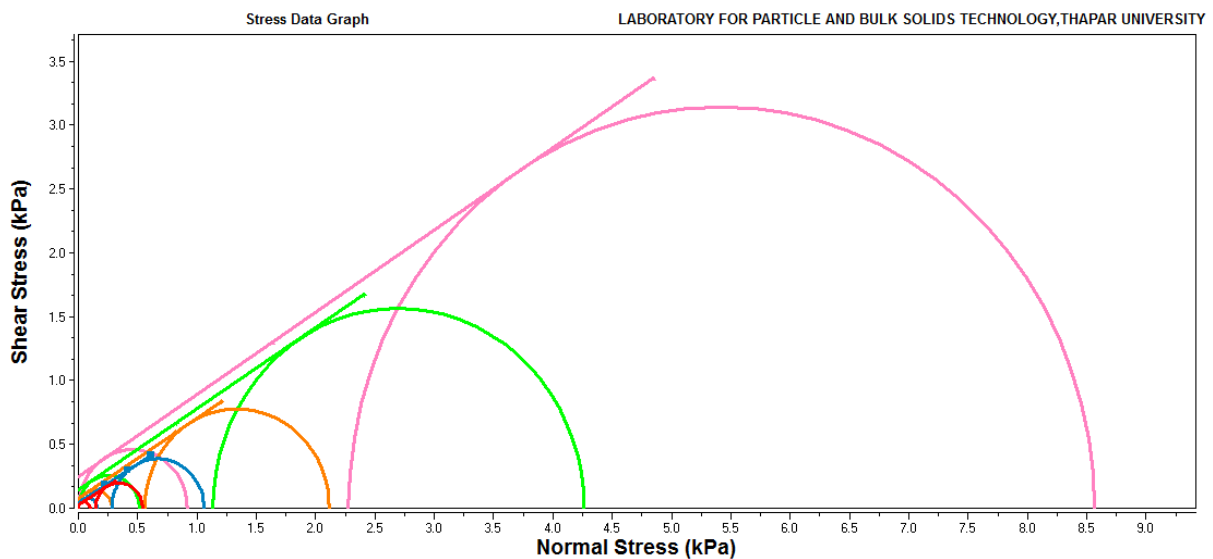


Figure 3.3: Yield locus for F1 fly ash at 0.317, 0.610, 1.207, 2.414 and 4.819kPa

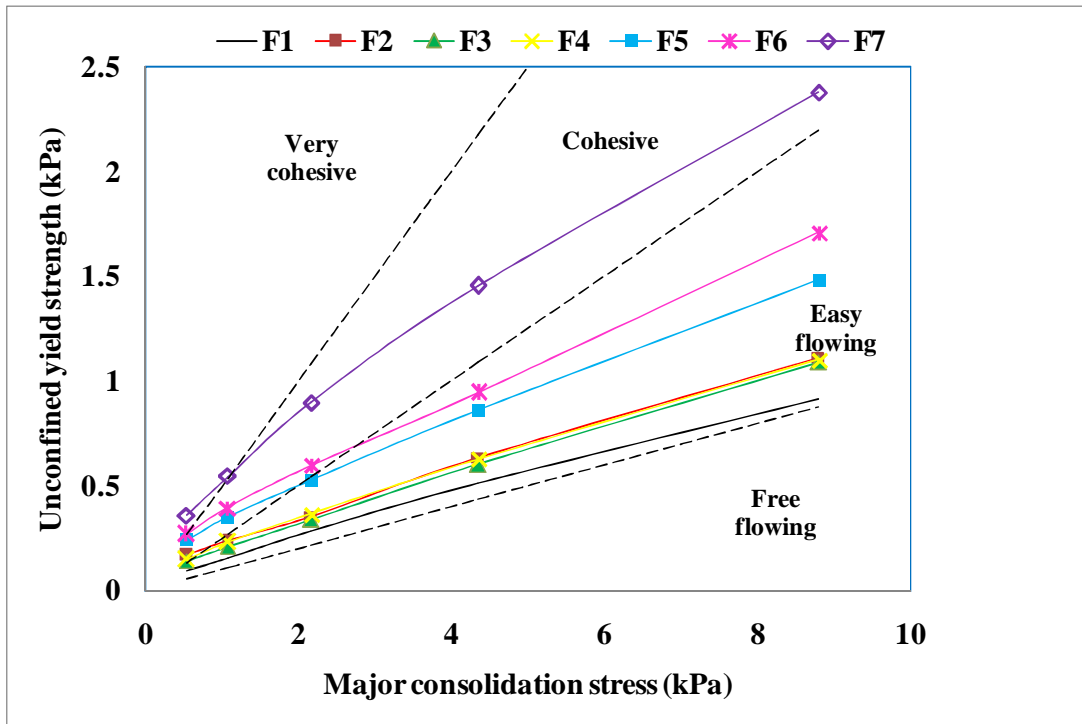


Figure 3.4: Flow function curves for seven fly ash samples

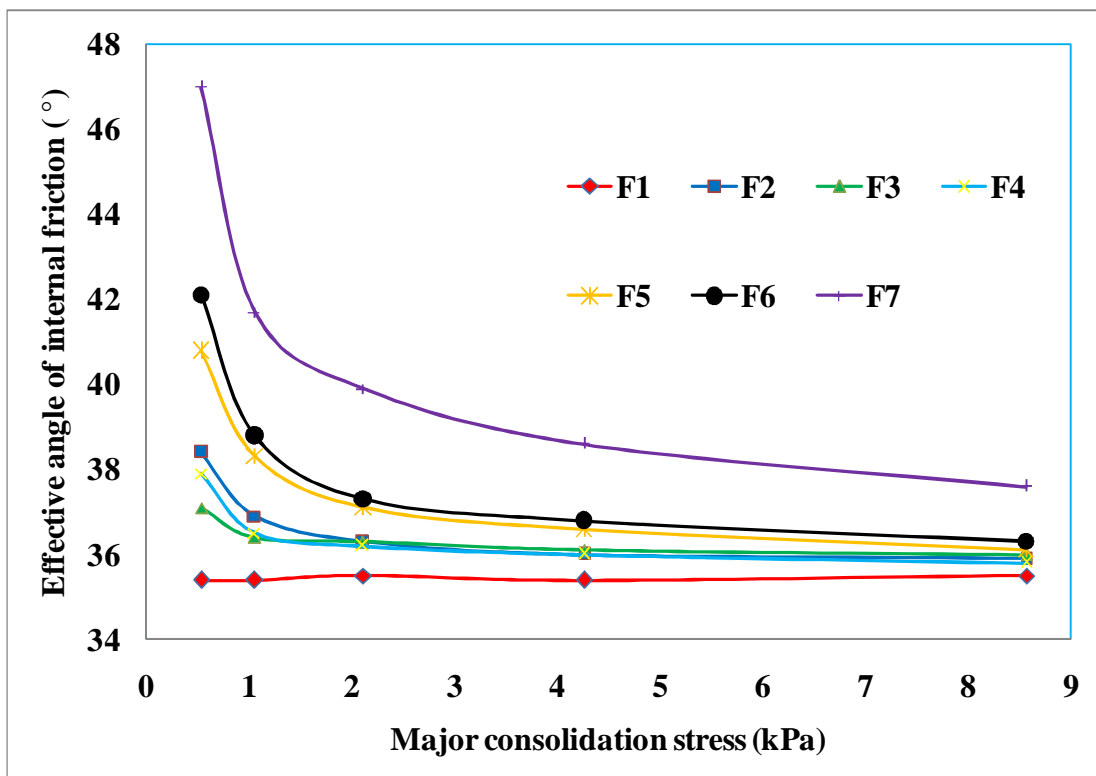


Figure 3.5: Variation of effective angle of internal friction with major consolidation stress

3.6.2 Wall friction and bulk density tests

The wall friction tests were conducted by using the standard wall friction lid made up of 304 stainless steel having 2B surface finish. The test procedure for the wall yield locus is similar to the flow function yield locus with the only difference that the slip is in between the wall and the powder instead of the layers of the powder. The wall yield locus was tested at a maximum of 4.817 kPa by rotating the wall friction lid 10 times with 0.006 m displacement. The intercept made by the wall yield locus represents the adhesion property of the sample with particular material. The wall yield locus for F7 is shown in Fig. 3.6. Effective angle of internal friction (ϕ_w) represents the friction between the wall material and the powder layer at given normal stress. The variation of ϕ_w with the major consolidation stress is shown in Fig. 3.7. The bulk density tests were conducted simultaneously at 10 stress points with the wall friction tests. The bulk density trends with the major consolidation stress are shown in Fig. 3.8.

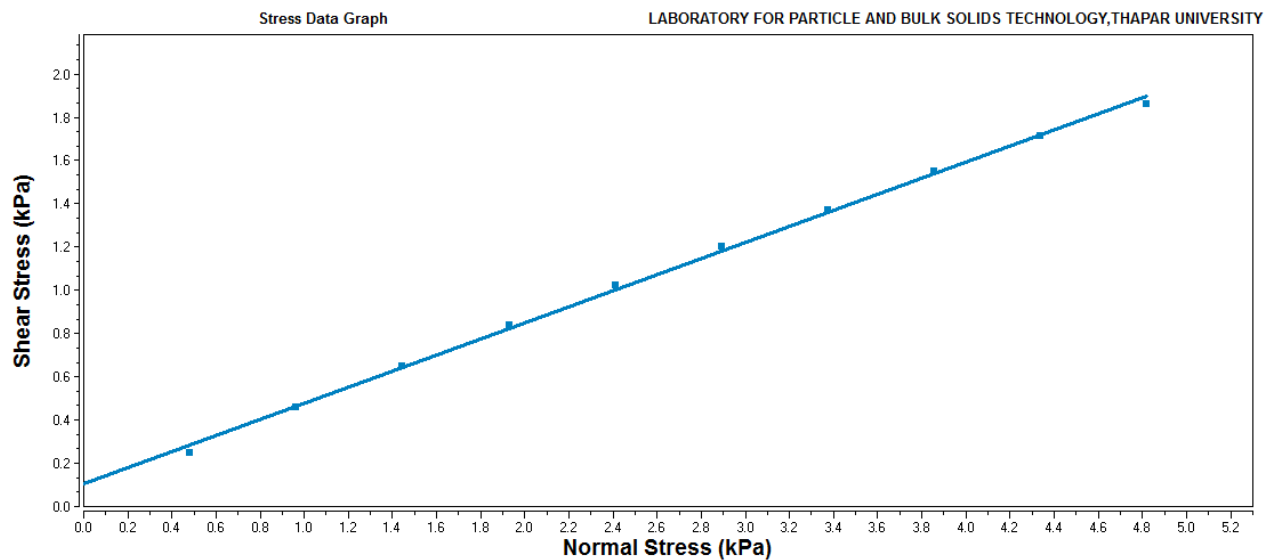


Figure 3.6: Wall yield locus for F7 fly ash sample

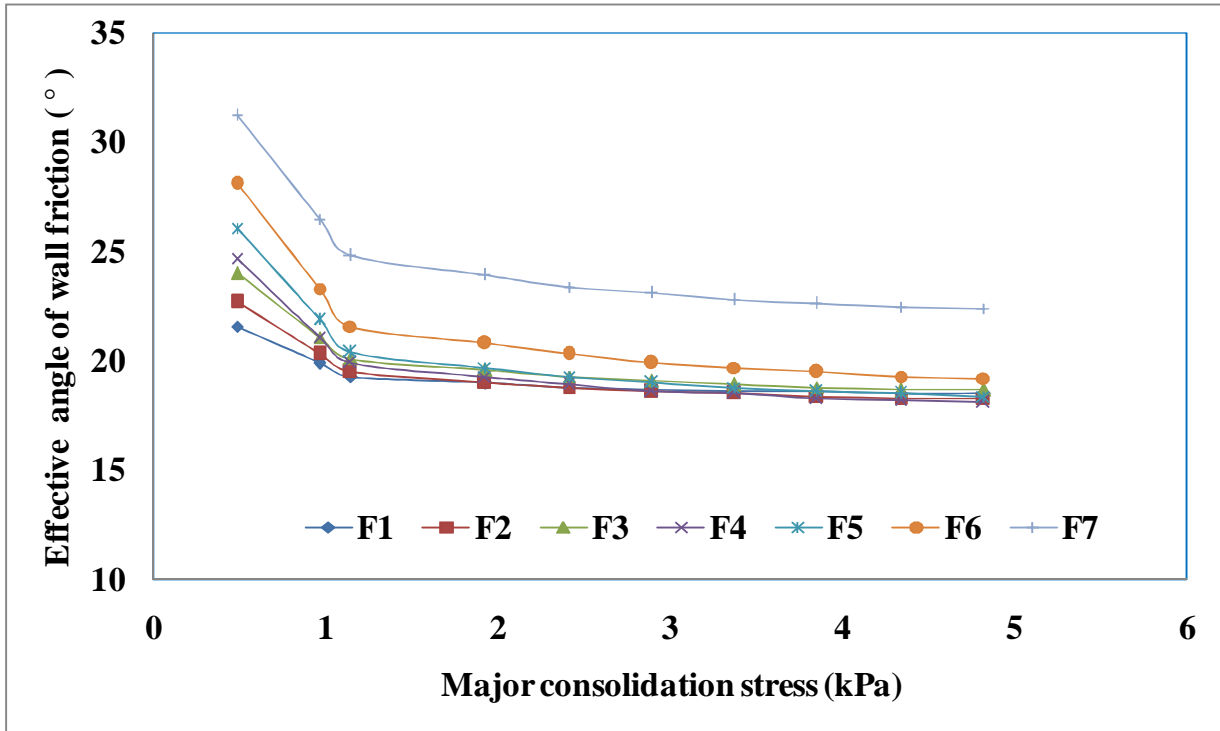


Figure 3.7: Trends of effective angle of wall friction with major consolidation stress

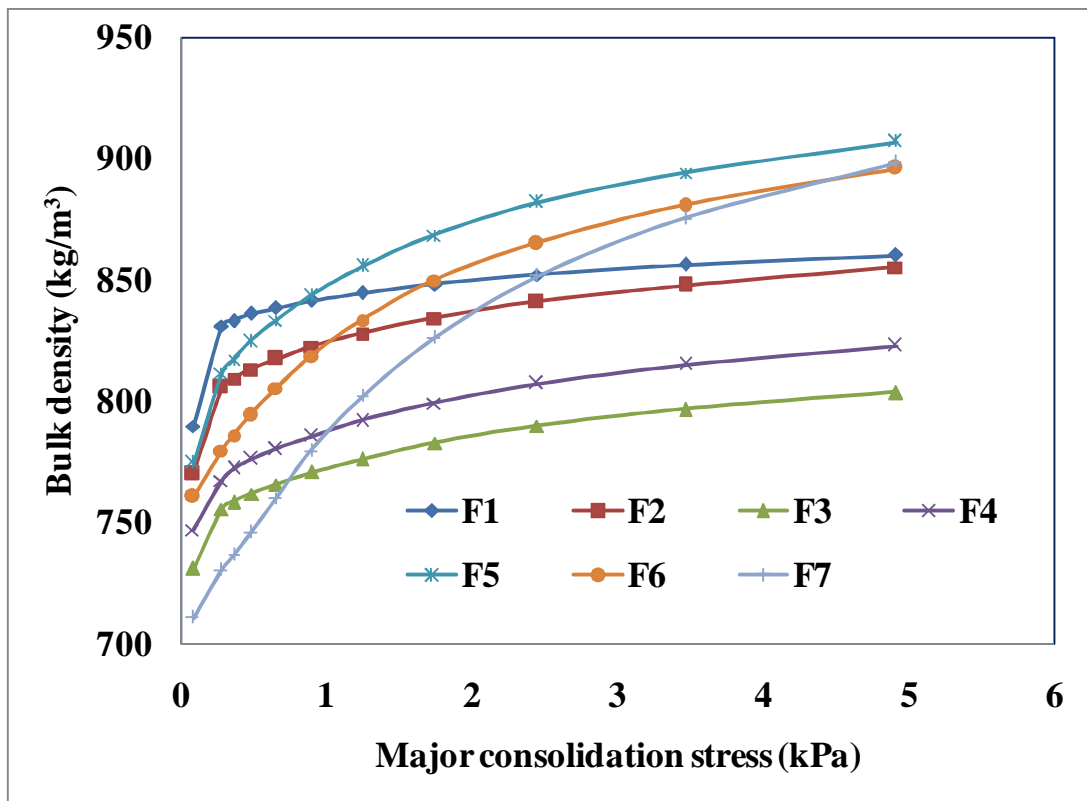


Figure 3.8: Bulk density curves for seven fly ash samples

3.7 Hopper designing procedure

3.7.1 Critical dimensions of the mass flow hopper

The hopper half angle (θ) and outlet opening (D_c) are the critical parameters for the mass flow pattern inside a hopper irrespective of its structural design. Jenike (1964) did pioneering work by deriving mathematical relations between the hopper critical dimensions and the powder flow properties. The results of his work were presented in form of the charts for the mass flow and the funnel flow hopper design. The details about the designing procedure and different types of the hopper configurations to achieve the mass flow can be found elsewhere, see Schulze (2008). The standard flow function tests and the wall friction tests were conducted at the five earlier mentioned pre-shear stresses (represented as Stress 1-Stress 5 in kPa). The hopper half angle and critical outlet opening were found by using the Eq. (3.2) and (3.3) by using the flow properties found at different pre-shear stresses (Arnold et al., 1980)

$$D_c = \frac{2 X \sigma_c X 1000}{\rho_b X g} \quad (3.2)$$

$$\theta = \left[90 - \frac{1}{2} \cos^{-1} \left(\frac{1 - \sin \delta}{2 \sin \delta} \right) \right] - \frac{1}{2} \left[\varphi_w + \sin^{-1} \left(\frac{\sin \varphi_w}{\sin \delta} \right) \right] \quad (3.3)$$

3.7.2 Hopper design for the funnel flow

A storage vessel operates as a funnel flow hopper when its half angle is larger than the mass flow limit. The wall friction is another parameter which can cause the funnel flow in a storage vessel. Hopper half angle (θ_f) for the funnel flow is given by Eq. (3.4).

$$\theta_f = 65^\circ - \varphi_x \quad (3.4)$$

Critical outlet opening for the funnel flow hopper for avoiding formation of rathole is given by Eq. (3.5). $G(\varphi)$ is a function of angle of wall friction which is given by Eq. (3.6) (W.2).

$$D_f = \frac{G(\varphi) \sigma_{crit}}{\rho_b g} \quad (3.5)$$

$$G(\varphi) = 0.7771 e^{0.03 \varphi} \quad (3.6)$$

3.7.3 Hopper design by using Jenike charts

The hopper design can also be done on the basis of the design diagrams given by Jenike as reported by Schulze (2008). This approach of designing the hopper is called flow factor approach.

Firstly the wall friction angle (φ_w) and angle of internal friction (δ) for the design purpose are measured by performing the flow property testing. Using the design diagrams with the value of φ_w and δ , it is possible to extract the value of hopper half angle θ . $H(\theta)$ value can be read from the graphs reported by Schulze (2008) for the circular outlet opening. Further we can also find the value of flow factor (ff) if the value of the wall friction angle and the hopper half angle are known. After determining the hopper half angle, next work is to get the value of outlet opening necessary to avoid arching in mass flow hopper. It is given by Eq. (3.7).

$$D_c = \frac{H(\theta) \times \sigma_c \times 1000}{\rho_b \times g} \quad (3.7)$$

Where, D is the outlet opening (m). The value of $H(\theta)$ remains nearly equal to 2 for circular openings. The value of σ_c and ρ_b are required at critical condition at which the material in the hopper is in between no flow and flow condition. The major consolidation stress on the powder element is represented by σ_1 and σ_1' represents the major stress acting in the arch just near the hopper opening. The flow factor (ff) is the ratio of σ_1 and σ_1' . The value of $\sigma_1' > \sigma_c$ is required for continuous deformation or flow of the powder element. In case of $\sigma_1' < \sigma_c$, the material will consolidate and forms an arch just near the outlet opening. The critical value is at $\sigma_1' = \sigma_c$, this corresponds to the condition at which there is transition between the non flow regime and the flow regime for a given hopper. This also corresponds to the condition of minimum hopper opening necessary to sustain the mass flow.

3.8 Exploring link between flowability and fluidizability

The flow mode of pneumatic conveying is also dependent on powder physical and the flow properties. The dense phase conveying of fine powders is more popular these days for their distinct advantages like the low requirement of air, low wear rate and low attrition rate etc. It is very important to find the possibility of the dense phase conveying capabilities of the Indian fly ash. Chawla (2015) in his M.E thesis did exhaustive study on the same problem of accessing the flow modes for Indian fly ash by conducting aeration and de-aeration experiments in a standard aeration chamber. In this study, the dense phase capabilities of Indian fly ash have been reinvestigated with special reference to their flow properties found by the shear testing. The following paragraph will comprehensively detail about the dense phase conveying criterion used by different researchers.

Wypych (1999) used Geldart, Dixon and other different criterions to evaluate dense phase capabilities for a long distance conveying. Sanchez et al. (2003) reviewed all the popular criterions for accessing the dense phase conveying capabilities of the material. Geldart classified the flow mode of different bulk solids on the basis of their fluidizing behaviour (Reported by Wypych, 1999). Although Geldart diagram was never developed to access the flow mode of the material but still some researchers advocated its importance. Geldart classified the bulk solids in 4 different categories namely A, B, C and D having different characteristics. Group A materials are easily aerea Table and have minimum bubbling velocity higher than minimum fluidization velocity. Group B materials have the same value for both these velocities. Group A and Group B material deareate very slowly and retain the fluid like properties for a longer time. Group C materials are difficult to fluidise and often form a complete plug in the aeration chamber. Group D materials have a large particle size and high bulk density. Dixon (Reported by Wypych, 1999) developed a 2 dimensional diagram for classifying the different bulk solids on the basis of their slugging nature. His theoretical diagram correlated well with Geldart original diagram and in both the diagrams A/C boundary was not completely demarcated. Dixon also classified the bulks solids in 4 categories namely Group A, B, C and D. Group A material shows no slug formation and very high solid loading ratio is possible with these materials. Group B materials also show the possibility of fluidized dense phase conveying but it has been observed that high solid loading ratio will cause vibrations in the pipeline. Group D materials have the solid loading ratio mare than group B but lower than group A. Dixon slugging diagram has been developed

for different pipeline geometries. It could be possible that a material may show dense phase mode in a smaller diameter pipe line but shows completely different behaviour in a higher diameter pipeline. Pan (1999) classified 3 flow modes namely PC1, PC2 and PC3 on the basis of 2 dimensional diagrams between median particle size diameter and loose pour bulk density of material. PC1 represents the material which can be transported from dilute to fluidized dense phase. PC2 represents the material which shows dilute phase or unstable flow while PC3 material show dilute phase only. John and Williams (Reported by Wypych, 1999) proposed a 2 dimensional diagram between loose pour bulk density and permeability factor. They demarcated the diagrams with derived conditions for fluidized dense (FD) and dilute phase. Table 3.4 shows the flow mode of Indian fly ash according to different researchers. It is worth mentioning that the materials which are present at the boundary between two groups can show the behaviour of either of them.

It can be observed from Table 3.4 that F1 to F7 sample have same flow mode for pneumatic conveying despite of having different flowability. Pan and Wypych (2000) gave a theoretical model to predict pressure drop for slug phase conveying by considering the powder flow properties. During this investigation it was found that, the flow properties like effective angle of wall friction and angle of internal friction were higher for the fly ash collected from the later stages of ESP (F5 to F7) which imply the requirement of more pressure drop and hence large compressor requirements.

Table 3.4: Flow mode classification of fly ash samples

Sample	Pan	Geldart	Dixon	Johns and Williams
F1	PC1	A	B	FD
F2	PC1	A	B	FD
F3	PC1	A	B	FD
F4	PC1	A	A/B	FD/Dilute
F5	PC1	A	A	FD
F6	PC1	A/C	A	FD
F7	PC1	C	A/C	FD/Dilute

Chapter 4

Effect of Physical Properties of Fly Ash on its Flow Properties

4.1 Introduction

In this chapter, the effect of the powder physical properties on the flow properties of the fly ash has been evaluated. Seven fly ash samples (F1 to F7) collected from the same thermal power station have been considered for study. The powder flow properties results discussed in chapter 3 have been utilized to describe the trend of the powder flow properties with median particle size and aerated bulk density. The critical particle size which caused transition of the flow behaviour from easy flowing to cohesive has been identified experimentally.

4.2 Analysis of the physical properties of fly ash

SEM images of F1- F7 samples have been shown in Fig. 4.1. It can be observed from SEM images that F1 sample is having a large number of angular shaped particles with similar sized spherical particles in between them. The size of the angular particles was greater than spherical particles for F2 to F4 samples. The size of the spherical particles and the angular particles became smaller for F5 to F7 samples. F7 sample had more quantity of small spherical shaped particles with a little quantity of the angular shaped particles in between them. Surface area of the fly ash is more in the later stages of ESP hoppers because of the presence of smaller spherical particles. More surface area implies more intermolecular forces between particles and such samples have poor flow properties which were observed during this study (Schulze, 2008). F1 sample had a large angular shaped particle but it was observed that they still have better flow properties. Weight forces in F1 sample largely outweighs the magnitude of intermolecular forces between the particles.

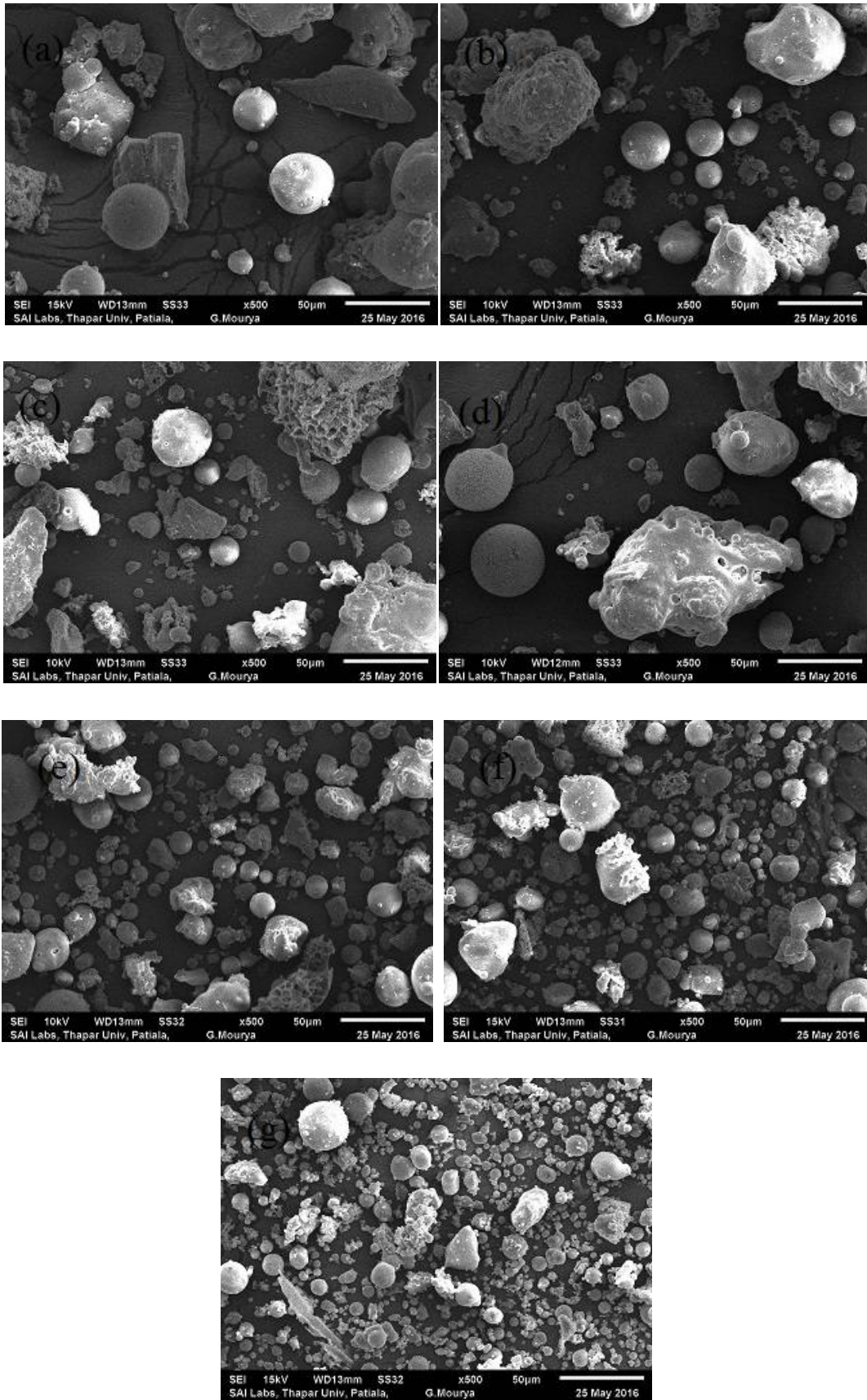


Figure 4.1: SEM images of seven fly ash samples F1 to F7 at 500 times magnification

It can be inferred from this observation that there exists a particular particle size (or sample) after which intermolecular forces become larger than weight forces. This critical particle size has been investigated and identified in this study. The presence of the angular particles in the sample affects the flow properties of the fly ash especially at low consolidation stresses. A decent trend of reduction in median particle size from sample F1- F7 was observed. The bulk density of the samples decreased from F1 to F7. The quenching rate of the fly ash is very high in later stages of ESP which captures the finest fly ash. The higher quenching rate inhibits the formation of crystalline phase (like α -Quartz and Mullite etc) in the fly ash and large quantity of amorphous glass content is produced. Amorphous glass has lower bulk density as compared with other mineralogical components (Lee et al., 1999). This could be the reason of reduction of the bulk density from F1 to F7 samples. Apart from this, the particles of fly ash may be hollow from inside with a thick wall outside. It has also been observed that hollow fly ash particle may encapsulate the finer particles in them. There was no trend observed in the particle density of fly ash with different samples for the same reason. The finer particle samples have good air retention capabilities which further reduce their bulk density.

4.3 Flowability classification of fly ash

The flow function curves for seven fly ash samples have been presented in Fig. 3.4. It can be observed from Fig. 3.4 that F1 sample remained easy flowing throughout the test stress range (up to 10 kPa). Samples F2, F3 and F4 were in cohesive region below stress 1 but gradually shifted to an easy flowing region. Sample F5 and F6 were in cohesive region for stress 1 to stress 3 and finally shifted to cohesive region for stress 3 to stress 5. The flow function curve classification shows the dynamic flow behaviour of fly ash sample which is dependent upon the working stress range. The material is cohesive or free flowing according to the stress level involved in the end application. For this study, FI at 1.2 kPa pre-shear stress has been taken as a standard to classify the flowability of fly ash. Table 3.1 reports flow index for seven fly ash samples (F1 to F7). The flowability classification has also been reported in Table 3.1. Sample F1 to F4 are of free flowing nature and F6 and F7 are of cohesive nature with sample F5 (53 μ m median particle size) being the transition sample between easy flowing and cohesive nature of fly ash. Similar observations about F5 sample being the transition sample were made by compaction dynamics of the seven fly ash samples reported in Fig. 3.8.

Regression analysis was used to fit the trend line for each fly ash sample in Fig. 3.8. Compaction dynamics of F1 to F4 easy flowing samples and F5 to F7 cohesive samples can be represented by Eq. (4.1) and (4.2) respectively.

$$\rho_b = A \log_n \sigma + \rho_o \quad (4.1)$$

$$\rho_b = \rho_o + A \sigma^4 + B \sigma^3 + C \sigma^2 \quad (4.2)$$

Where, ρ_o is the loose pour bulk density, σ is the major consolidation stress and A, B, C are the constants dependent on the material. The Flow index of sample F2 and F4 were same but there compaction dynamics were entirely different (refer Table 3.1 and Fig. 3.8). This observation shows the significance of the compaction dynamics for characterising different powders (Lumay et al., 2012). It can also be observed from compaction dynamics (refer Fig. 3.8) that sample F5 had the highest bulk density among all the samples. According to a study by Abdullah and Geldart (1999), there is an optimum percentage of the fine fractions in the powder which gives the densest packing. A sample consisting of 100% fine or 100% coarse particles have lower bulk density. The optimum mixture has just sufficient number of the fine particles to fill all the voids when the powder is compacted. This could be the reason for the highest bulk density of F5 sample during its compaction although its loose pour bulk density was sufficiently lower than F1 to F4 samples. Loose pour bulk density for an easy flowing sample was higher than cohesive fly ash samples because the easy flowing samples pack well. The overall flowability of the sample depends upon the magnitude of intermolecular force in between them. Bond number (Bo) is the ratio of intermolecular forces of attraction (F_a) and particle weight (mg). It has been observed that, the powders which pack well have good flowability characteristics also because they have more weight force as compared to the magnitude of intermolecular forces in between them (Castellanos, 2005).

4.4 Effect of particle size on cohesion

The effect of particle size on cohesion in seven fly ash samples at different pre shear stresses have been reported in Fig. 4.2. It can be observed from Fig. 4.2 that cohesion in fly ash decreases with an increase in median particle size. Fine particle samples (F5 to F7) are more cohesive because they have more surface area as compared to coarse particle samples (F1 to

F4) which increases intermolecular forces of attraction (Schulze, 2008). Cohesion of the sample depends upon the particle geometry, particle size and number of contact points. The compaction of the sample reduces intermolecular distance causing an increase in cohesion. The power law variation was observed for decrease in cohesion with an increase in the particle size, although the experimental data slightly deviated from the power law at higher pre shear stresses. The contact points between the particles of powder undergo deformation on increasing normal load over them. The flat contact point's increased surface area dependent forces (like van der wall forces) which increases net intermolecular forces between the particles. The increased intermolecular forces cause an increase in bulk cohesion in the sample. Cohesion increases more quickly in fine samples as compared coarse samples with increasing pre shear stress. Fine samples have good air retention capabilities and they deareate very slowly. The fine powders deareate after application of normal load over the sample and after deareation there flow properties deteriorates further. Air within the fine samples acts as a lubricant and improves there flowability. The particles of fly ash come closer after deareation and increasing normal load results in more number of direct contact points among the particles. Deareation phenomenon is more prominent in fine powders for increasing cohesion. It can also be observed that cohesion is fairly constant for the coarse samples (F1 to F4) at low pre shear stresses although, there were some deviations noticed at higher pre shear stress. At lower pre shear stress range (stress 1 to stress 2) cohesion becomes independent of particle size after transition sample (F5). This observation reconfirms the presence of critical particle size after which the weight force of the particle is balanced by net intermolecular forces of attraction (Bond number, $Bo = 1$) (Castellanos, 2005). Capece et al. (2015) recently developed multi component granular bond number and correlated it with flow index of powder. They identified the boundary for powders at Bond number, $Bo = 1$ as the condition after which particle weight force dominates particle intermolecular force resulting transition of their flow behaviour.

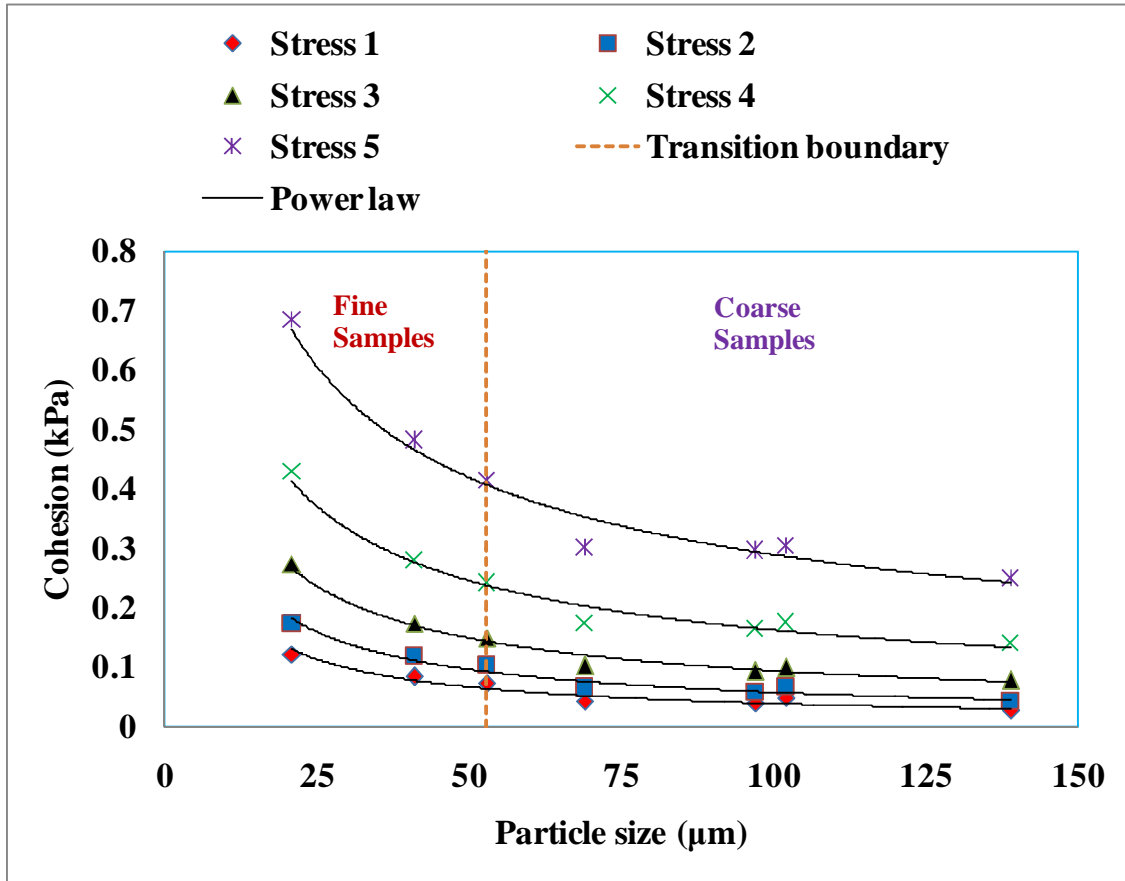


Figure 4.2: Effect of median particle size on cohesion in seven fly ash samples at different pre shear stresses.

4.5 Effect of particle size on angle of internal friction

The angle of internal friction (δ) is the measure of the friction between the layers of the powders at the given pre shear stress. It can be observed from Fig. 4.3 that δ for F1 sample is constant for all the pre shear stresses confirming its easy flowing behaviour. The flowability classification of F1 to F4 samples showed that all of them are easy flowing powders. The variation in angle of internal friction with median particle size gave more insight about their flowability characteristics. A free flowing material should have constant angle of internal friction throughout the stress range which was only observed for F1 sample. It was observed that the power law fairly represents ($R^2 = 0.95 - 0.85$) the variation of δ with median particle size at different pre shear stresses. Power law curves converged at a point for F1 sample (particle size 139 μm) after their diverging for samples F2 to F7. The maximum divergence in power law curves was observed for F7 sample. The range of effective angle of internal

friction (δ^*) which is the difference between the highest (δ_{\max}) and the lowest (δ_{\min}) value of δ observed for the sample is able to differentiate among free flowing samples and cohesive samples. Table 4.1 shows the values of δ^* for seven fly ash samples. Each sample had different values of δ^* representing the difference of the flowability among easy flowing and cohesive samples. Table 4.1 also reports flowability classification of fly ash samples on the basis of flow index. It can be inferred that δ^* can serve as a parameter to differentiate among samples which have been classified under the same category according to the flow index classification. The fly ash having particle size of more than 139 μm will come under the category of the free flowing samples in absence of any moisture content as shown in Fig. 4.3.

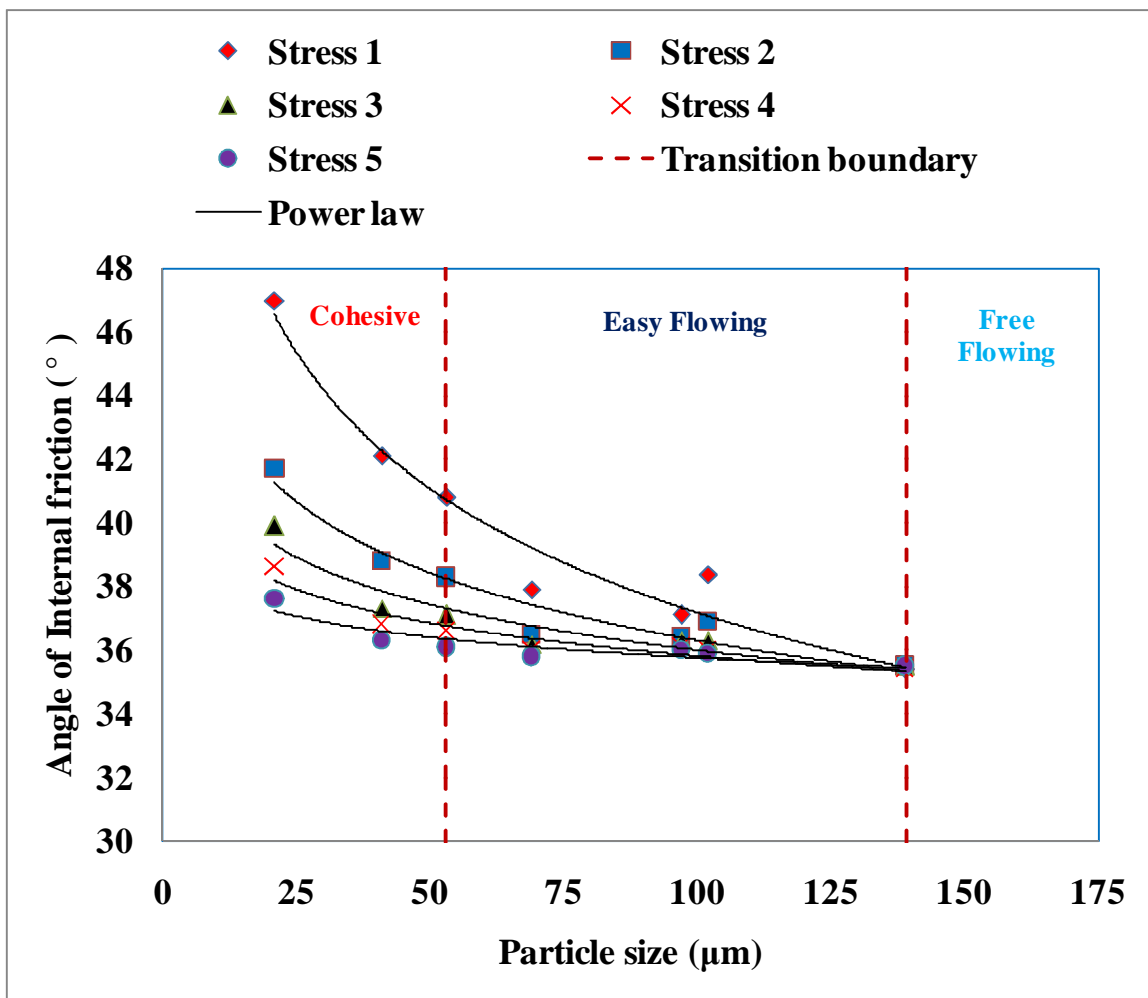


Figure 4.3: Effect of particle size on Angle of internal friction

Table 4.1: Comparison of range of angle of internal friction with fly ash flowability

Sample	Range of δ ($\delta^* = \delta_{\max} - \delta_{\min}$)	Flowability Classification
F1	0.1	Easy flowing
F2	2.5	Easy flowing
F3	1.1	Easy flowing
F4	2.1	Easy flowing
F5	4.7	Easy flowing/ Cohesive
F6	5.8	Cohesive
F7	9.4	Cohesive

4.6 Effect of particle size on unconfined yield strength

Figure 4.4 reports the variation of unconfined yield strength with median particle size.

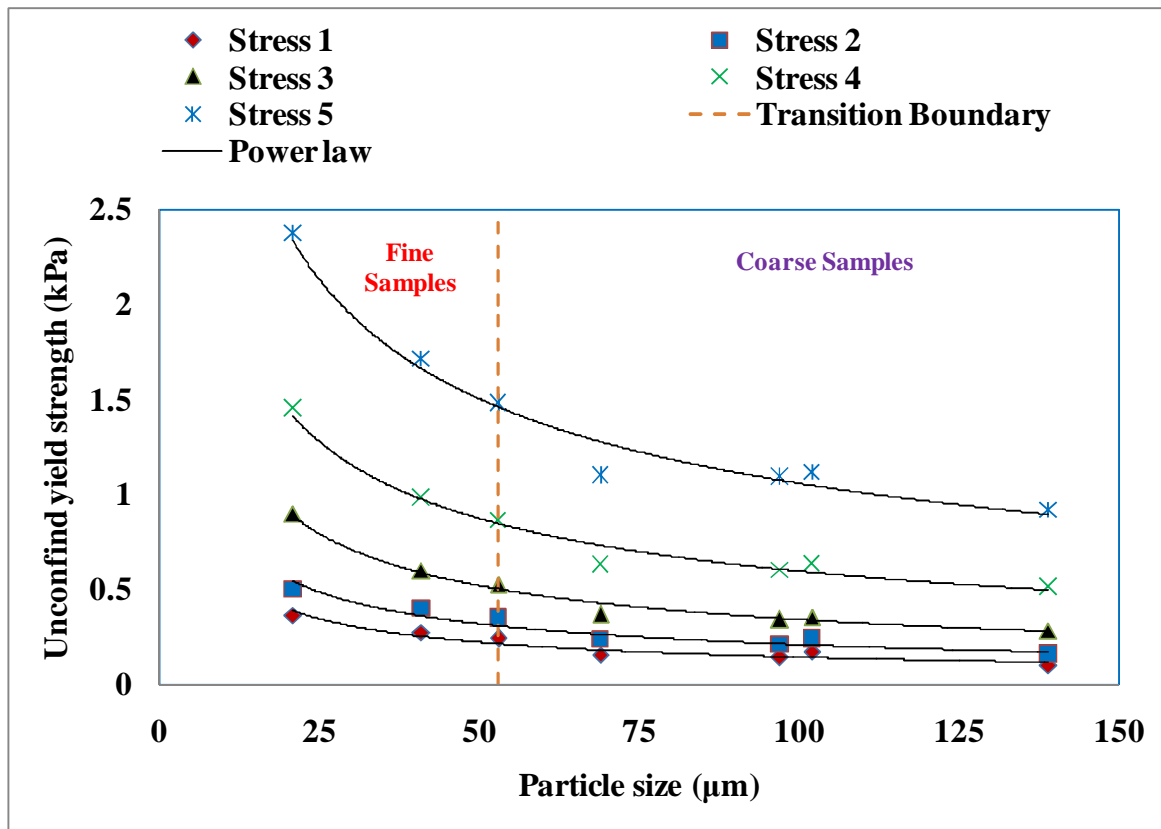


Figure 4.4: Effect of particle size on unconfined yield strength

It was observed that the trend follows the power law especially at the lower pre shear stresses. The fine samples had higher unconfined yield strength because of their capability to form the stable structures. SEM images of F5 to F7 sample revealed presence of small

spherical particles which gives a compact structure by filling all the voids when any normal stress is applied over these samples. On the other hand, the coarse samples had fairly constant unconfined yield strength especially at lower pre shear stresses. Transition particle size boundary has also been shown in Fig. 4.4 revealing the transition in unconfined yield strength of the fly ash samples. Unconfined yield strength affects the critical outlet opening of the mass flow hopper (refer Eq. 3.2).

4.7 Effect of particle size on wall friction angle

The wall friction angle (ϕ_w) variation with the particle size has been reported in Fig. 4.5. Stress 1 to stress 10 represents ten equally spaced normal stresses ranging from 0.482 kPa to 4.817 kPa in an increasing order. It was observed that all the fly ash samples followed non linear power law variation especially at low normal stress.

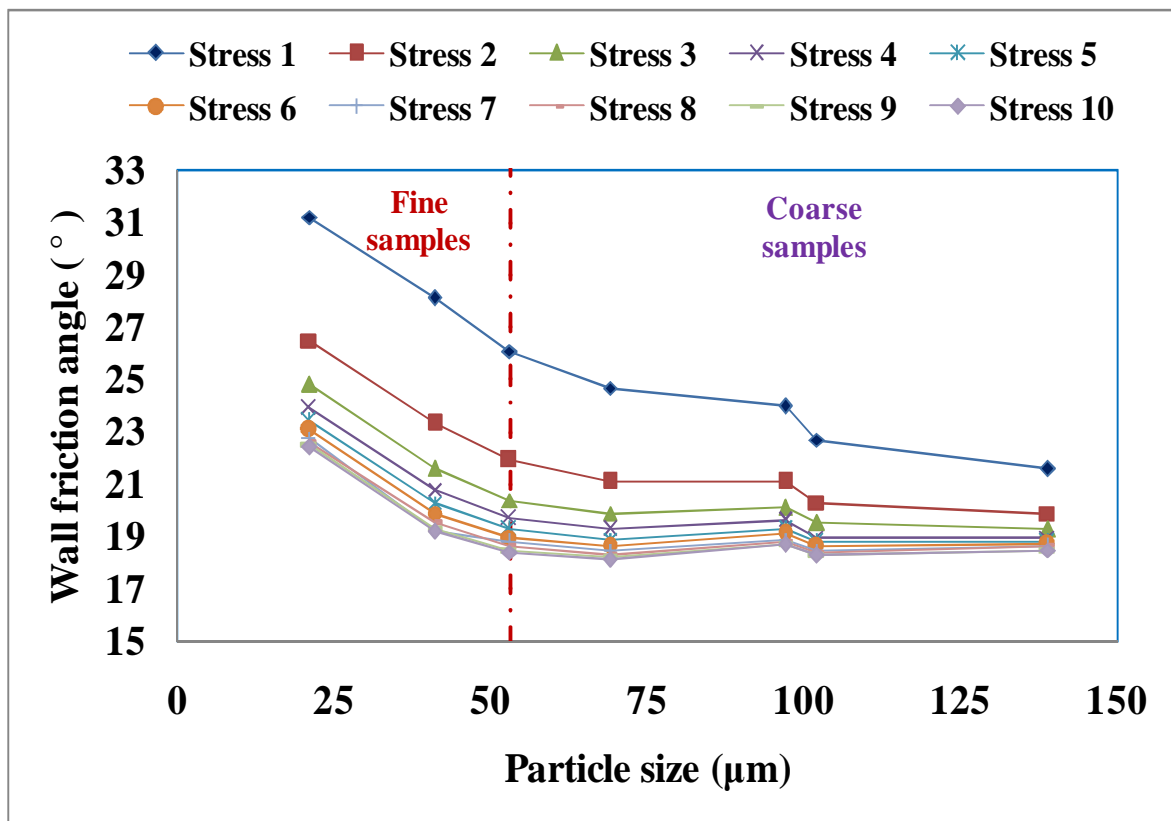


Figure 4.5: Effect of particle size on wall friction angle at different normal stresses

It can be inferred from the experimental data that change in magnitude of ϕ_w keeps on diminishing with increasing normal stress over the sample. Reduction in ϕ_w at higher consolidation stresses can be explained by smoothening of powder asperities contact. Smoothening of asperities with increasing consolidation load was recently reported by Chirone et al. (2016) in his experimental data for radius of curvature of particle asperities. The fine sample particles get struck in the asperities of the wall material resulting in higher ϕ_w as compared to the coarse samples. An average roughness (Ra) for 2B surface finish stainless steel material ranges from 0.3 μm to 0.5 μm (W.3). The fine samples have more quantity of smaller fly ash particle size (represented by d_{10}) as compared to the coarse samples (refer Table 3.1).

4.8 Effect of aerated bulk density on Flow Index (FI)

The Flow Index is used to rank the powders on the basis of their flow properties. More flow index means better are the flowability characteristics of the sample. The bulk density can also serve as the indicator of the flowability and this parameter has been considered while developing model for cohesion which is discussed later in the thesis. Fig 4.6 shows the variation of the bulk density with FI for 7 fly ash samples. It can be very well observed that the variation is linear and freely flowing materials have higher flow index. This variation is obvious and could be expected for every type of material because there exists a critical particle size for each material after which gravity forces in the powder sample become more than inter-molecular forces. The gravitational forces dominance gives the advantage of free rolling, flowing and mixing of the powder.

Table 4.2: Aerated bulk density of 7 fly ash samples

Sample name	Aerated bulk density (Kg/m ³)
F1	848
F2	839
F3	830
F4	818
F5	804
F6	780
F7	759

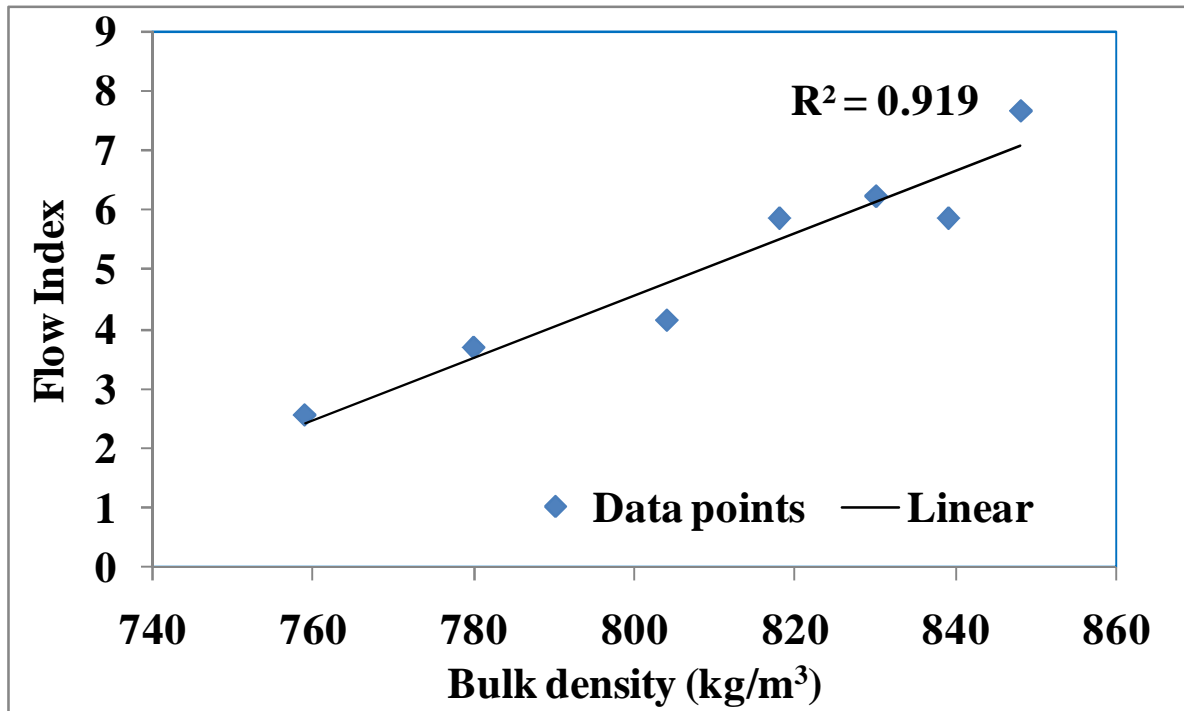


Figure 4.6: Effect of aerated bulk density of FI

4.9 Effect of aerated bulk density on Cohesion.

The effect of the bulk density on cohesion can be fairly represented by the power law variation as shown in Fig. 4.7. Table 4.2 shows the aerated bulk density of the seven samples of fly ash. Similar variation was observed with median particle size as well. The cohesion depends upon the magnitude of the pre shear stress. Increasing pre shear stress increases the cohesion more in case of lower bulk density samples as compared to the higher bulk density samples. It has been observed that lower bulk density samples generally have lower median particle size as well.

This curve has great significance because the bulk density can be used as a parameter to model cohesion. In the previous chapter it was discussed that the particle size distribution also contributes to magnitude of cohesion in the sample.

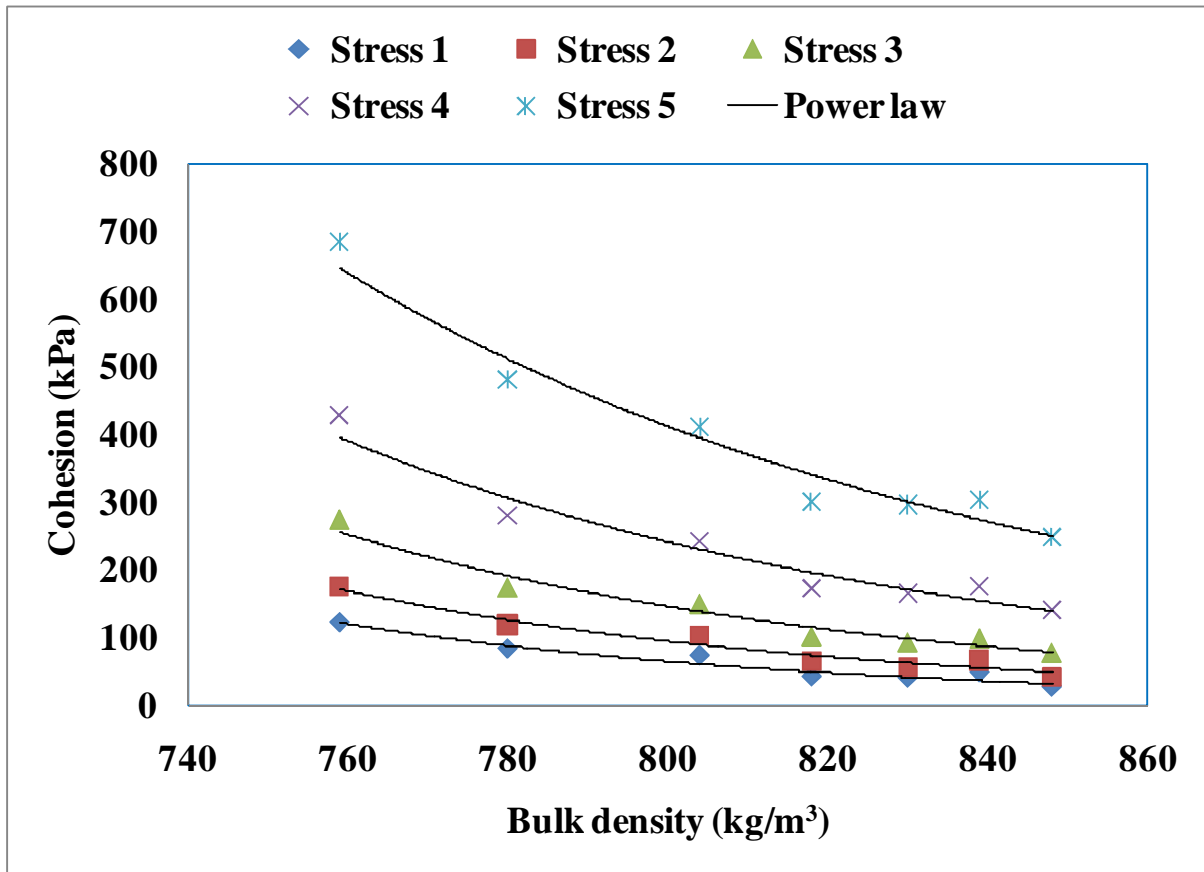


Figure 4.7: Effect of aerated bulk density on cohesion in the sample

A model comprising of these two parameters can be used to predict magnitude of cohesion in the sample with relatively low error. These models have been developed during this study and have been discussed in the subsequent chapters. The similar variation in other powder flow properties will be noticed because the bulk density is proportional to median particle size (Refer Table 3.1)

Chapter 5

Effect of Flow Properties of Fine Powders on Hopper Geometry

5.1 Introduction

In this chapter, the effect of the flow properties of the fly ash on the hopper geometry has been discussed. The fly ash samples were classified into three categories according to Jenike (1964) classification. The hopper half angle versus the critical outlet opening curves for the twenty two available fly ash samples collected from ESP hoppers have been analysed. The variation of the critical outlet opening in the funnel flow hopper with the depth of the fly ash has also been studied. Finally, seven fly ash samples (F1 to F7) from the same thermal power plant were studied separately to evaluate their flowability from specified dimensions of ESP hopper. A qualitative idea has been given regarding aeration rate necessary to achieve continuous discharge from the ESP hopper.

5.2 Effect of flow properties of fly ash on mass flow hopper geometry

The critical dimensions of the mass flow hopper are its outlet opening and the hopper half angle. Arching is a no flow condition commonly encountered in the mass flow hoppers. Arching is caused when the strength of powder due to compaction is more than abutment stress provided by the hopper (Cannavacciuolo et al., 2009). Arching in the mass flow hopper can be avoided by keeping hopper outlet opening such that the strength of powder element just above the hopper opening is less than its unconfined yield strength at a particular normal stress. The normal stress is provided horizontally on the powder element in the hopper section. Arnold et al. (1980) used Eq. (3.1) and (3.2) to find critical outlet opening and hopper half angle for reliable and continuous discharge from the mass flow hopper. Fig. 5.1

to 5.3 reports the hopper geometry for easy flowing, cohesive and very cohesive fly ash. A typical ESP hopper has 100 mm diameter of outlet opening and 30° wall edge angle (wall angles with vertical are 18° and 25°). ESP hoppers are aerated continuously to ensure continuous evacuation of fly ash.

The ESP dimensions have also been demarcated in Fig. 5.1 to Fig. 5.3 for the sake of analysis. It can be observed in Fig. 5.1 that the hopper dimensions are sufficient for the discharge of easy flowing fly ash by gravity only. There is no need to aerate easy flowing fly ash having Compressibility Index (CI) ranging from 8.20 to 9.22. The sample ‘Rel 1’ showed the need of steep hopper half angle despite of being easy flowing according to the flowability classification. The sample ‘Rel 1’ had 5.23 Flow Index which is close to the transition boundary to cohesive samples. Further it could be inferred that the easy flowing samples do require hopper half angle more than 30° for all outlet openings (refer Fig. 5.1). The fly ash requires steeper hopper half angle as its flowability is reduced. The outlet opening is selected on the basis of discharge rate necessary from the mass flow hopper. Theoretical discharge rate (Q) can be calculated by modified Beverloo’s Eq. (5.1) reported by Schulze (2008).

$$Q = C \rho_b \sqrt{g + \frac{1}{\rho_b} \left(\frac{dP}{dZ} \right)} (d - kx)^{2.5} \quad (5.1)$$

Where C and k are the parameters found from curve fitting, d is the hopper outlet opening and x is the mean particle size of the fly ash. The mass flow rate is dependent upon the pressure gradient, (dP/dZ) present just at the outlet of the hopper. Air rushes in to the hopper because of the vacuum created by dilation of the powder during discharge. The net effect of pressure gradient is to reduce the discharge rate of fine powders from the hopper.

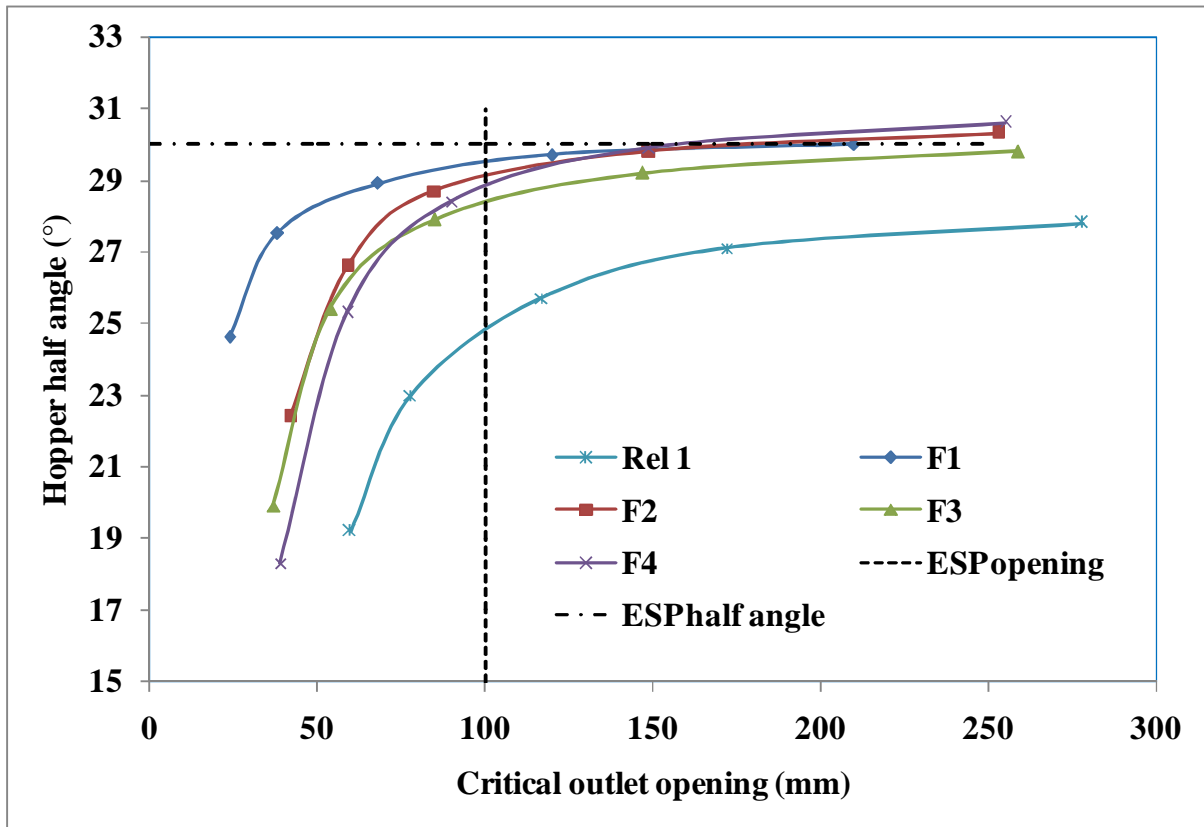


Figure 5.1: Mass flow hopper geometry for easy flowing fly ash

The hopper half angle is selected on the basis of the space constraints. It is not feasible to have storage vessel having 10° hopper half angle for same storage capacity. This will result in very large height of the hopper which contradicts the space constraints. The expanded flow hoppers can be used in such conditions as they provide the advantage of reliable mass flow discharge and storage capacity. There is a steep half angle present just near the outlet of the hopper while rest of the hopper has large hopper half angle. Cone in cone inserts can be used to change the flow pattern inside the storage vessel. The half angle for the cone in storage vessel must correspond to the hopper half angle for the mass flow. More details about the hopper configurations and inserts used commercially can be found elsewhere see, Schulze (2008).

Figure 5.2 show the variation of hopper geometry for cohesive fly ash.

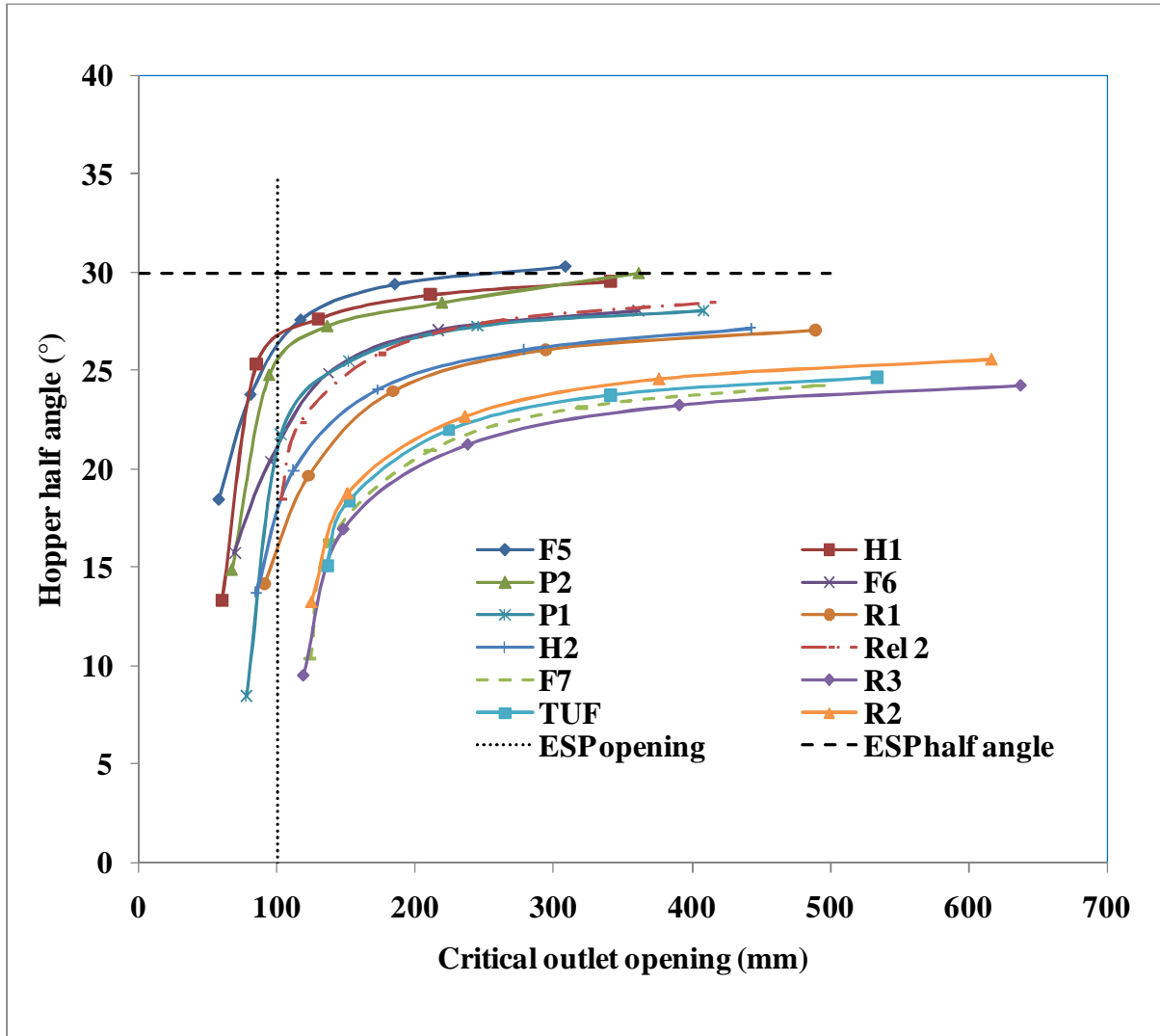


Figure 5.2: Mass flow hopper geometry for cohesive fly ash

It can be observed from Fig. 5.2 that cohesive fly ash cannot be discharged completely by gravity only. The hopper half angle necessary for cohesive fly ash ranges from 15° to 25°. Continuous supply of air by aeration pads is necessary for the fly ash with Compressibility Index (CI) ranging from 14.59 to 17.17. Some cohesive fly ash samples having CI ranging from 20.85 to 21.67 present near the boundary of very cohesive material cannot be discharged from ESP hopper by gravity only and will require even higher aeration rate.

Figure 5.3 shows that very cohesive fly ash samples cannot be discharged from an ESP hopper. Such fly ash samples have CI ranging from 22.79 to 29.67. These samples require high and continuous aeration rate to evacuate fly ash completely. Very cohesive samples require the hopper half angle ranging from 12° to 5° for 100 mm outlet opening of ESP hopper.

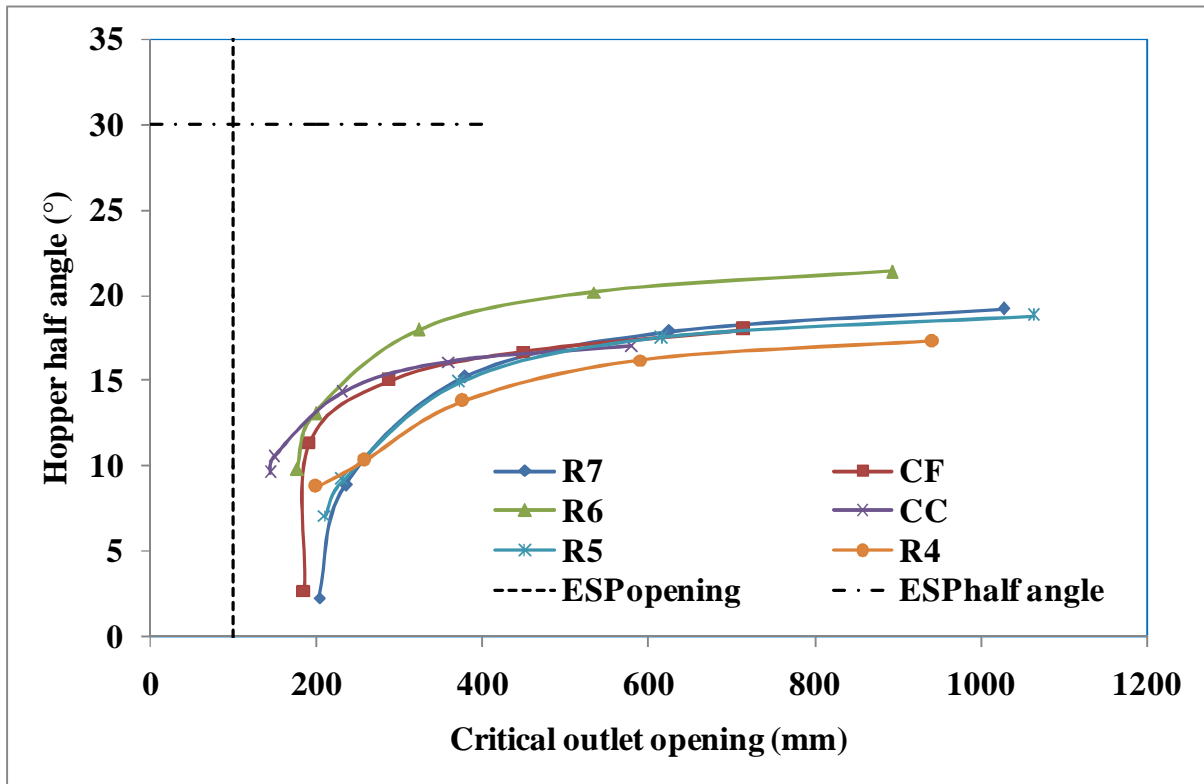


Figure 5.3: Mass flow hopper geometry for very cohesive fly ash

Qualitative analysis on aeration rate necessary for reliable discharge

It has been observed during the study that cohesive and very cohesive fly ash cannot be discharged by gravity only. The flow promoting devices and discharge aids have to be used in such conditions. The flow promoting devices are of two types, the mechanical flow promoting devices and the pneumatic flow promoting devices (Schulze, 2008). The mechanical flow promoting devices like the mechanical agitators and the pneumatic hammers produce mechanical impact on the hopper and produce a mechanical shock wave to overcome the flow obstruction. These devices harm the structural strength of the hopper and deform its geometry resulting in changed flow pattern inside the vessel. The pneumatic discharge aids like pneumatic nozzles, aeration pads, pneumatic cannon etc introduce air into the powders and fluidise them to promote their flow. More details about commercially used discharge aids could be found elsewhere see Schulze (2008). In this study, seven fly ash samples (F1 to F7) collected directly from an ESP hopper unit were studied separately for their mass flow hopper geometry. Figure 5.4 shows mass flow hopper geometry for F1 to F7 samples.

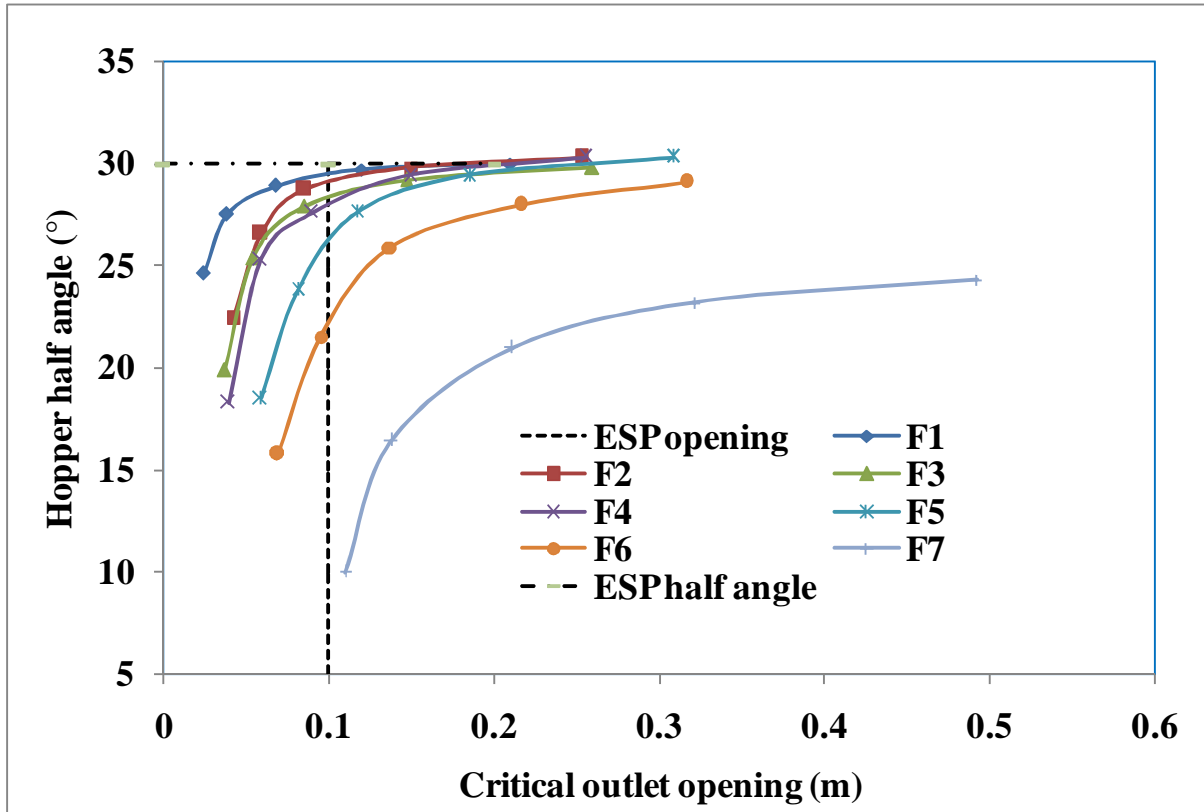


Figure 5.4: Mass flow hopper geometry for samples (F1 to F7) collected from consecutive ESP hoppers

Table 5.1 reports minimum fluidisation velocity and permeability factor for the samples F1 to F7. It can be observed from the Table 5.1 that minimum fluidization velocity progressively increases for the samples F1 to F7 in the order of their decreasing FI. The permeability factor also increased from samples F1 to F7. It can be inferred from this observation that all ESP hoppers do not required the same aeration rate because there is a difference in their minimum fluidization velocity. Air introduced into ESP hopper fluidises the material and expands the active flow zone (Schulze, 2008). The unconfined yield strength of the powder significantly decreases after the material is in fluidised state (Johanson, 2003). The minimum fluidisation velocity denotes the onset of the fluidisation in the powder. The fluidised fly ash is capable of flowing through a narrow opening because its unconfined yield strength is substantially reduced due to the presence of air between the particles of the fly ash. The wall friction of the fluidized fly ash also reduces because aeration pads acts as air slides for the air and fly ash mixture. Sample F1 do not require any aeration because its hopper dimensions required for mass flow are the same as that of the ESP hopper.

Table 5.1: Minimum fluidization velocity and permeability factor for sample F1 to F7
(Chawla, 2015)

Sample	Minimum fluidization velocity (m/s)	Permeability factor (m ² /kPa-s)
F1	0.0285	0.00578
F2	0.016	0.00454
F3	0.018	0.00403
F4	0.030	0.0182
F5	0.036	0.0112
F6	0.040	0.0092
F7	0.122	0.0416

The fly ash is under normal load in the hopper and the aeration rate necessarily depends upon it. It was observed while studying the compaction dynamics of the fly ash that, its voids fraction is reduced and cohesion is increased further with an increase in the consolidation load. Reduced void fraction will cause large pressure drop and more aeration rate will be needed to fluidise the material. The proportion of aeration rate will remain the same as of the minimum fluidisation velocity. Samples F2 to F6 will require progressively higher aeration rates. According to this qualitative analysis, sample F7 will require approximately seven times more aeration rate as compared to the F2 sample.

5.3 Effect of flow properties on fly ash on funnel flow hopper geometry

The discharge from the funnel flow hopper geometry is dependent upon the stagnant zones formed near the walls. The funnel flow mode of discharge occurs when hopper half angle exceeds half angle necessary to initiate the mass flow. The high wall friction can also produce stagnant zones and hence funnel flow pattern (Lee et al., 2015). A rathole or standpipe is formed into the vessel causing no flow condition. The material at the top of outlet opening is discharged continuously while rest of the material is the part of stagnant zone (Lee et al., 2015). The depth of the powder causes consolidation of powder in the lower parts of the hopper. The powder gains strength due to the consolidation and is able to support stand pipe. The circumferential stress or hoop stress in the standpipe element must exceed the unconfined yield strength of the material under given normal load. The consolidation stress at the bottom of the hopper is dependent on the depth of material (Schulze, 2008). Therefore the

rathole profile can be reported as a function of the material depth instead of the major consolidation stress. A brief introduction for designing of the funnel flow hopper has been reported in chapter 3. More details about the same could be found elsewhere, see (Schulze, 2008). The rathole will collapse if the hoop stress in the powder element present just at the outlet exceeds unconfined yield strength. The outlet dimension of the funnel flow hopper must be kept greater than the critical rathole diameter. The rathole diameter is greater than the critical diameter of the hopper to avoid arching. This is because the flow factor for ratholing is greater than the flow factor for arching. The rathole diameter is dependent on the geometry of vessel (height of material and diameter of vessel) because the normal consolidation load at the bottom of the vessel is dependent on the height of material filled in the vessel. The geometry of the funnel flow hopper has been assumed of 6 m diameter and 20 m height for calculation purpose. Figure 5.5 shows the variation of rathole profile for the easy flowing samples.

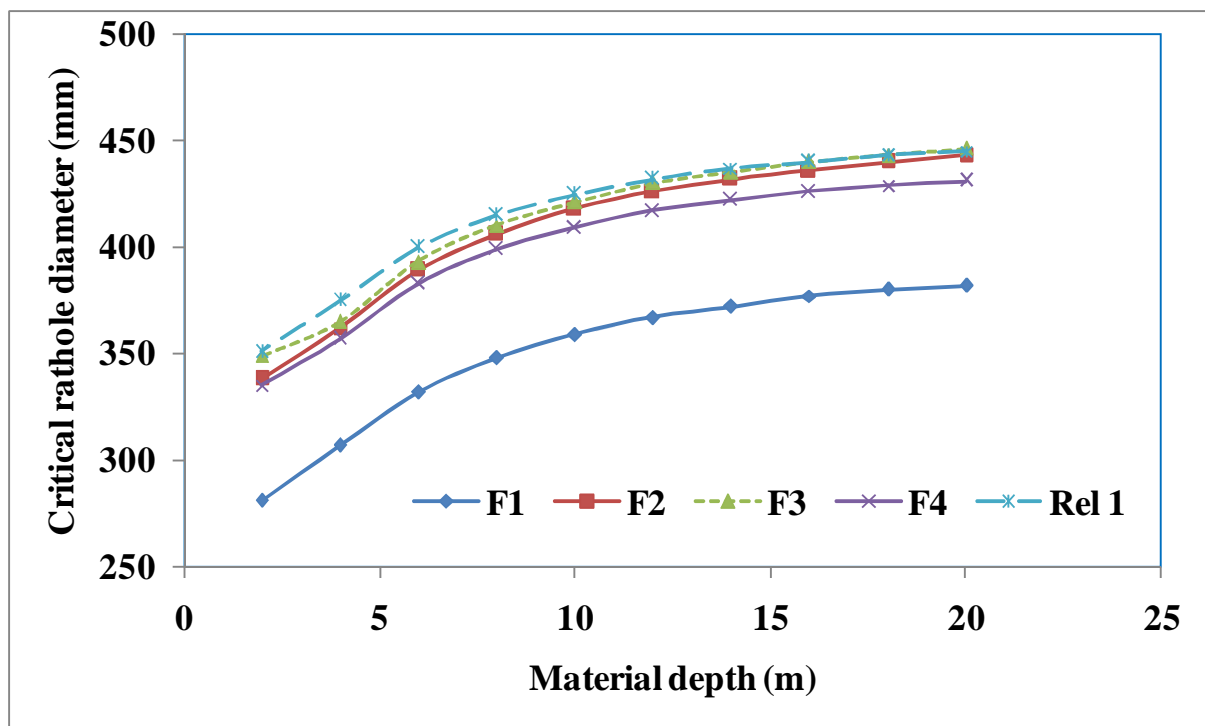


Figure 5.5: Critical rathole diameter profile for easy flowing fly ash

It can be observed that an easy flowing fly ash requires a maximum of 450 mm outlet opening to ensure the collapse of standpipe. Similarly, cohesive samples required maximum outlet opening of 942 mm to ensure continuous discharge (refer Fig. 5.6).

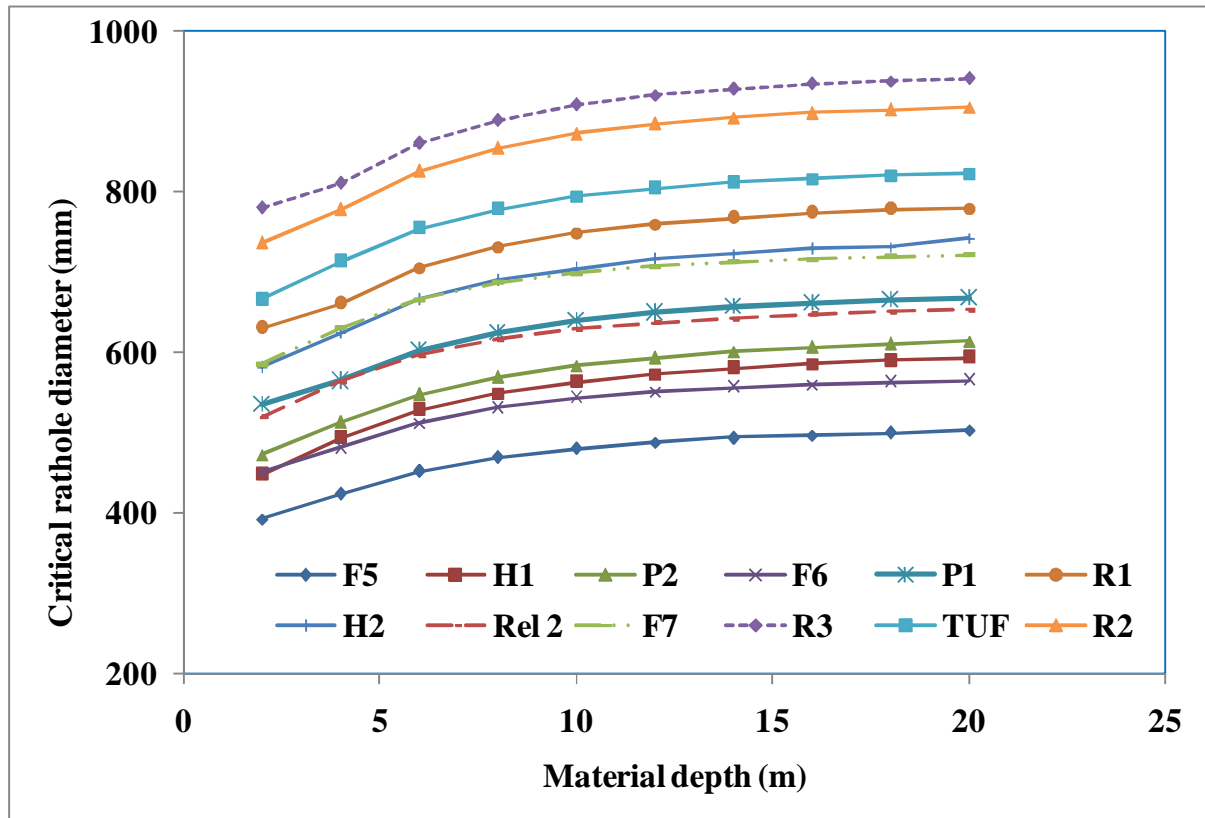


Figure 5.6: Critical rathole diameter for cohesive fly ash samples

Very cohesive samples can gain large strength after consolidation. This was also reflected in their rathole profile, the maximum outlet opening observed was 1232 mm diameter (refer Fig. 5.7). There was no particular trend found between flow index and rathole profile. The rathole diameter depends upon the wall friction characteristics and flow properties of fly ash. FI classification is only on the basis of the flow properties of fly ash and does not take the wall friction characteristics into account. The difference of the wall friction characteristics causes the difference in the rathole profile and hopper half angle for the mass flow hoppers as well.

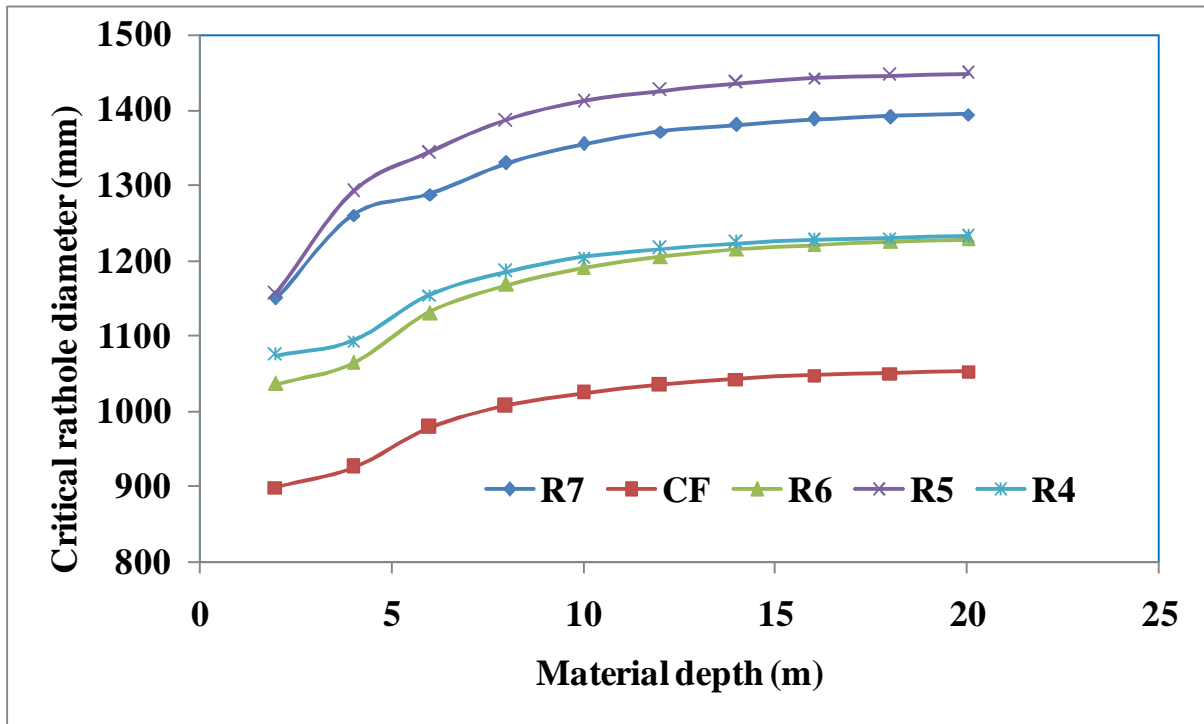


Figure 5.7: Critical rathole diameter for very cohesive fly ash

Chapter 6

Modelling of Cohesion and Unconfined Yield Strength for Fine Powders

6.1 Introduction

In this chapter we will discuss cohesion models for different fine powders. The magnitude of cohesion in the sample is the indicator of its flowability. Saw et al. (2013) proposed a model for the cohesion by incorporating the powder physical properties and ratio of the unconfined yield strength. This model gives very good predictions, but on the other has a major limitation also. Saw's model requires the ratio of the unconfined yield strength which can only be found after performing shear testing. Thus this model is partially helpful. In this study, shear testing has been performed over 25 fine powder samples and an attempt has been made to correlate powder physical properties with cohesiveness in the sample.

6.2 Existing correlation between particle physical properties and cohesion

6.2.1 Unconfined yield strength ratio model

Saw et al. (2013) gave an empirical model to show the effect of the particle physical properties on cohesion in a sample. The model proposed is given as Eq. (6.1).

$$C = m \left(\frac{\rho_b}{\rho_p d} \right)^a \left(\frac{\sigma_c}{\sigma_{c \min}} \right)^b \quad (6.1)$$

Where, C is the cohesion of the sample in Pa, ρ_b and ρ_p are the bulk density and particle density respectively in kg/m^3 , d is the particle size in μm . σ_c and $\sigma_{c \min}$ are the unconfined yield strength in Pa. Model constants m, a and b were found by regression analysis tool in MS Excel 2007. The new Eq. (6.2) formed after regression analysis is given as,

$$C = 591.04 \left(\frac{\rho_b}{\rho_p d} \right)^{0.408} \left(\frac{\sigma_c}{\sigma_{c \min}} \right)^{0.887} \quad [R^2 = 0.898] \quad (6.2)$$

The summary of the output from the results of regression analysis can be found in appendix B. The model was proposed by using the same equipment (PFT), so it was expected that the model will give good results. The R^2 value for the model tested over 25 powders was 0.898 which show that the model can predict for 89% of the data. The samples were classified as easy flowing, cohesive and very cohesive as described in the Table 3.1. Saw's model was evaluated at five pre shear stresses (stress 1 to stress 5) mentioned in chapter 3. Fig. 6.1 to 6.5 represents cohesion prediction by Eq. (6.2) at stress 1 to stress 5 respectively. It was observed that the Saw et al. (2013) model gives an error of $\pm 50\%$. The error boundaries representing $\pm 50\%$ have been demarcated in Fig. 6.1 to 6.5.

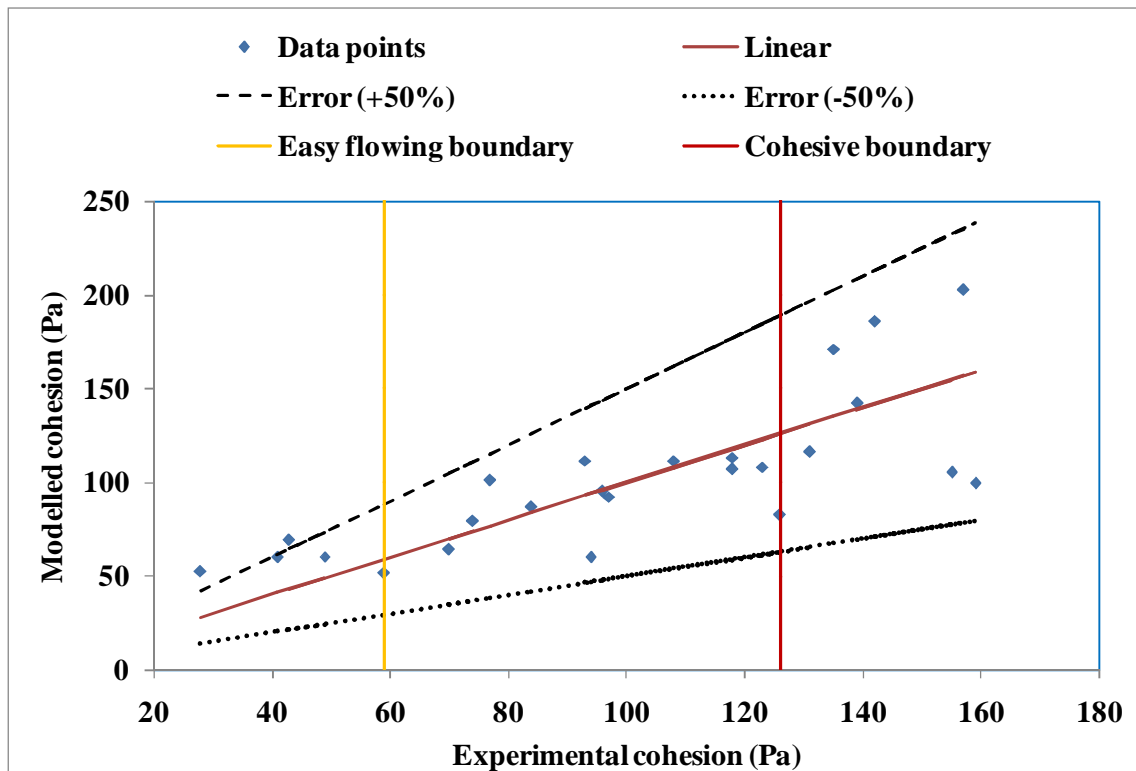


Figure 6.1: Comparison of experimental cohesion and modelled cohesion by using Saw et al. (2013) model at stress 1

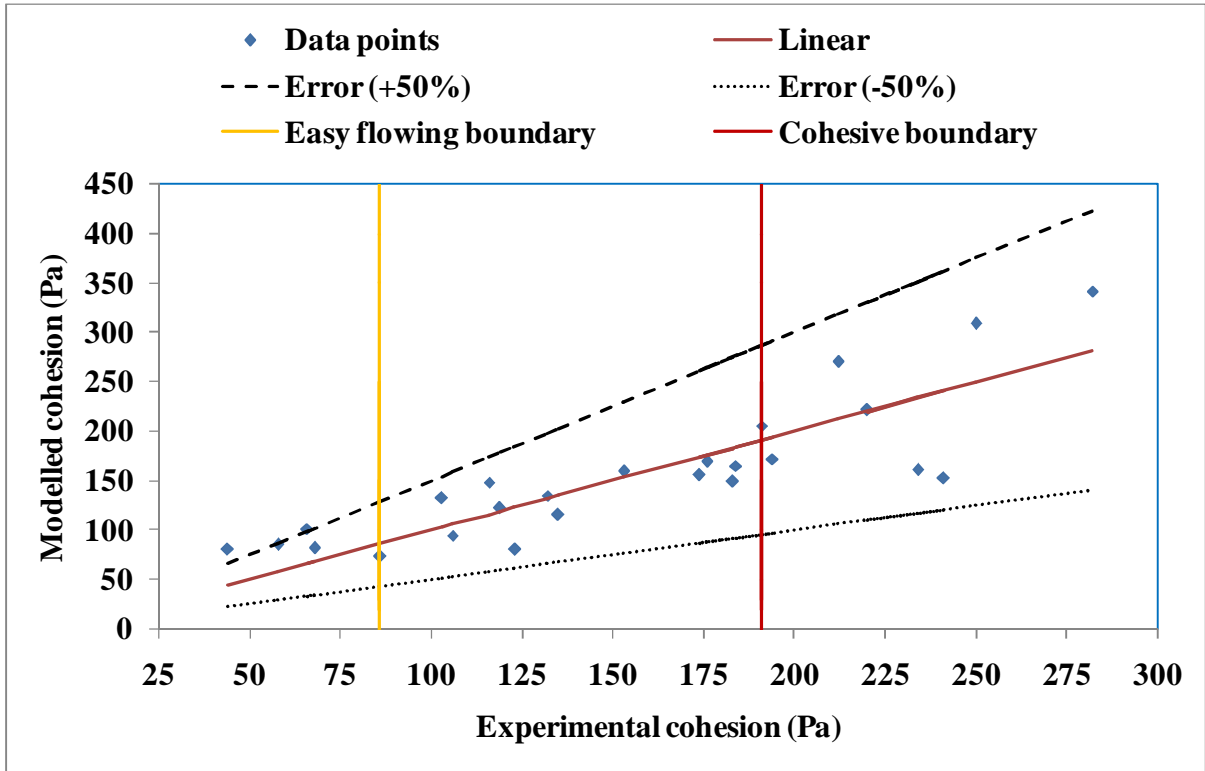


Figure 6.2: comparison of experimental cohesion and modelled cohesion by using Saw et al. (2013) model at stress 2

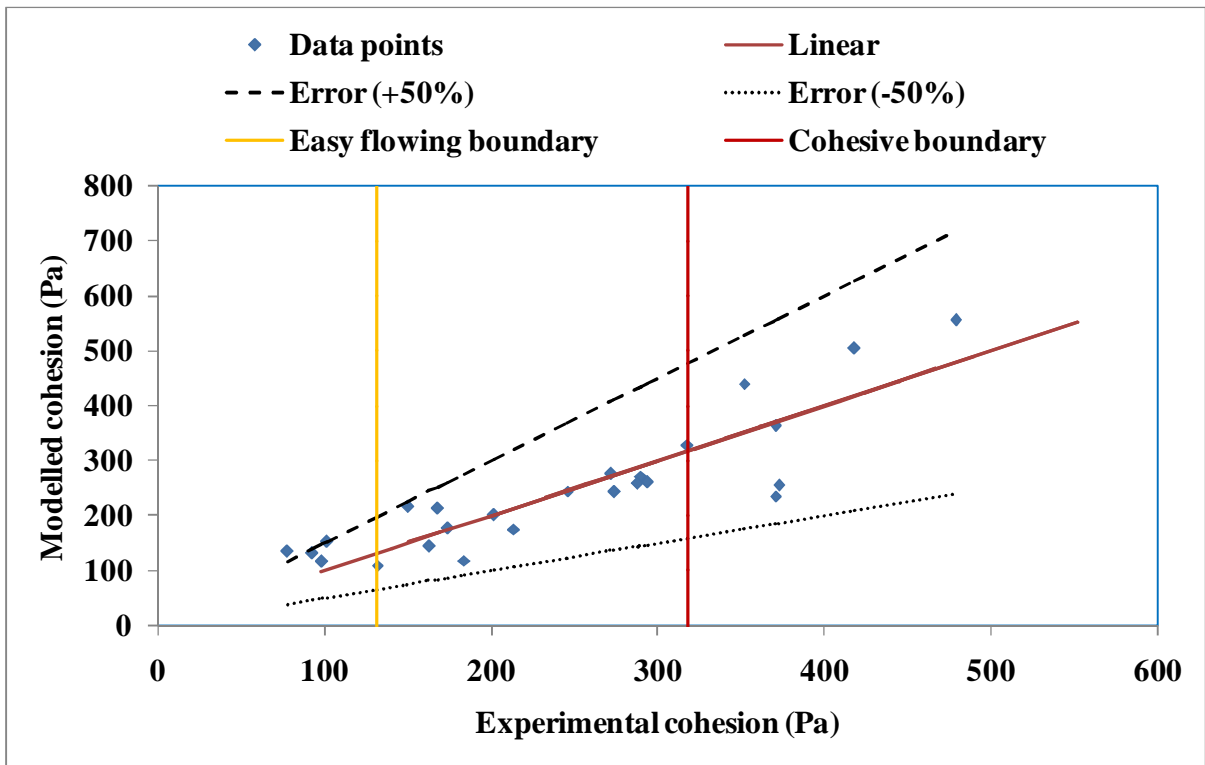


Figure 6.3: Comparison between experimental cohesion and modelled cohesion by using Saw et al. (2013) model at stress 3

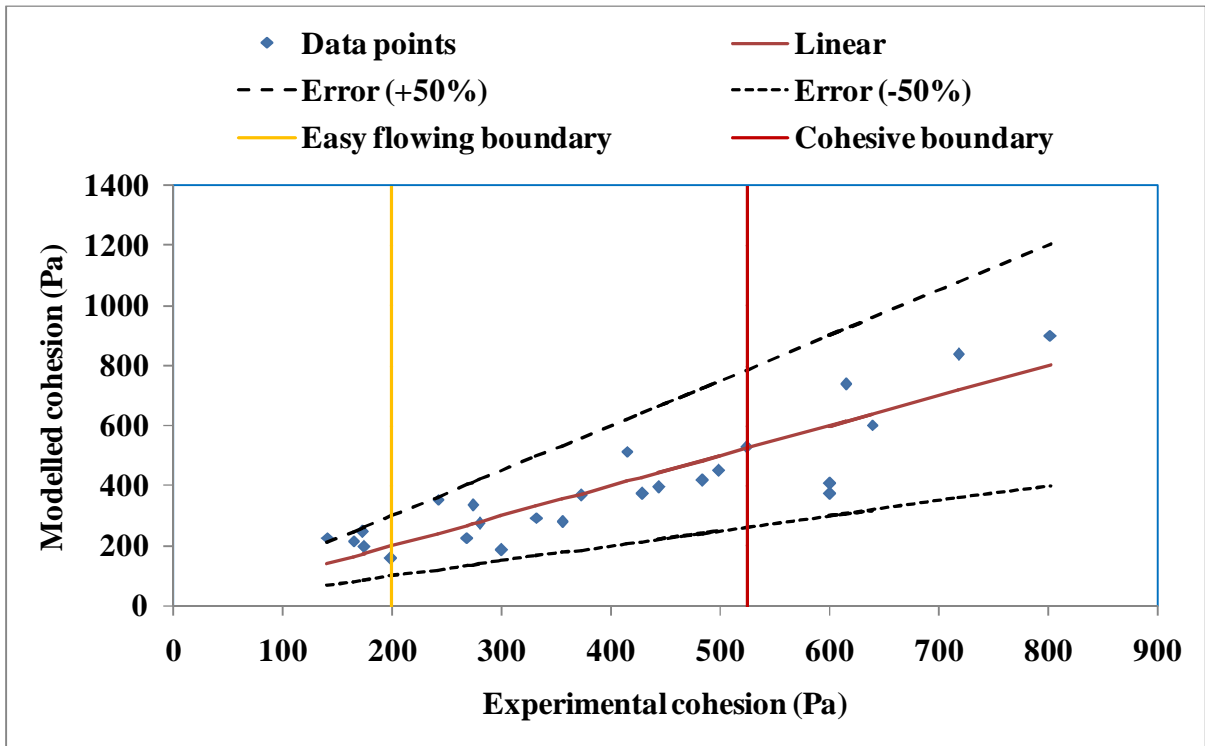


Figure 6.4: Comparison between experimental cohesion and modelled cohesion by using Saw et al. (2013) model at stress 4

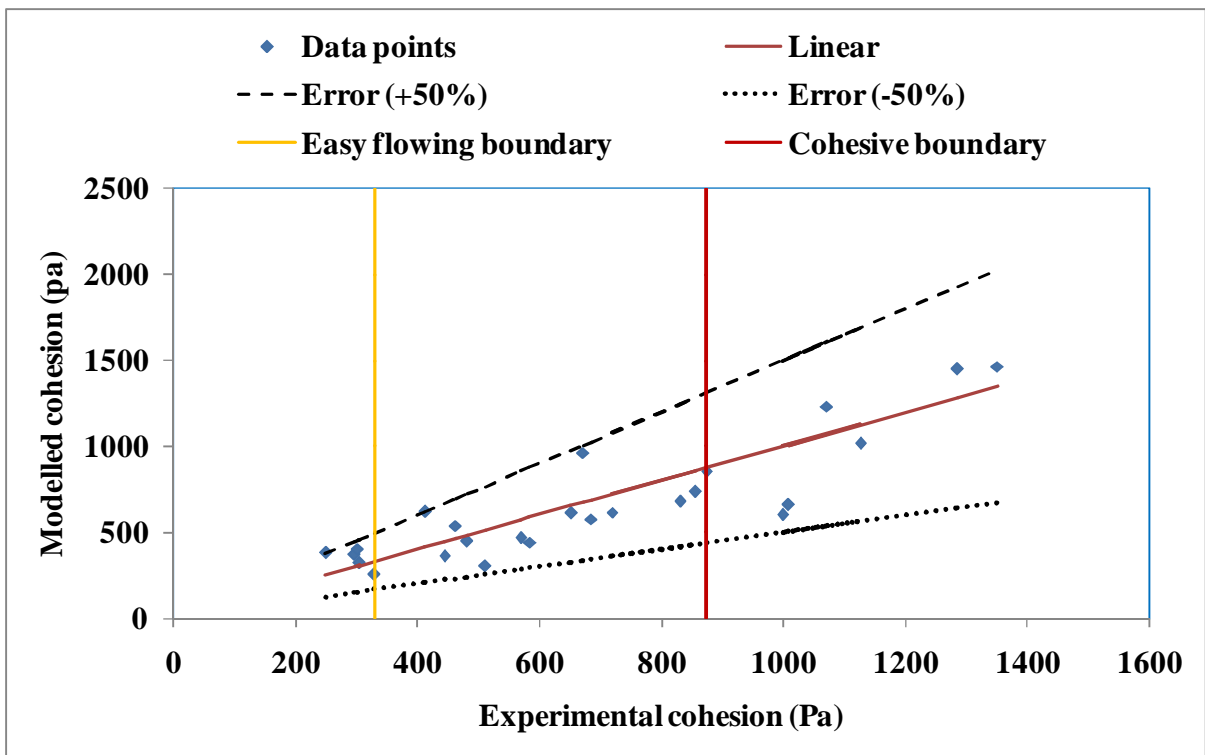


Figure 6.5: Comparison between experimental cohesion and modelled cohesion by using Saw et al. (2013) model at stress 5

The easy flowing boundary and the cohesive boundary have also been demarcated to separately evaluate the performance of the model for the fine powders having different flowability. It can be observed from Fig. 6.1 to 6.5 that Eq. (6.2) always gives an over prediction for the easy flowing samples with the maximum error up to 46.42 %. The predictions were slightly better at higher pre shear stresses with maximum error of 34.61% (refer Table 6.3 to 6.8). The model predicted well for cohesive samples, although both under predictions and over predictions were observed. The maximum error was less at lower pre shear stresses (maximum up to 24.10%) and higher at larger pre shear stresses (maximum up to 33.57%). Both under predictions and over predictions were found very cohesive samples as well. The maximum error observed was 59% for very cohesive samples. Some very good predictions can be observed for cohesive samples at stress 4 and stress 5. This observation implies that the model is well applicable for cohesive samples at pre shear stresses above stress 3. In general, it can be inferred from above observations that Saw et al. (2013) model gives an error of $\pm 50\%$ for predicting cohesion.

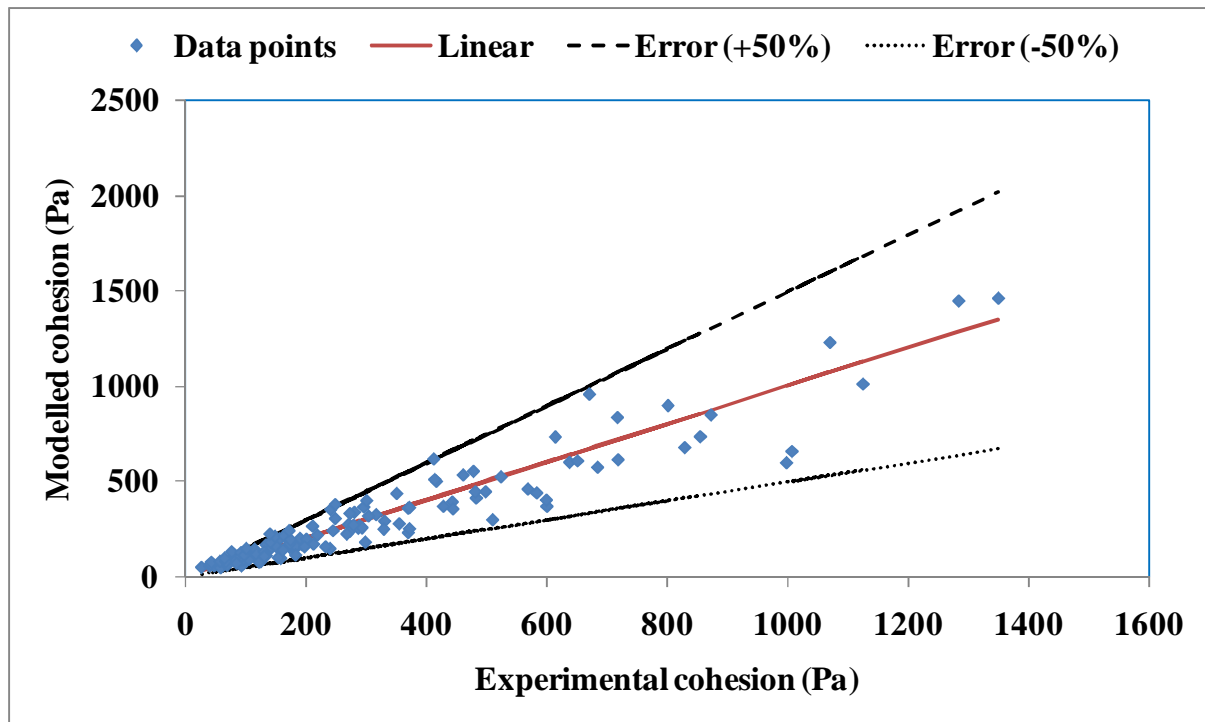


Figure 6.6: Comparison of experimental cohesion and modelled cohesion by using Saw et al. (2013) model at all the pre shear stresses

6.2.2 Trend line modelling technique based cohesion model

Saw et al. (2015) proposed another model for the cohesion by using trend line modelling technique. They used Hausner Ratio (HR) as the parameter to predict cohesion in 18 powders of different flowability. Firstly, power law base cohesion models were made at different pre shear stresses. The power law constants were dependent upon the pre shear stresses and were approximated by regression analysis. Finally, the modelled constants were substituted back to the final model. The model predicted by the final trend line modelling is given as Eq. (6.3).

$$C^* = \log[\sigma_{pre}^{0.6096 HR-0.7250}] + 0.4695 HR - 0.5180 \quad (6.3)$$

Where C^* (kPa) is the cohesion in sample predicted by using the HR at the different pre shear stresses (σ_{pre}). This model was also investigated for validity by using the HR of 25 different powders mentioned in Table 3.1. All the values were entered in an MS Excel sheet to find the difference between cohesion predicted by Eq. 6.3 and experimental values found by PFT. Figure 6.7 shows the comparison between two values at the lowest pre shear stress level (stress 1 = 0.318 kPa). It can be observed from that Eq. (6.3) under predicts cohesion with a large error percentage (75%). An absolute error was even larger at higher pre shear stresses. It can be inferred from this observation that the trend line modelling technique cannot provide an approximation for cohesion. The probable cause for a large error in the model could be its dependence on the powders used for modelling purpose. Another reason for the under prediction by the Saw et al. (2013) model was its assumption that cohesion varies linearly with HR which was not observed during the experiments. It can be concluded that Saw et al. (2013) model predicts better than Saw et al. (2015) model. The model has another limitation that it will predict the same cohesion for the powders having same HR. It was observed in this study that the powders with same HR can have different cohesion.

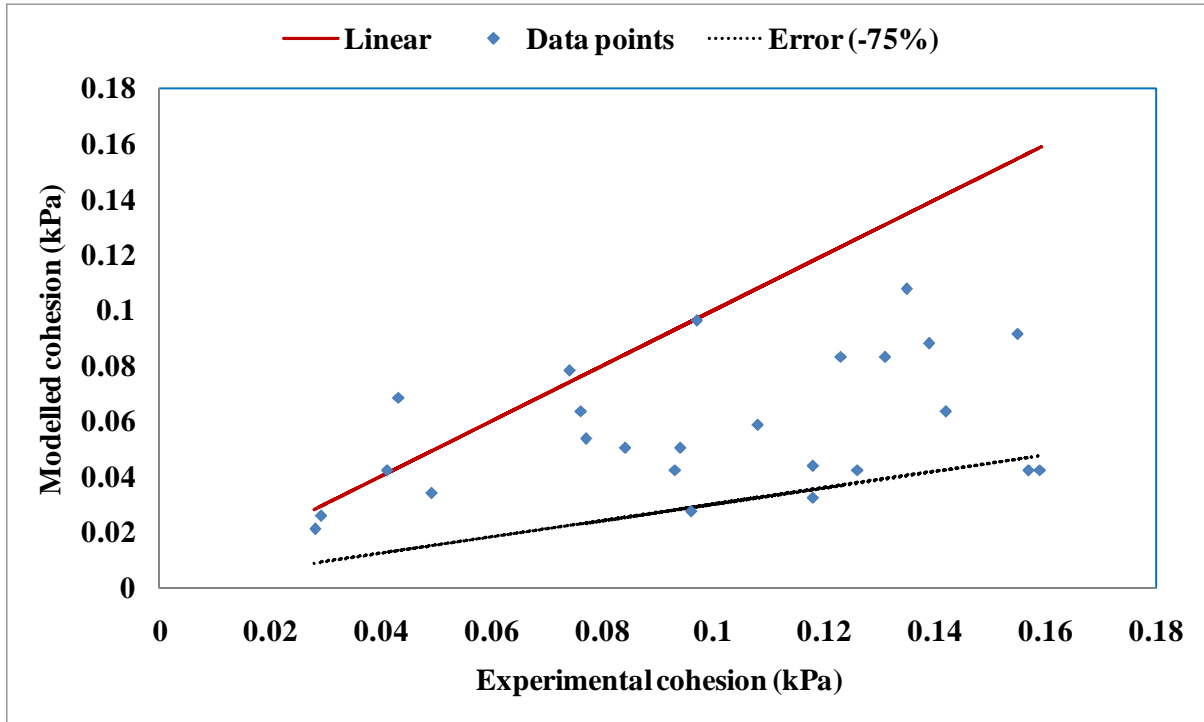


Figure 6.7: Comparison between experimental cohesion and modelled cohesion by using Saw et al. (2015) model at stress 1

6.3 Modelling cohesion on the basis of particle size distribution.

6.3.1 Particle size distribution model (PSD model)

The cohesion in the sample is dependent on particle size distribution, bulk density, tapped density and the pre-shear stress at which cohesion has been measured. A new parameter ‘D’ has been used to represent the span of particle size distribution in the model. The various parameters used in the model are reported in the Table 6.1. The format of the new model developed for predicting cohesion is given by Equation (6.4)

$$C = K (D)^a (CI)^b (\sigma_{pre})^c \tag{6.4}$$

The exponents of the model were determined by using experimental data obtained by using PFT. The final model Eq. (6.5) formed after regression analysis is,

$$C = 0.0555 (D)^{0.0779} (CI)^{1.1722} (\sigma_{pre})^{0.69185} \quad [R^2 = 0.9619] \quad (6.5)$$

The various stress levels or the pre-shear stresses used for the study have been reported again in the Table 6.2 for the sake of convenience.

Table 6.1: Particle size distribution model parameters for 25 tested powders

Samples	D ₁₀ (µm)	D ₅₀ (µm)	D ₉₀ (µm)	Span	Compressibility Index
				$\left[D = \frac{D_{90} - D_{10}}{D_{50}} \right]$	$\left[CI = \frac{\rho_t - \rho_b}{\rho_t} \times 100 \right]$
F1	42	139	316	1.97	8.2
F3	23	97	213	1.95	9.05
F2	23	102	235	2.07	9.93
F4	18	69	170	2.20	9.22
Rel1	38	126	170	1.04	11.33
F5	14	53	141	2.39	14.59
H1	16	87	238	2.55	14.57
P2	4	25	103	3.96	12.4
F6	12	41	108	2.34	15.09
P1	20	106	235	2.02	13.21
R1	6	28	120	4.07	17.17
H2	7	35	105	2.80	19.9
JK	3	19	49	2.42	17.37
Rel 2	5	48	170	3.43	15.65
F7	6	21	63	2.71	20.85
R3	2	17	111	6.41	21.81
TUF	3	19	140	7.21	27.16
R2	3	21	63	2.85	21.67
JKW	3	19	49	2.42	19.23
R7	1	4	33	8	22.79
CF	4	22	83	3.59	23.94
R6	1	4	25	6	22.04
CC	3	19	75	3.78	25.63
R5	1	4	29	7	22.82
R4	1	8	69	8.5	29.67

Table 6.2: Pre-shear stress level and magnitude

S.No	Stress levels	Stress Magnitude (kPa)
1	Stress level 1	0.316
2	Stress level 2	0.611
3	Stress level 3	1.206
4	Stress level 4	2.411
5	Stress level 5	4.846

6.3.2 Physical significance of model parameters

Cohesion has been modelled by using three parameters namely, Particle size distribution span (D), compressibility index (CI) and pre shear stress (σ_{pre}). The span of particle size distribution is a statistics term used to describe the relative width of the particle size distribution. It was observed that cohesive samples had large span as compared to free flowing samples. Large span size refers to availability of particles of all possible particle sizes in some fraction. These fine particles can accommodate in all the voids formed in the powder and increase compactness of the sample. Fine particles increase intermolecular forces and hence bulk cohesion in the sample. Compressibility index (CI) incorporates tapped density (ρ_t) found at 4.186 kPa normal load and loose pour bulk density (ρ_b). Any change in physical property or flowability of the sample is represented by change in its compressibility index. It was observed during the experiments that cohesive samples had higher CI as compared to freely flowing samples. Cohesion in the sample increases with normal stress on the sample. Pre shear stress (σ_{pre}) represents the normal stress used to homogenise the material before conducting shear tests. The combination of D and CI can model cohesion for any sample. It is very rare that any sample has same D and CI but different flowability or cohesion.

6.3.3 Relative importance of the model parameters

It can be observed from Eq. (6.6) that all the exponents are positive which shows that all the selected parameters of the model have positive effect (directly proportional) on the magnitude of cohesion. Compressibility index (CI) had the highest effect on cohesion followed by pre shear stress (σ_{pre}) and span (D). The particle size distribution of the sample remains the same provided that there is no attrition in the sample. In such cases, the parameters which affect the

cohesion are CI and pre shear stress. Change in the flow properties of the sample due to factors like moisture content, temperature etc will affect CI of the sample. Doubling the CI will result in increased cohesion roughly by 2.25 times. Similarly, doubling the normal stress on the sample will increase the cohesion by 1.61 times.

6.3.4 Evaluation of applicability and error in the model

Figure 6.8 to 6.12 shows the comparison between experimental cohesion and modelled cohesion by using the newly developed particle size distribution (PSD) based model. The newly developed PSD model has substantially reduced the error in predicting cohesion. Saw et al. (2013) model gives the maximum error of $\pm 50\%$ while PSD model has $\pm 30\%$ maximum error in predicting cohesion. The new model gives 20% more accurate predictions as compared to Eq. (8.2). The model gives an accurate prediction for free flowing samples especially at the higher pre shear stresses (Refer Table B.1 to B.5 in appendix B). There were both under predictions and over predictions for cohesive and very cohesive samples. The maximum over prediction and under prediction for cohesive sample was 26.58% and 29.35% respectively. The model gives fairly accurate results for very cohesive samples and the maximum error was 15.17% only. Fig 5.16 represents the maximum error boundary of $\pm 30\%$ for predictions by PSD based model. It can be observed by comparing Fig. 6.6 and Fig. 6.13 that the scatter in PSD based model is lesser as compared to Saw et al. (2013) model. The R^2 value for PSD based model is higher than Saw et al. (2013) model. The model is applicable for easy flowing and cohesive samples although it can give good predictions for some very cohesive samples also.

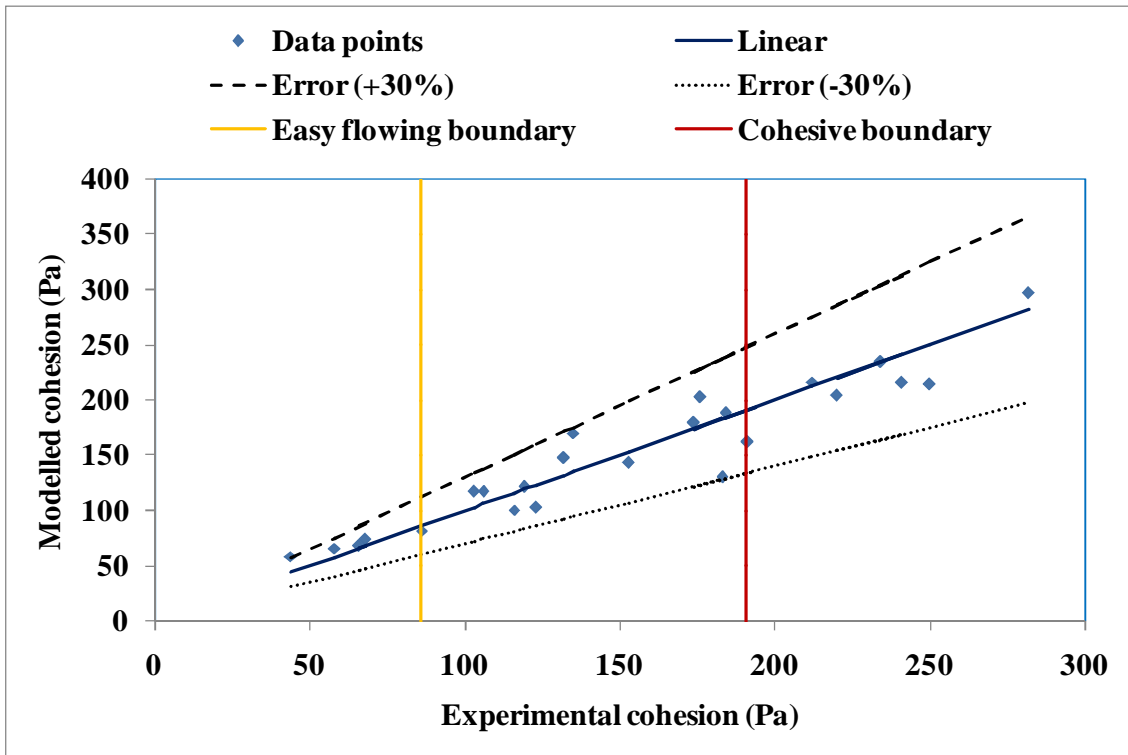


Figure 6.8: Comparison of experimental cohesion and modelled cohesion by using newly developed particle size distribution model at stress 1

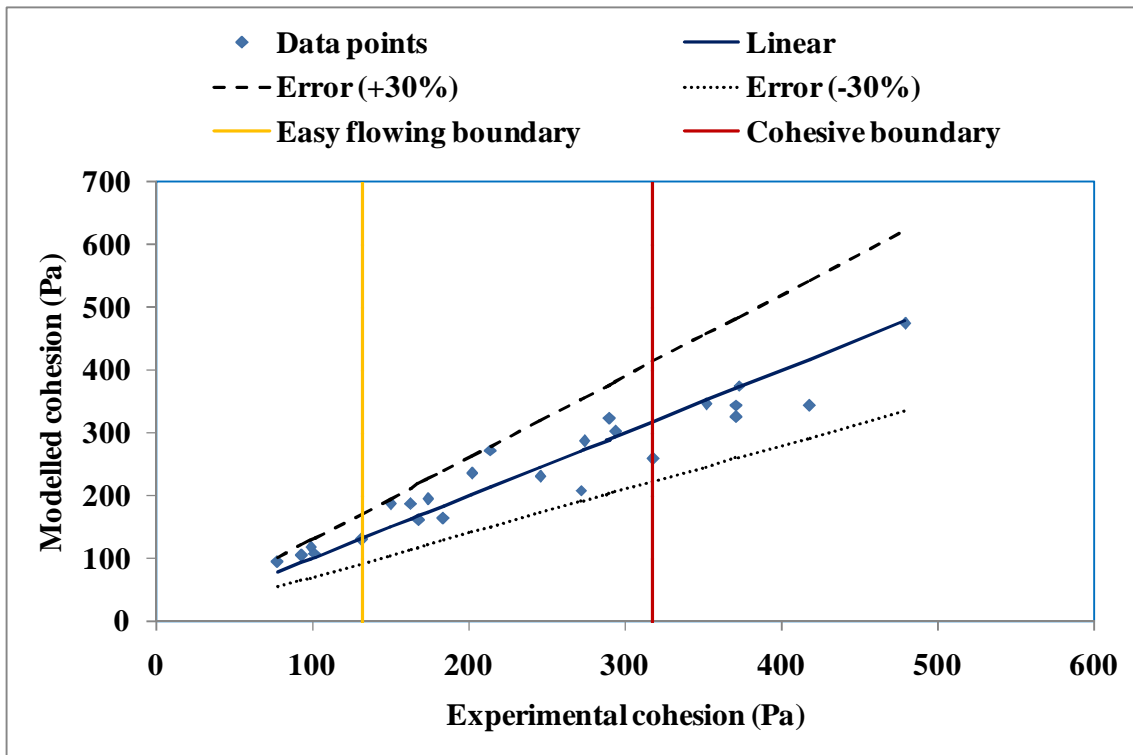


Figure 6.9: Comparison between experimental cohesion and modelled cohesion by using newly developed particle size distribution model at stress 2

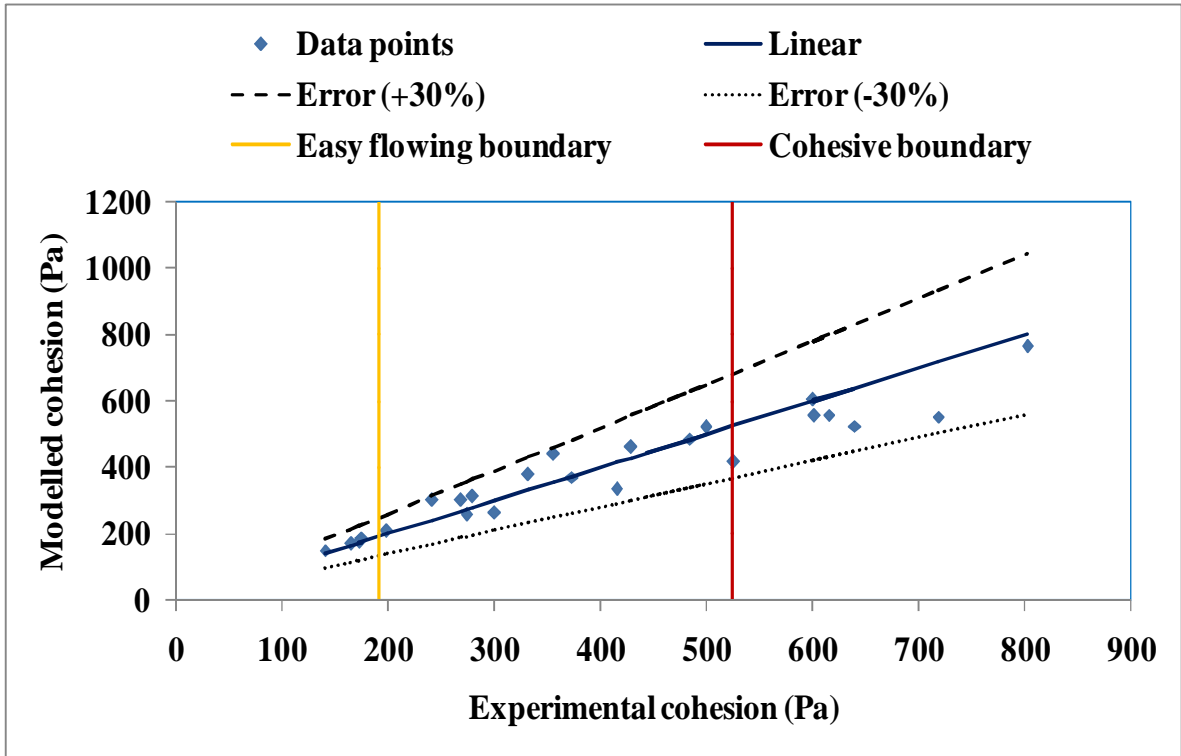


Figure 6.10: Comparison between experimental cohesion and modelled cohesion by using newly developed particle size distribution model at stress 3

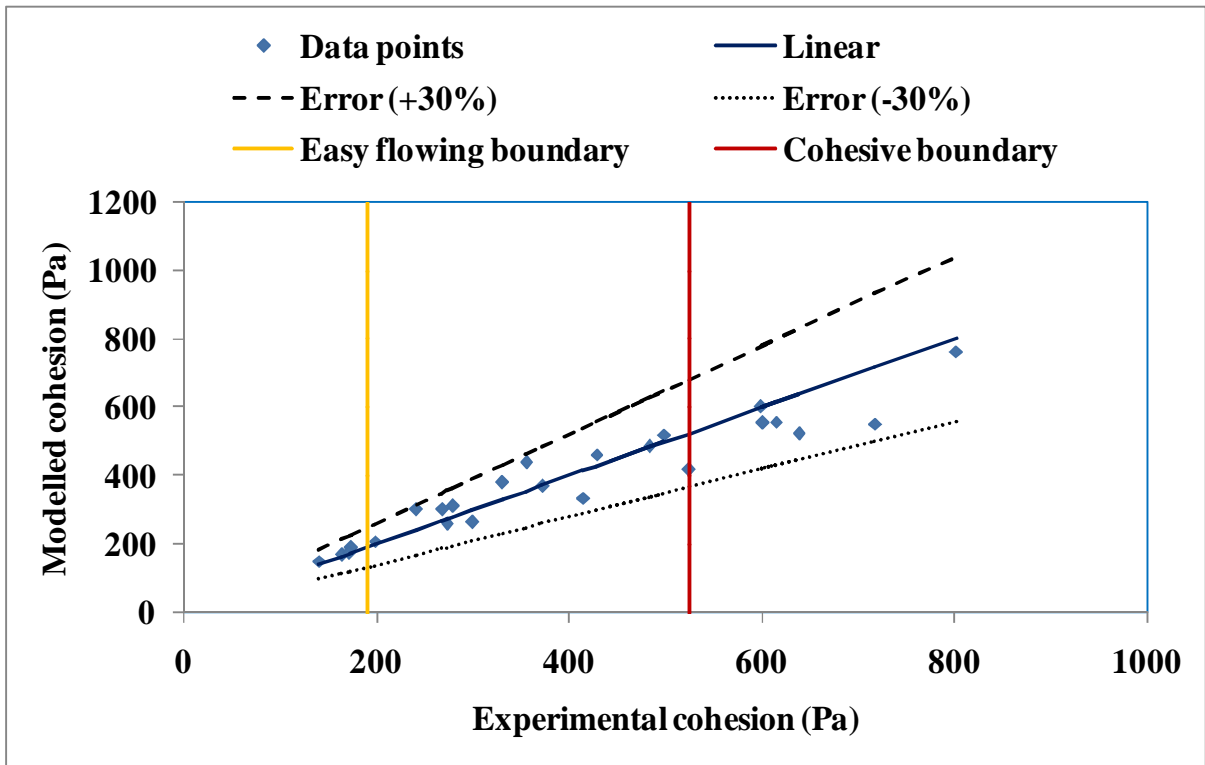


Figure 6.11: Comparison between experimental cohesion and modelled cohesion by using newly developed particle size distribution model at stress 4

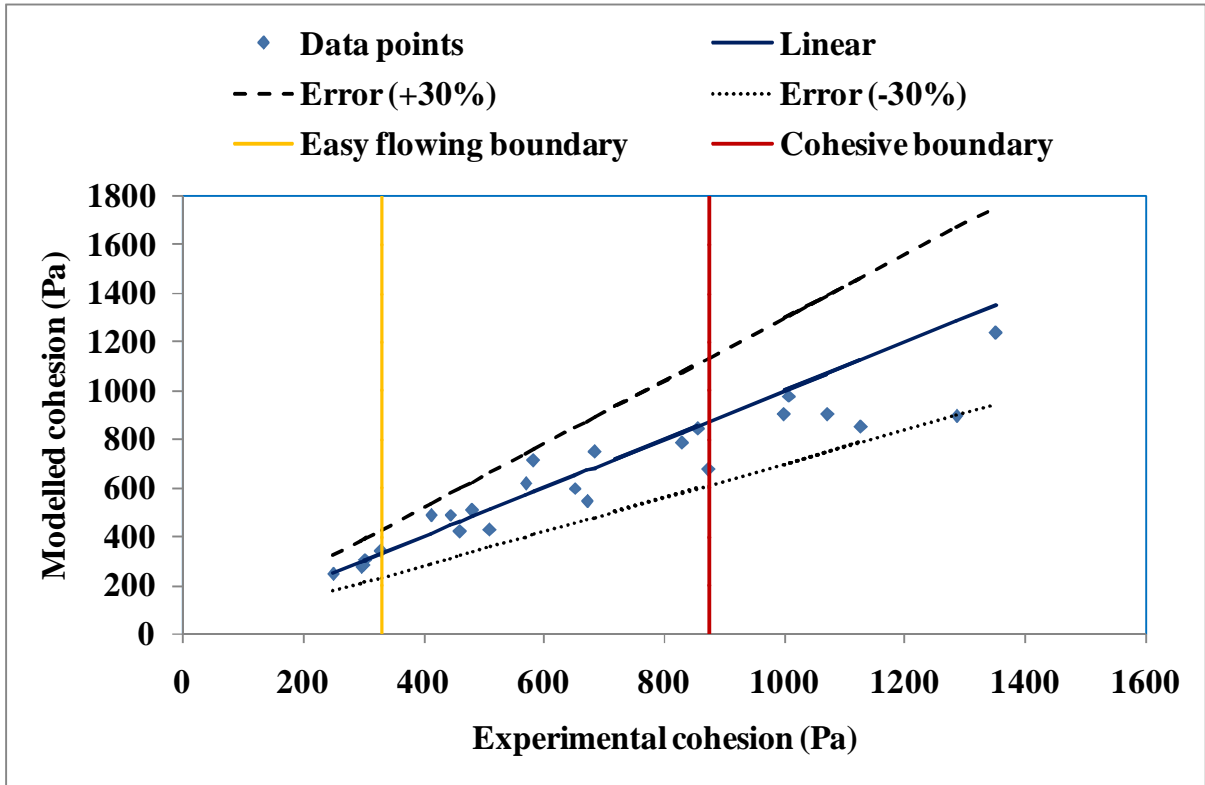


Figure 6.12: Comparison between experimental cohesion and modelled cohesion by using newly developed particle size distribution model at stress 5

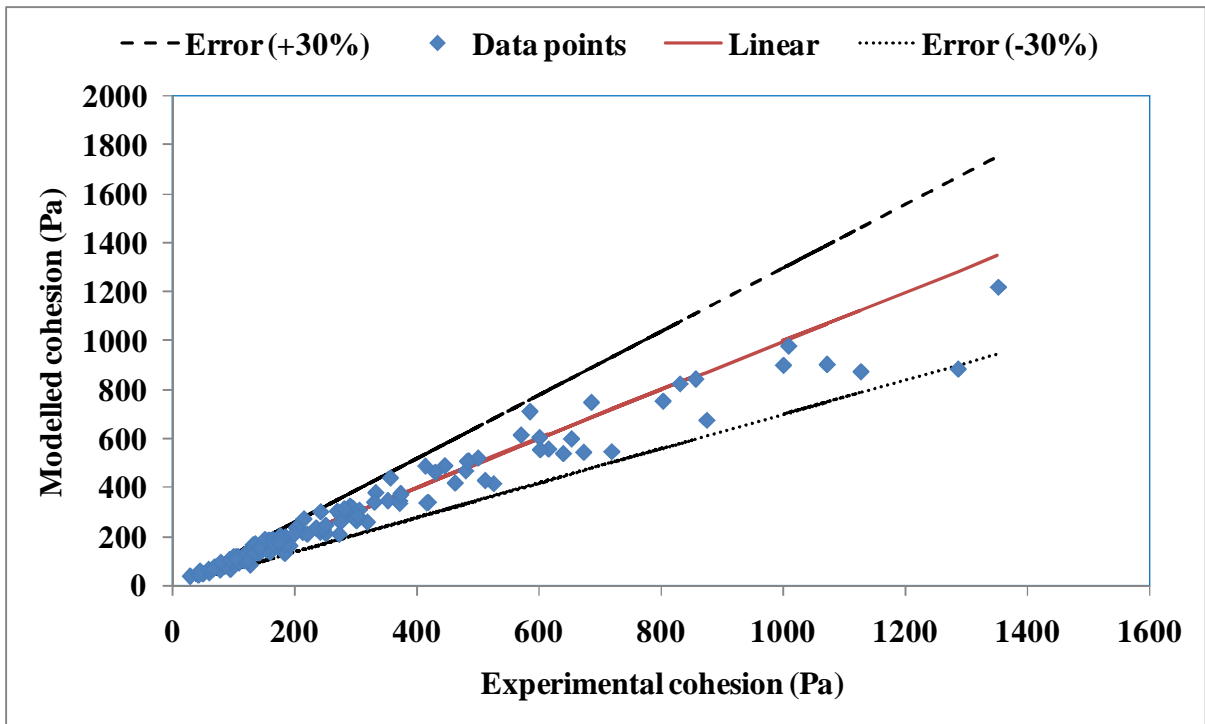


Figure 6.13: Comparison of experimental cohesion and modelled cohesion by using particle size distribution based model at stress 1 to stress 5

6.4 Modelling Unconfined yield strength by using particle size distribution

The cohesion is the intercept made by yield locus on ordinate in σ - τ curve at a particular σ_{pre} . On the other hand, the unconfined yield strength of the powder is defined as compressive stress necessary to cause incipient failure in the powder column which has been consolidated under a known normal load. Both these parameters are used to access the flowability characteristics of powders. Very good correlation was found between C and σ_c ($R^2 = 0.99$) as shown in Fig. 6.14. It can be inferred from this observation that σ_c can be modelled by using similar parameters to access the flowability of the powders. The proposed model for unconfined yield strength is given in Eq. (6.6).

$$\sigma_c = 0.0281 (D)^{0.056} (CI)^{1.099} (\sigma_{pre})^{0.729} \quad [R^2 = 0.965] \quad (6.6)$$

Fig. 6.15 to 6.17 reports the comparison of modelled and experimental σ_c at all pre shear stresses. It can be observed that the maximum error range predicted by Eq. (6.6) is $\pm 25\%$ which is slightly better than Eq. (6.5).

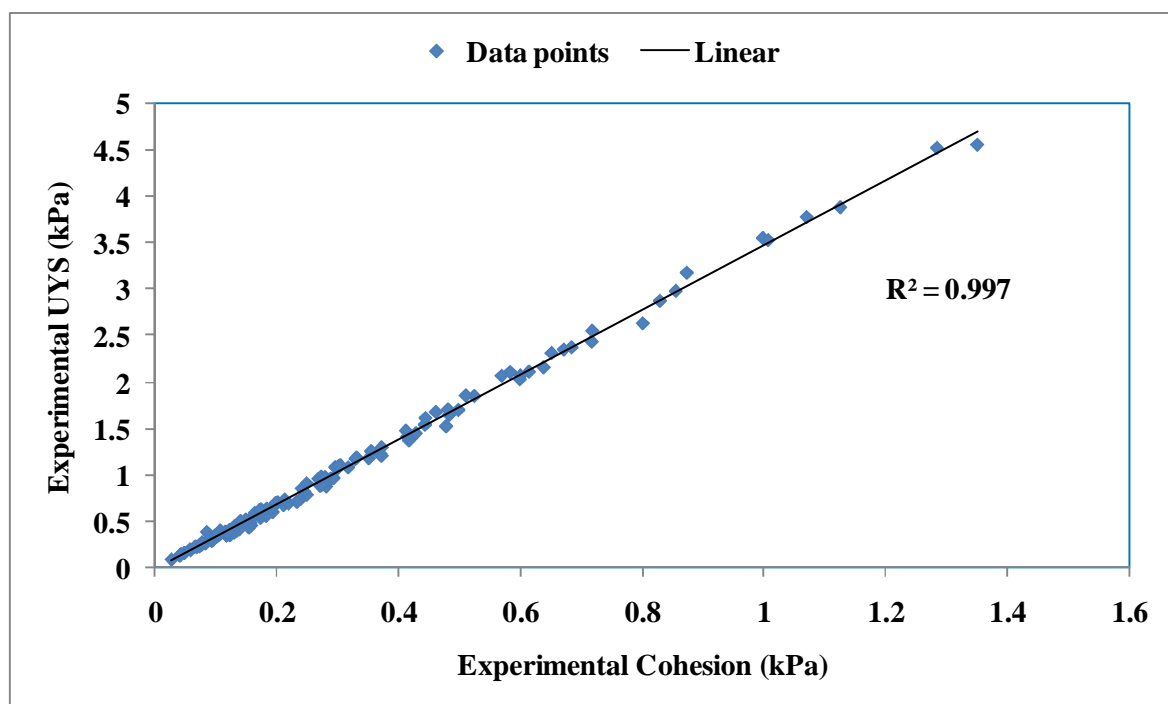


Figure 6.14: Comparison of Experimental cohesion and unconfined yield strength at all σ_{pre} .

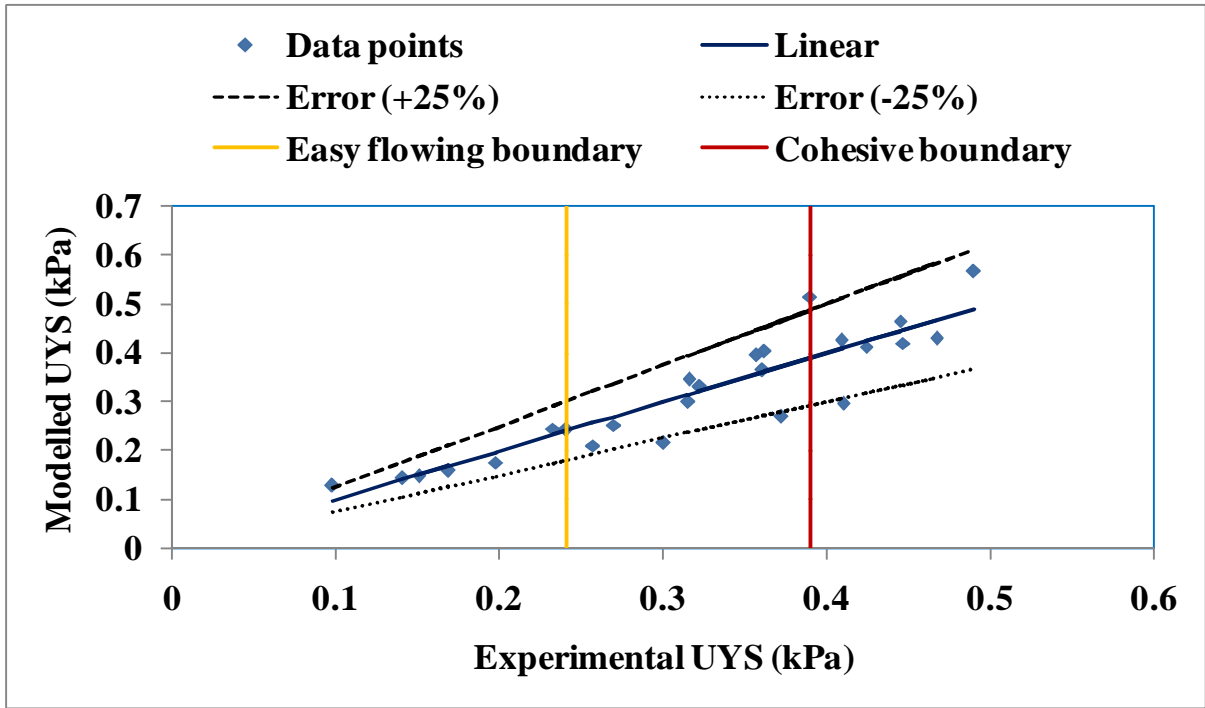


Figure 6.15: Comparison of experimental and modelled unconfined yield strength (UYS) at stress1

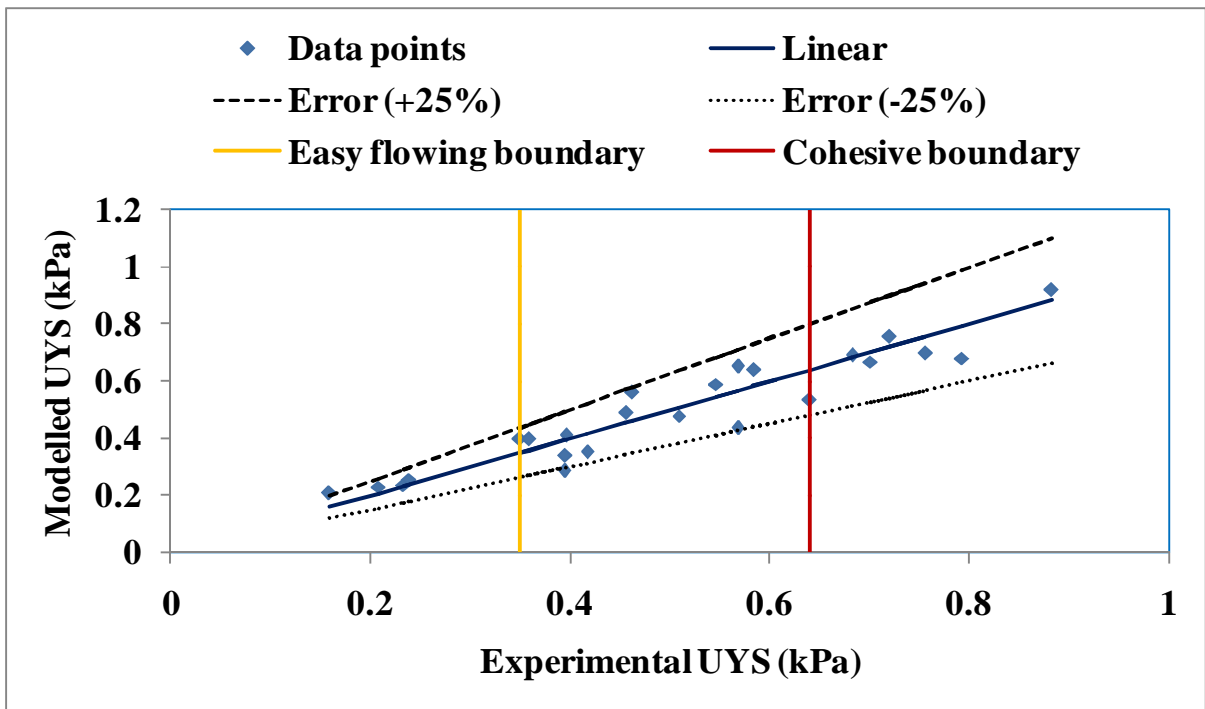


Figure 6.16: Comparison of experimental and modelled unconfined yield strength (UYS) at stress 2

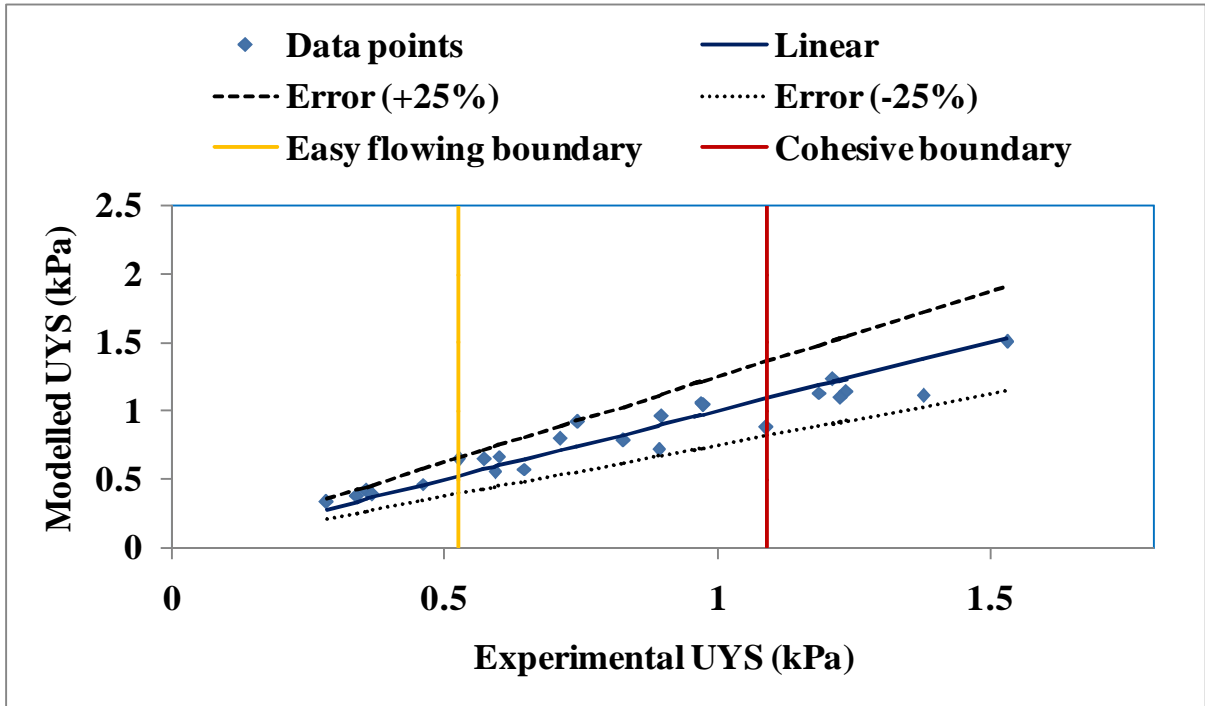


Figure 6.17: comparison of experimental and modelled unconfined yield strength (UYS) at stress 3

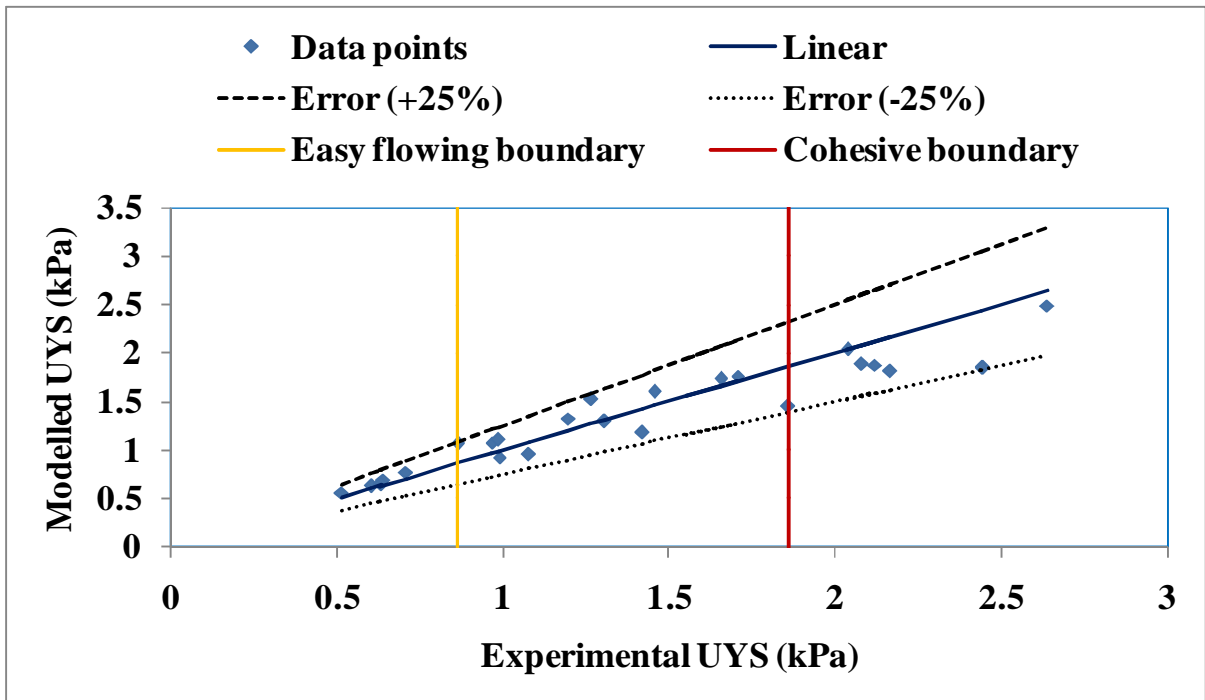


Figure 6.18: Comparison of experimental and modelled unconfined yield strength (UYS) at stress 4

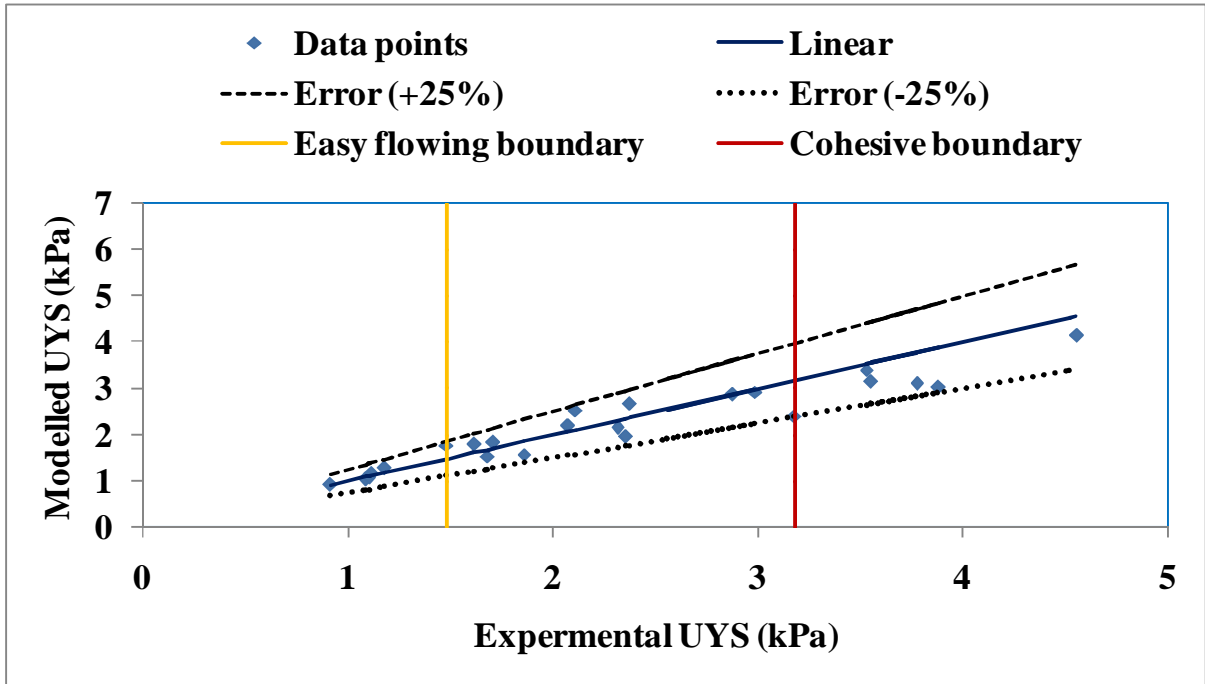


Figure 6.19: Comparison of experimental and modelled unconfined yield strength (UYS) at stress 5

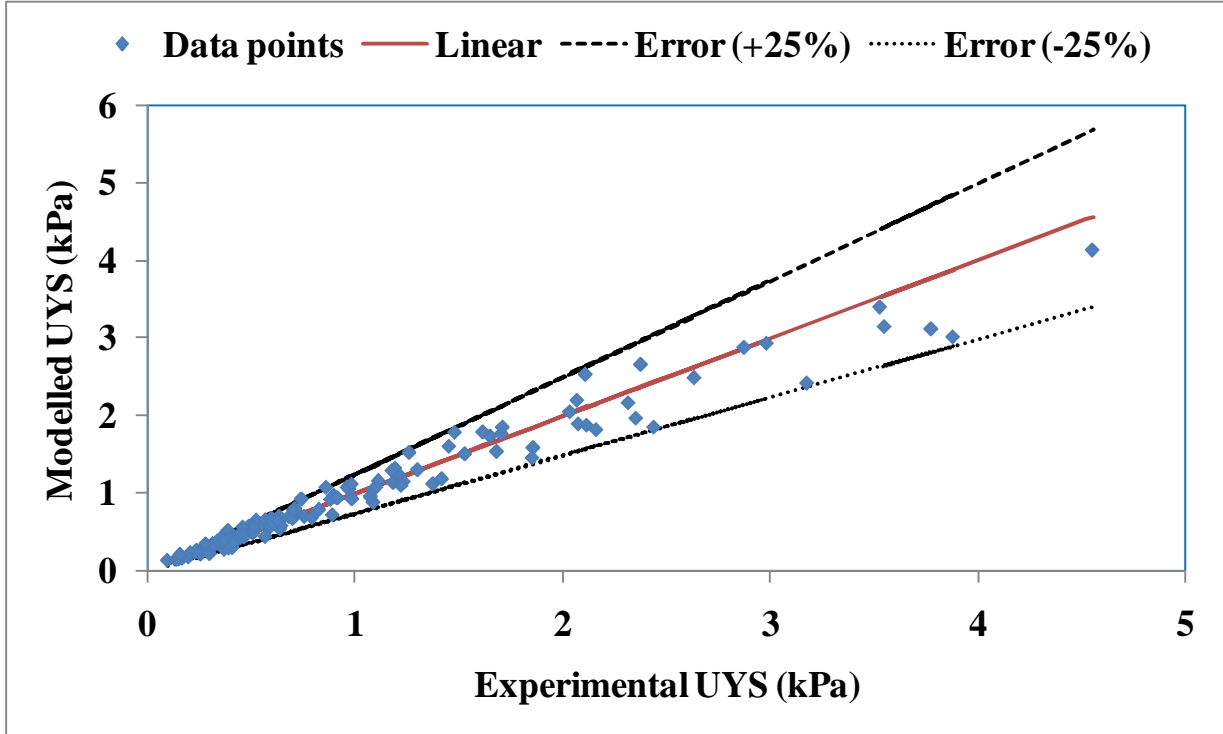


Figure 6.20: comparison of experimental and modelled unconfined yield strength at all pre shear stresses

6.5 Comparison of maximum and minimum error in the models

The table (6.3) reports the maximum and the minimum error observed in different models at $\sigma_{pre} = 1.2$ kPa. Error in the models was evaluated by Eq. (6.7).

$$Error \% = \frac{Model-Experimental}{Model} \times 100 \quad (6.7)$$

It was observed that Saw et al. (2013) model (Eq. 6.2) gives an error up to 46.72%, 56.84% and 59.80% for the easy flowing, cohesive and very cohesive samples respectively. This correlation moreover requires ratio of unconfined yield strength making the shear testing compulsory to access the flowability characteristics of the powder. Newly developed cohesion PSD based model (Eq. 6.5) shows significant improvement from Eq. (6.2) in predicting cohesion. The model predicts well for easy flowing powders giving the maximum error of 24.19%. Saw et al. (2015) modelled cohesion by using trend line modelling technique and their correlation was showing error up to 127% for easy flowing powders. Eq. (6.5) predicts better and hence can be used to predict cohesion in easy flowing powders. Similarly the model also performed better for cohesive and very cohesive samples with an error of 24.28% and 13.53% respectively. Newly developed UYS model (Eq. 6.6) showed further improvement from PSD base cohesion model (Eq. 6.5) which can be observed from Table 6.3. Error range further reduced for easy flowing powders by using Eq. (6.7). Refer appendix C for the error analysis in UYS model at all pre shear stresses. Both newly developed models perform better than previously existing model Saw's model (Eq. 6.2).

Table 6.3: Maximum and Minimum error in models at $\sigma_{pre} = 1.2$ kPa

Flowability classification	Saw's Cohesion model (Eqn. 6.2)		New cohesion model (Eqn. 6.5)		New UYS model (Eqn. 6.6)	
	Maximum	Minimum	Maximum	Minimum	Maximum	Minimum
Easy flowing	46.72%	-13.45%	24.19%	-14.24%	23.58%	-6.44%
Cohesive	24.10%	-56.84%	21.67%	-20.93%	24.28%	-22.23%
Very cohesive	-47.40%	-59.80%	15.17%	-16.37%	13.53%	-8.53%

Chapter 7

Conclusion and Future Scope

7.1 Conclusion

The flow properties and the physical properties of the fly ash were investigated in this thesis. Seven fly ash samples were collected directly from ESP hoppers to study their flow properties by using the Powder Flow Tester (PFT). It was observed that fly ash collected from initial stages of ESP (F1 to F4) was of the easy flowing nature while the fly ash from later stages (F5 to F7) was of cohesive nature. The transition particle size after which the flowability of fly ash changed from easy flowing to cohesive was identified experimentally by using Jenike (1964) flowability classification and compaction dynamics. The change in the flowability was due to large magnitude of net intermolecular forces as compared to the weight force of a particle. All flow properties like angle of internal friction, cohesion, unconfined yield strength etc, showed asymptotic nature after transition particle size of 53 μm (F5 sample). It was also observed during the experiments that fine or cohesive samples have different compaction trends as compared to the coarse or easy flowing samples. Effect of flow properties of twenty two available fly ash samples on the hopper geometry was evaluated. The samples were classified as easy flowing, cohesive and very cohesive and their feasibility to flow from an ESP hopper of specified dimensions was observed. It was found that only easy flowing samples have the capability to discharge completely under gravity for an ESP hopper while the rest of the fly ash samples require some discharge aids. A qualitative idea about the aeration rate necessarily has also been given on the basis of minimum fluidisation velocity and permeability factor. The minimum fluidisation velocity was the highest for seventh fly ash field sample which implies that more aeration rate will be necessary to achieve continuous discharge. It was found that all the samples do not require the same aeration rate which is generally the practice in industries. A new cohesion model based on the particle size distribution for predicting cohesion in fine samples was developed which showed a good correlation with experimental data as compared to the Saw et al. (2013) model. Another new model for the unconfined yield strength has been proposed which gives an error of $\pm 25\%$ with experimental data. This new model can be used to access the

flowability ranking of the powder. The new models use only the powder physical properties eliminating the need to conduct full shear testing of powder.

7.2 Future Scope

This thesis was an attempt to explain the bulk behaviour of the powders by using the physical properties. Cohesion in the sample has been successfully modelled by using the powder physical properties with the help of regression analysis. A major effort in this thesis has been devoted to the shear testing and the data collection of the different fine powders. The powder characterization and the powder flow properties have very large application and one thesis certainly cannot address all the issues related to the powder flowability. Further work on the powder flow properties can include the following areas.

1. Using Atomic Force Microscope to identify intermolecular forces and their effect on the bulk behaviour of the powders.
2. The minimum aeration rate necessary in wedge shaped ESP hoppers for evacuating fine powders can be investigated.
3. The numerical simulation of the mass flow, funnel flow pattern and the hopper discharge can be performed and can be validated with the experimental data provided in this thesis.

References

- Abdullah, E.C. and Geldart, D., 1999. The use of bulk density measurements as flowability indicators. *Powder Technology*, 102(2), pp.151-165.
- Arnold, P.C., McLean, A.G. and Roberts, A.W., 1980. Bulk solids: storage, flow and handling. TUNRA. Bulk solids handling research associates. University of Newcastle, Australia.
- Bian, Q., Sittipod, S., Garg, A. and Ambrose, R.K., 2015. Bulk flow properties of hard and soft wheat flours. *Journal of Cereal Science*, 63, pp.88-94.
- Cannavacciuolo, A., Barletta, D., Donsì, G., Ferrari, G. and Poletto, M., 2009. Arch-Free flow in aerated silo discharge of cohesive powders. *Powder Technology*, 191(3), pp.272-279.
- Capece, M., Ho, R., Strong, J. and Gao, P., 2015. Prediction of powder flow performance using a multi-component granular Bond number. *Powder Technology*, 286, pp.561-571.
- Castellanos, A., 2005. The relationship between attractive interparticle forces and bulk behaviour in dry and uncharged fine powders. *Advances in Physics*, 54(4), pp.263-376.
- Chawla, A. (2014). An Investigation Into Effect of Variation of Particle Size on Fluidization and Deaeration Characteristic to Access Fluidised Dense Phase Pneumatic Conveyability, M.E Thesis, Thapar University, Patiala.
- Chirone, R., Barletta, D., Lettieri, P. and Poletto, M., 2016. Bulk flow properties of sieved samples of a ceramic powder at ambient and high temperature. *Powder Technology*, 288, pp.379-387.
- Colbert, M.J., Grandbois, M. and Abatzoglou, N., 2015. Identification of inter-particle forces by atomic force microscopy and how they relate to powder rheological properties measured in shearing tests. *Powder Technology*, 284, pp.396-402.

- Danjo, K., Kinoshita, K., Kitagawa, K.A., Iida, K., Sunada, H. and Otsuka, A., 1989. Effect of particle shape on the compaction and flow properties of powders. *Chem Pharm Bull*, 37(11), pp.3070-3.
- Fitzpatrick, J.J., Barringer, S.A. and Iqbal, T., 2004. Flow property measurement of food powders and sensitivity of Jenike's hopper design methodology to the measured values. *Journal of Food Engineering*, 61(3), pp.399-405.
- Freeman, R., 2007. Measuring the flow properties of consolidated, conditioned and aerated powders—a comparative study using a powder rheometer and a rotational shear cell. *Powder Technology*, 174(1), pp.25-33.
- Ganesan, V., Rosentrater, K.A. and Muthukumarappan, K., 2008. Flowability and handling characteristics of bulk solids and powders—a review with implications for DDGS. *biosystems engineering*, 101(4), pp.425-435.
- Geldart, D., Abdullah, E.C. and Verlinden, A., 2009. Characterisation of dry powders. *Powder Technology*, 190(1), pp.70-74.
- Iqbal, T. and Fitzpatrick, J.J., 2006. Effect of storage conditions on the wall friction characteristics of three food powders. *Journal of Food Engineering*, 72(3), pp.273-280.
- Jager, P.D., Bramante, T. and Luner, P.E., 2015. Assessment of Pharmaceutical Powder Flowability using Shear Cell-Based Methods and Application of Jenike's Methodology. *Journal of pharmaceutical sciences*, 104(11), pp.3804-3813.
- Jenike, A.W., 1964. Storage and flow of solids, bulletin no. 123. *Bulletin of the University of Utah*, 53(26).
- Johanson, K. and Barletta, D., The Influence of Air counter Flow Through Powder Material on the Measurement, *The 4th International Conference for Conveying and Handling of Particulates Solids, Budapest, Hungary, May, 2003*. pp. 4.39-4.44.
- K. Smolders, J. Baeyens, A Characterisation of Cohesive (C) and Free Flowing (A) Powders, *The proceedings of 4th International Conference for conveying and Handling of Particulate Solids, Budapest, Hungary, May 2003*, pp. 4.8–4.13.

- Krantz, M., Zhang, H. and Zhu, J., 2009. Characterization of powder flow: Static and dynamic testing. *Powder Technology*, 194(3), pp.239-245.
- Koynov, S., Glasser, B. and Muzzio, F., 2015. Comparison of three rotational shear cell testers: Powder flowability and bulk density. *Powder Technology*, 283, pp.103-112.
- Lee, S.H., Sakai, E., Daimon, M. and Bang, W.K., 1999. Characterization of fly ash directly collected from electrostatic precipitator. *Cement and Concrete Research*, 29(11), pp.1791-1797.
- Lee, Y.J. and Yoon, W.B., 2015. Flow behavior and hopper design for black soybean powders by particle size. *Journal of Food Engineering*, 144, pp.10-19.
- Leturia, M., Benali, M., Lagarde, S., Ronga, I. and Saleh, K., 2014. Characterization of flow properties of cohesive powders: A comparative study of traditional and new testing methods. *Powder Technology*, 253, pp.406-423.
- Liu, Y., Guo, X., Lu, H. and Gong, X., 2015. An Investigation of the Effect of Particle Size on the Flow Behavior of Pulverized Coal. *Procedia Engineering*, 102, pp.698-713.
- Lu, H., Guo, X., Liu, Y. and Gong, X., 2015. Effect of Particle Size on Flow Mode and Flow Characteristics of Pulverized Coal. *KONA Powder and Particle Journal*.
- Lumay, G., Boschini, F., Traina, K., Bontempi, S., Remy, J.C., Cloots, R. and Vandewalle, N., 2012. Measuring the flowing properties of powders and grains. *Powder Technology*, 224, pp.19-27.
- Maarup, C., Hjuler, K. and Dam-Johansen, K., 2014. High temperature cement raw meal flowability. *Powder Technology*, 253, pp.686-690.
- Mallick, S.S. and Wypych, P.W., 2009. Modeling solids friction for dense-phase pneumatic conveying of powders. *Particulate Science and Technology*, 27(5), pp.444-455.
- Pan, R. and Wypych, P.W., Pressure Drops of Slugs in Unstable Zone of Pneumatic Conveying, *The Third Israeli Conference for Conveying and Handling of Particulate Solids, Dead Sea, Israel, May 2000*. pp. 10.31-10.36.
- Pan, R., 1999. Material properties and flow modes in pneumatic conveying. *Powder Technology*, 104(2), pp.157-163.

- Ripp, M., Debele, Z.A. and Ripperger, S., 2015. Determination of Bulk Flow Property of tef Flour and Seed and Design of a Silo. *Particulate Science and Technology*, 33(5), pp.494-502.
- Sanchez, L., Vasquez, N., Klinzing, G.E. and Dhodapkar, S., 2003. Characterization of bulk solids to assess dense phase pneumatic conveying. *Powder Technology*, 138(2), pp.93-117.
- Sarkar, S., 1974. *Fuels and combustion*. Universities Press.
- Saw, H.Y., Davies, C.E., Jones, J.R., Brisson, G. and Paterson, A.H., 2013. Cohesion of lactose powders at low consolidation stresses. *Advanced Powder Technology*, 24(4), pp.796-800.
- Saw, H.Y., Davies, C.E., Paterson, A.H. and Jones, J.R., 2015. Correlation between Powder Flow Properties Measured by Shear Testing and Hausner Ratio. *Procedia Engineering*, 102, pp.218-225.
- Schulze, D., 2008. Powders and bulk solids. *Springer, Berlin/Heidelberg. doi,10(1007)*, pp.978-3.
- Sindel, U. and Zimmermann, I., 2001. Measurement of interaction forces between individual powder particles using an atomic force microscope. *Powder technology*, 117(3), pp.247-254.
- Teunou, E., Fitzpatrick, J.J. and Synnott, E.C., 1999. Characterisation of food powder flowability. *Journal of Food Engineering*, 39(1), pp.31-37.
- Wypych, P.W., 1999. Pneumatic conveying of powders over long distances and at large capacities. *Powder Technology*, 104(3), pp.278-286.
- Xanthakis, E., van Ommen, J.R. and Ahrné, L., 2015. Flowability characterization of nanopowders. *Powder Technology*, 286, pp.156-163.
- Zafar, U., Hare, C., Calvert, G., Ghadiri, M., Girimonte, R., Formisani, B., Quintanilla, M.A.S. and Valverde, J.M., 2015. Comparison of cohesive powder flowability measured by Schulze Shear Cell, Raining Bed Method, Sevilla Powder Tester and new Ball Indentation Method. *Powder Technology*, 286, pp.807-816.

Web references:

W.1 Fly ash coal combustion residue, <http://mineral.eng.usm.my>, (accessed on - 2 June 2016)

W.2 PFT Manual, <http://www.brookfieldengineering.com>, (accessed on – 2 June 2016)

W.3 Surface roughness, <http://www.worldstainless.org>, (accessed on – 4 June 2016)

Appendix A

An overview of stresses in storage vessel (Schulze. 2008)

The determinations of the stresses in the hopper/silo are of paramount importance. These stresses are relevant for designing of the silo for strength and flow. Apart from traditional and direct applications, the knowledge about stresses in storage vessels find importance in the calculation of load on the feeders, inserts, driving torque necessary to run a screw feeder etc. This section contains the overview of the stresses that occur in the hoppers. The knowledge about the stresses in the hoppers is also important because the powder flow properties have to be tested under similar stress conditions for obtaining a realistic view on the flowability of the bulk solid out of the given storage vessel.

A.1 Stresses in storage vessels

The civil engineering design is completely a separate research article as that design is more focused on the stability of structure. The various design codes are available in the literature which deals with this designing part. The study in this thesis has been concentrated in the hopper design on the basis of the flowability of the bulk solid. The designing on the basis of the flowability deals with the determination of the nature of the flow pattern inside the storage vessel, hopper half angle and outlet opening size only. The stresses in the hopper are studied in 3 different parts described as follows.

- a) Stresses in the vertical section of storage vessel.
- b) Stresses in the hopper during storage (Filling state).
- c) Stresses in the hopper during discharging process.

The following section describes about the stresses in these sections of the storage vessels in detail.

A.2 Stresses in vertical section

A storage vessel consists of two parts namely vertical section and the hopper section. The vertical section in a conical silo is the cylindrical portion present on its top. The stresses in the vertical section are relatively easy to find and the results have been found experimentally

over the last 100 years. Janssen was the first to describe the problem of the storage of wheat in a conical silo. His analysis yielded a famous Janssen Equation which is valid even today as the large number of erected silos is designed using the modification of the same principle Equation. The pressure at wall, σ_w for the conical vessel containing liquid is directly proportional to its depth according to Pascal law. The maximum pressure is at the bottom of the vessel. This is not the case with the bulk solids/powders, σ_w becomes fairly constant after a particular depth because the walls start supporting the bulk material. The stress distribution depends upon the frictional behaviour the wall and the bulk solid. This has been pictorially represented in Fig. A1.

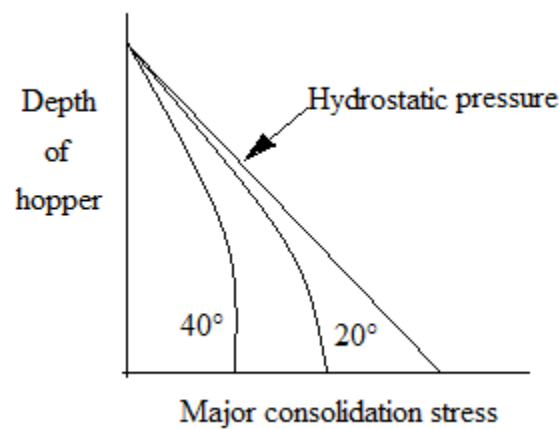


Figure A1: Dependence of the major consolidation stress on the wall friction angle.

(W.2)

The differential Equation formed after assuming static element in the vertical section can be rewritten as Eq. (A1).

$$\frac{d\sigma_v}{dz} + \sigma_v \lambda \left(\frac{U}{A} \right) \tan \varphi_x = g\rho_b \quad (A1)$$

Where σ_v is the vertical stress on the bulk solid, z is the depth of the vessel, $\lambda = \sigma_v / \sigma_h$ is the ratio of vertical and horizontal stress, U is the perimeter of the vessel, A is the surface area of the vessel containing bulk solid, $\varphi_x = \tau_w / \sigma_v =$ coefficient of friction between wall and the bulk solid, τ_w is the wall shear stress. The solution of this Eq. (A1) is given by Eq. (A2).

$$\sigma_v = \frac{gA\rho_b}{\lambda \tan \varphi_x U} \left[1 - e^{-\frac{\lambda U z \tan \varphi_x}{A}} \right] + \sigma_{v0} e^{-\frac{\lambda U z \tan \varphi_x}{A}} \quad (A2)$$

Where σ_{v_0} is the vertical surcharge stress introduced in the solution while imposing the boundary conditions. If the silo is open and having stress free surface on the top then this value is zero. We know that λ is the ratio of horizontal stress on the bulk solid and vertical stress on the bulk solid element. This λ is similar to the term used in soil mechanics describing the ratio of the two abovementioned stresses. The precise calculation of λ is the key concept on which the applicability of Janssen Equation is dependent. The lambdameter is the ISO standard equipment for measuring λ . According to German standard DIN 1055, stress ratio is given by Eq. (A3).

$$\lambda = 1.2(1 - \sin \varphi) \quad (A3)$$

Where φ = angle of internal friction of bulk solid. For rough calculations λ is taken as 0.4 and for practical purposes the range is in between 0.3-0.6. Using the value of λ , we can calculate σ_w or σ_h by using Eq. (A4).

$$\sigma_h = \lambda \sigma_v \quad (A4)$$

A.3 Stresses in hopper section (During Storage condition)

The value of λ is in between 0.3-0.6 which shows that the complimentary horizontal stresses are lower than vertical stresses. In other words, vertical stress, σ_v is the major consolidation stress σ_1 and horizontal or wall stresses σ_w is the minimum principle stress, σ_2 . The Mohr circle analysis can be used to specify the stress state of the bulk solid in the vertical vessel. On the other hand, the problem is not so straight forward in the case of stresses in the hopper section. In simple words it can be said that the material has major principle stress σ_v in vertical section which changes to σ_w in hopper section. The differential Equation formed after force balance on a slice element in the hopper section can be written as Eq. (A5) and (A6).

$$\frac{d\sigma_v}{dz} - n \left(\frac{\sigma_v}{z} \right) = -g\rho_b \quad (A5)$$

$$\text{Where } n = (m + 1) \left\{ K \left[1 + \frac{\tan \varphi_x}{\tan \theta} \right] - 1 \right\} \text{ and } K = \frac{\sigma_w}{\sigma_v} \quad (A6)$$

Where, m represents the parameter accounting for the shape of the hopper. The parameter $m=0$ for wedge shaped hoppers and $m=1$ for circular hoppers. Θ represents hopper half angle. K and n are the parameters dependent upon the flow properties of bulk solids and the mode of operation (discharge or filling state). The solution of this differential Equation requires numerical methods. SSTOOL is the commercially available freeware software tool by Dietmar Schulze (Schulze, 2008). The solution of this differential Equation provides σ_v and σ_w distribution in a silo. The arching phenomenon occurs just at the outlet of the hoppers and the normal and vertical stresses at that affect the flowability of the bulk solid. Knowledge of these stresses is of paramount importance as it gives an estimate at which stress points the flowability of the bulk solid has to be investigated. Wall friction angle must be investigated in the stress range near σ_w and angle of internal friction of powder must be investigated near σ_v stress range. The knowledge of σ_v and σ_w is not enough because the shear testing has to be performed at a particular pre shear stress, σ_{pre} . According to a rough estimate $\sigma_{pre} = 0.8 \sigma_1$, where σ_1 is the major consolidation stress or the stress point found from the stress distribution. SS TOOL gives the stress distribution in the complete silo with height as shown in Fig. (A2).

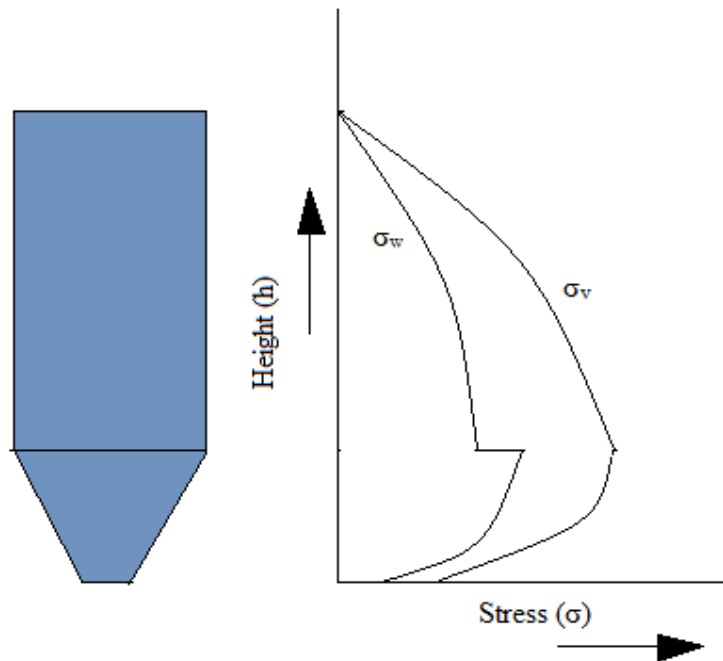


Figure A2: Stress distribution in a silo

A.4 Stresses in hopper (During discharge state)

The hopper is designed on the basis of filling condition because discharge condition stresses are much lower as compared to them. There is a stress peak which occurs at the transition of the vertical conical section to the hopper section. This stress peak is called the “switch” and a similar condition is found when there is a dent in the silo or there is a screw protruding in the hopper. Inserts also face switch conditions during discharge state. In more technical terms, one can say that the bulk solid is transformed from active stress state to passive stress state. Active state of the stress is represented by the greater value of the vertical stresses and passive state of stress is represented by the greater value of the horizontal stresses. More details about the discharge stress states can be found elsewhere (Schulze, 2008). The powder actually expands due to horizontal squeezing action of the walls as it moves just near to the outlet. This phenomenon sometimes create vacuum inside the hopper giving unreliable discharge in case of fine powders. Providing of nozzles, vibrators and inserts with air nozzles are some of the suggested solutions for this problem.

Appendix B

Table B.1: Comparison of maximum and minimum error in cohesion models at stress 1

Sample type	Saw model (% error)		New PSD based model (% error)	
	Minimum	Maximum	Minimum	Maximum
Easy flowing	-13.45	46.72	-14.24	24.19
Cohesive	-56.84	24.10	-20.93	21.67
Very cohesive	-59.80	-47.40	-16.37	15.17

Table B.2: Comparison of maximum and minimum error in cohesion models at stress 2

Sample type	Saw model (% error)		New PSD based model (% error)	
	Minimum	Maximum	Minimum	Maximum
Easy flowing	-16.42	45.22	-5.39	25.01
Cohesive	-22.41	22.31	-19.59	26.58
Very cohesive	-57.92	21.51	-11.63	3.56

Table B.3: Comparison of maximum and minimum error in cohesion models at stress 3

Sample type	Saw model (% error)		New PSD based model (% error)	
	Minimum	Maximum	Minimum	Maximum
Easy flowing	-20.06	42.12	-1.87	16.86
Cohesive	-55.37	30.67	-22.81	31.84
Very cohesive	-57.13	20.16	-23.07	0.66

Table B.4: Comparison of maximum and minimum error in cohesion models at stress 4

Sample type	Saw model (% error)		New PSD based model (% error)	
	Minimum	Maximum	Minimum	Maximum
Easy flowing	-23.76	38.19	5.33	6.72
Cohesive	-61.04	31.99	-23.23	34.78
Very cohesive	-60.55	16.60	-31.20	0.82

Table B.5: Comparison of maximum and minimum error in cohesion models at stress 5

Sample type	Saw model (% error)		New PSD based model (% error)	
	Minimum	Maximum	Minimum	Maximum
Easy flowing	-31.07	34.61	-6.59	3.06
Cohesive	-68.13	33.57	-29.35	34.79
Very cohesive	-65.73	13.14	-44.99	-2.87

Appendix C

Table C1: Error in UYS model at stress 1

Sample	Maximum % error	Minimum % error
Easy flowing	23.58	-6.44
Cohesive	24.28	-22.23
Very cohesive	13.53	-8.53

Table C2: Error in UYS model at stress 2

Sample	Maximum % error	Minimum % error
Easy flowing	23.92	2.7
Cohesive	17.73	-30.19
Very cohesive	4.58	-16.32

Table C3: Error in UYS model at stress 3

Sample	Maximum % error	Minimum % error
Easy flowing	16.90	1.89
Cohesive	19.32	-24.67
Very cohesive	2.06	-23.17

Table C4: Error in UYS model at stress 4

Sample	Maximum % error	Minimum % error
Easy flowing	9.06	1.89
Cohesive	19.64	-24.67
Very cohesive	2.06	-23.17

Table C5: Error in UYS model at stress 5

Sample	Maximum % error	Minimum % error
Easy flowing	9.06	2.26
Cohesive	19.64	-27.63
Very cohesive	0.477	-19.22

Communications

Rohilla, L., Mallick, S.S. and Setia, G. An Experimental Investigation on Flow Properties of Fly Ash. **Powder Technology, Elsevier.** (Under communication)

Rohilla, L., Mallick, S.S. and Setia, G. Modelling Cohesion and Unconfined yield strength of Fine Powders. **Powder, Granule and Bulk Solids: Innovations and Applications. 1 to 3 December, 2016, Jaipur, Rajasthan, India.** (Under Communication)